Empirically detecting colour: Can we use Solar Cells as Colour Sensors?

by

Sergio Majluf Suárez

A thesis submitted to the
School of Graduate and Postdoctoral Studies in partial
fulfillment of the requirements for the degree of

Master of Science in Material Science

Faculty of Science
University of Ontario Institute of Technology (Ontario
Tech University)
Oshawa, Ontario, Canada
August, 2021

THESIS EXAMINATION INFORMATION

Submitted by: **Sergio Majluf Suárez**

Master of Science in **Material Science**

Thesis Title : Empirically detecting colour: Can we use solar cells as colour sensors?

An oral defense of this thesis took place on July 28, 2021 in front of thefollowing examining committee:

Examining Committee:

Chair of Examining Committee	Dr. Brad Easton
Research Supervisor	Dr. Franco Gaspari
Research Co-supervisor	Dr. Alberto Tagliaferro, Politecnico di Torino
Examining Committee Member	Dr. Aaron Slepkov, Trent University
Examining Committee Member	Dr. Nisha Agarwal, Ontario Tech University
Thesis Examiner	Dr. Mark Green, Ontario Tech University

The above committee determined that the thesis is acceptable in form and content and that a satisfactory knowledge of the field covered by the thesis was demonstrated by the candidate during an oral examination. A signed copy of the Certificate of Approval is available from the School of Graduate and Postdoctoral Studies.

ABSTRACT

The purpose of this thesis was to explore the possibility of using solar cells as a colour sensor. Colour sensors already exist, yet they are either costly or fail at correctly sensing monochromatic light. Our experiment was set up in order to see if a solar cell would create a unique current response to a specific monochromatic wavelength.

We tested our solar cells by measuring their individual current response at different voltages with different monochromatic light inputs. We concluded that the use of a single solar cell is not a feasible colour sensor due to high Delta E values.

We then combined the colour matching functions of multiple solar cells. The Micromorph and DSSC combination had a lower Delta E average value in comparison to all single solar cells tested. At a light bandwidth of 60 nm, a Delta E value of less than 10 was achieved.

Keywords: physics ; colour sensors ; solar cells

AUTHOR'S DECLARATION

I hereby declare that this thesis consists of original work of which I have authored. This is a true copy of the thesis, including any required final revisions, as accepted by my examiners.

I authorize the University of Ontario Institute of Technology (Ontario Tech University) to lend this thesis to other institutions or individuals for the purpose of scholarly research. I further authorize University of Ontario Institute of Technology (Ontario Tech University) to reproduce this thesis by photocopying or by other means, in total or in part, at the request of other institutions or individuals for the purpose of scholarly research. I understand that my thesis will be made electronically available to the public.

Sergio Majluf Suárez

STATEMENT OF CONTRIBUTIONS

I hereby certify that I am the sole author of this thesis and that no part of this thesis has been published or submitted for publication. I have used standard referencing practices to acknowledge ideas, research techniques, or other materials that belong to others. Furthermore, I hereby certify that I am the sole source of the creative works and/or inventive knowledge described in this thesis.

ACKNOWLEDGEMENTS

Throughout the writing of this dissertation, I have received a great deal of support and assistance. I would first like to thank my supervisor, Professor Franco Gaspari, whose expertise was invaluable in formulating the research questions and methodology. Your insightful feedback pushed me to sharpen my thinking and brought my work to a higher level.

I would like to acknowledge my colleagues from my internship at Politecnico di Torino (Polito) for their wonderful collaboration. I would particularly like to single out my supervisor at Polito, Alberto Tagliaferro. Dr. Tagliaferro, I want to thank you for your patient support and for all of the opportunities I was given to further my research.

I would like to thank Massimo Rovere, for not only creating the code that made all of the analysis in this thesis possible, but for taking the time and effort to teach me how to properly use it, some very useful tips and tricks, and for the talks we had while having lunch together while I was in Polito. He truly made the stay at a foreign environment that much easier.

I would also like to thank my tutors, Dr. Valeri Kapoustine and Dr. Joe MacMillan, for their valuable guidance throughout my studies. You provided me with the tools that I needed to choose the right direction and successfully complete my dissertation. In addition, I would like to thank my parents for their wise counsel and sympathetic ear. As well as my family.

Finally, I could not have completed this dissertation without the support of my friends, Sasha Weiler, Adam Kozak, Hector Robinson, Jacob Demoe, Christian Morrison and

Nicole Noriega, who provided stimulating discussions as well as happy distractions to rest my mind outside of my research.

Muchas gracias,

Sergio Majluf Suárez

Contents

List of Tables

List of Figures

1. CHAPTER 1 - INTRODUCTION

1.1 What is colour?

Colour is a physical property of an object. A physical colour is the combination of pure spectral colours. Spectral colours are composed of a single wavelength in the visible spectrum. The range of the visible spectrum goes from 400 nanometres (nm) to 700 nm. Every wavelength of light is perceived as a spectral colour. Our eyes can perceive colours thanks to our trichromatic colour vision. Most mammals only have dichromatic colour vision. About 90 million years ago, we used to be able to see in the ultraviolet part of the spectrum, but we lost this ability as we shifted into trichromatic vision in order to be able to see blue light (Albrecht, M , 2010).

For humans to be able to see the colour of objects, rays of light must be reflected off said object. The lens behind our cornea focuses the reflected light into the back of the eye, where the retina is located. Photoreceptors cells in the retina then convert the light energy into nerve impulses. These nerve impulses are then sent through the optic nerve towards the brain. Once the signal reaches the necessary parts in the brain, the final image is created.

The textile industry has been using colour recognition in order to detect discrepancies in the tones of fabrics, and overall quality control of the pieces. For the aging population, having to consume multiple pills a day is a reality. These pills, with many

of them simply resembling a circular or capsule shape, use colour as a great way to distinguish them from each other, which is crucial especially for some of the aging population. Colour consistency and clear distinction are imperative in that regard. Another example is colour coding used in the health sector, which is the systematic process of displaying information using different colours in classification and identification (Bosch, S , 2012).

Colour is also used in order to monitor safety in quality control of products such as meats and produce. The ripeness and health of produce can be deduced by colour alone, leading to less waste product being produced at the end of the day. The great majority of the food industry uses two main colour measurement techniques, these being colorimetry and spectrophotometry.

One important aspect of colour sensing is how we describe colours. In figure 1.1, one can see colour being described in terms of hue, saturation, and value. In 1913, Albert Munsell, an American art instructor and painter created a system for designating colours based on a colour arrangement system.

This system is the “Munsell colour system”, and it was introduced in “The Atlas of the Munsell Colour system”. The publication included fifteen colour charts that consisted of hundreds of colour chips arranged to the colour characteristics. The characteristics listed in the system define colour by measured scales of hue, value, and chroma. Hue corresponds to the dominant wavelength. Hue is defined in physics as the subjective sensation related to the intensity of light which emanates from a surface or from a point surface. Value relates to the brightness. It distinguishes one colour from another. Chroma is the strength/weakness or purity of the colour (Monsen, H , 2005).

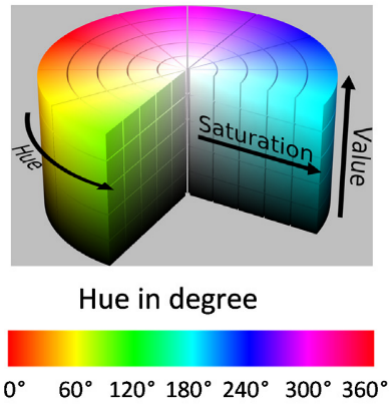

Figure 1.1: Hue, saturation, and value represented in a 3D space. (Reproduced from (Alaya, M , 2019))

1.2 The Human Eye

Our eyes can perceive the world around us thanks to cones and rods which are located in the retina of the human eye. The rods are for low light intensity and night vision. Humans have three different types of cones. We have red, green, and blue cones, which are distributed throughout the retina. Each type of cone has a distinct opsin, which are light sensitive proteins. Only one opsin type is found in any one cone, this leads to us only having three different cones as seen in figure 1.2.

The colour recognition of the human eye is not without its limitations. Colour blindness is one such common ailment in the human race. Dichromatic colour blindness can be sectioned off into red-green (the most common) and blue-yellow colour blindness. In individuals of northern European ancestry, "as many as 8 % of men and 0.5 % of women experience the common form of red-green colour blindness (Wong, B , 2011)."

Protanopia, deuteranopia, and tritanopia are red blindness, green blindness, and

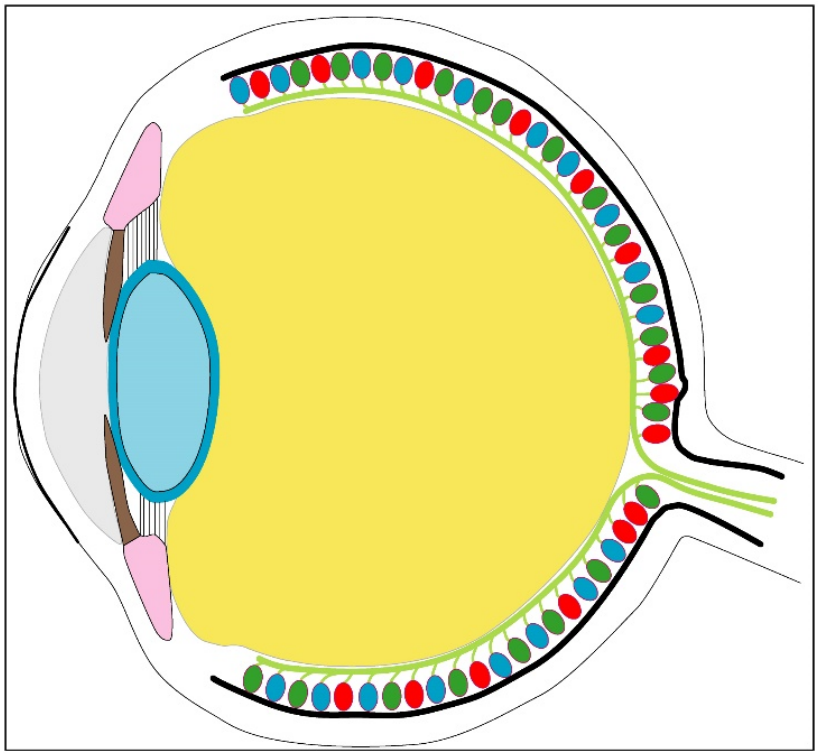

Figure 1.2: Human eye with the locations of our cones. Reproduced from Joshua Heafield (https://droso4schools.wordpress.com/l5-vision/)

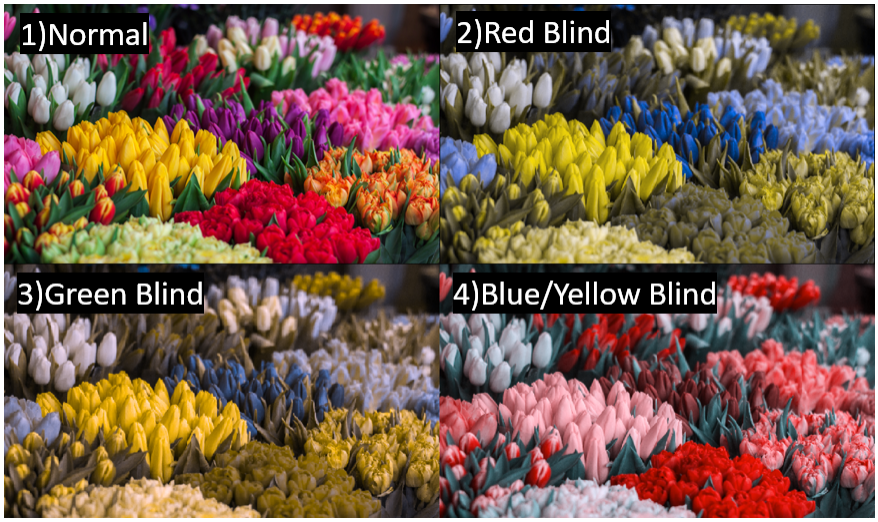

Figure 1.3: Photo by John-Mark Smith on Unsplash. Appearance of natural light seen to individuals with normal colour vision and simulated images perceived by different types of vision defective individuals. In this image we can see 1) Normal Vision, 2) Protanopia, 3) Deuteranopia, 4) Tritanopia. The simulation was performed by software from VisCheck (freely available at vischeck.com).

blue-yellow blindness respectively. These types of colour blindness are ever present for the individuals living with those genetic mutations. Keeping figure 1.3 in mind, colour blindness, be it mild or acute, will affect the colour perception of the individual, and when it comes to commercial, pharmaceutical, artistic, industrial, and manufacturing sectors, we need to be as precise and correct as possible in the way we communicate and keep things up to standard.

1.3 Colour Sensing

As mentioned previously, the main techniques used to detect and describe colours are colorimetry and spectroscopy. Colorimetry measures the three primary colours that can be observed by the human eye (Red Green Blue [RGB]). The shortcoming of

this technique is that it can not detect the secondary or tertiary colours individually which limits its efficiency. On the other hand, Spectroscopy can measure the different wavelengths of visible light, 400 to 700 nm. The reading is given either by spectral reflectance or by the transmittance of the object. Its use then is to standardize colour. It is a reliable piece of technology, yet it requires complex equipment setup in order to work (Alaya, M , 2019).

If we wanted to detect a wavelength, denoted by λ, of a single monochromatic signal, one can make use of a spectrometer. It works by having the optical signal diffracted by a grating at different angles. The angle depends on the incident wavelength. After the signal is diffracted, it will be detected by either a photodiode array, or a fixed photodiode with a rotatable grating.

The other option is to use an RGB sensor. This is made up of three photodiodes which have either a red, green, or blue filter in front of them. Yet another wavelength sensing device, which senses the intensity of the incoming single monochromatic signal is a photodiode colour sensor. This sensor type, when exposed to monochromatic light uses two stacked p-n junctions. These provide two unique and distinct outputs representing responsivity in different regions of the photodiode. The first signal is more sensitive to red light, and the other to blue light. If an incoming monochromatic signal is within the region between 450 and 780 nm, the sum or difference of the two signals will be a monotonically increasing function. The drawback from this sensor is that the responsivities are temperature dependent. In order to calibrate the colour sensor, its temperature must be read in the absence of light, and thenonce the temperature is determined, the responsivities can be adjusted (Udd, E , 2014). As stated, typical colour sensors are based on either photo emissive cells, photo conductive cells, or photo junction devices.

Colour sensor measurements can provide all the colour frequencies, yet there are errors when it comes to the measurement of short-range colour degrees. They have a short degree range for the orange [from 8° to 19°], while the blue range is quite large [from 180° to 309°]. This leads to error if a measurement were to be made near one of these limits. This error would lead to a conflict of reading which would impede a proper reading of the colour at hand. Therefore, the system is highly susceptible to errors in classifications at short ranges. Not only that, but it has difficulty in detecting the colour yellow, as readings in near yellow have a high chance of reflecting light off the sensor.

Additional limitations of readily available colour sensors are the limited range of colours they can detect, and the limited abilities to quickly change setups or handling multiple colours. Also, colour sensors have problems when they need to detect subtle differences among similar or highly reflective colours. An example would be metallic paint used in the automotive industry, which in turn makes it difficult to differentiate among shades of metallic colours like silver or gold. Being able to do this is imperative, as when matching subassemblies, e.g., the mirrors or bumpers to park assist-sensors in the car (Letterle, B , 2006).

With all of this in mind, the purpose of this thesis is to try to create a product that will be able to address some of these problems, be readily available, and be inexpensive as well. In particular, we have tested out solar cells in place of the standard current colour sensors. An ideal colour sensor should be able to recognize all wavelengths, be able to capture monochromatic and combined light, and be able to create a distinct current response signal to each corresponding wavelength. A solar cell by itself can provide an electric output for different optical inputs, including

visible light. Therefore, we tested whether solar cells can be used in order to absorb incoming monochromatic or combined light from an object, to transform that incoming wavelengths into an electric current, and then transform that combination of signals into a correct reading of the colour of the target.

1.4 Solar Cells as Colour Sensors

Since the discovery of the photoelectric effect, we know that photons can transfer enough energy to electrons to overcome their bonding energy and leave the surface of a metal. In a semiconductor material, the energy of the photon needs to overcome what is commonly called the "energy gap". This is the energy required to excite an electron from the valence band (bound state) to the conduction band (free electron state). A solar cell material is essentially a semiconductor, which can create a current when photons are irradiated onto its surface. The excitation of the electron by the absorption of light creates an electron-hole pair. These photons can come from artificial light, or from sunlight. The electron-hole pair would eventually recombine due to them not straying too far off each other in the absence on an external force (Bube, R , 1998). Different solar cells have widely different levels of efficiency when transforming energy from photons into electricity. The efficiency of a solar cell is at its maximum when the product of voltage (ϕ_m) and current density (J_m) in the cell is at maximum as well.

1.5 Quantum Efficiency

Quantum efficiency is another important metric to investigate in addition to the fill factor and efficiency of solar cell. The quantum efficiency of a solar cell is defined as the ratio between the number of photons of a given wavelength that strike the surface of the cell, and the number of electrons produced in the external circuit. In

other words, it is the density of electrons due to light in external circuit divided by the density of photons absorbed (Lan, D , 2015).

Quantum efficiency can be divided into two parts: External quantum efficiency (EQE), and Internal quantum efficiency (IQE). For the EQE value, all photons striking the solar cell surface are taken into consideration. In comparison, the IQE value depends only on the photons that are not being reflected. As a non-destructive technique, spectral analysis of IQE has long been an important part of solar cell characterization. For wavelengths that do not penetrate to the rear surface, the traditional plot of inverse-IQE versus absorption length was used to extract bulk minority-carrier diffusion lengths for thick planar devices. QE analysis allows for extraction of both electrical and optical properties in near bandgap wavelengths in modern solar cells that have textured surfaces and long diffusion lengths (Lan, D , 2015).

For our purposes, an alternative to quantum efficiency is measuring the spectral response of a solar cell. This was achieved by getting the current vs voltage and current vs wavelength responses of our chosen solar cell from -5 V to 5 V. A monochromator, a solar simulator, and a precision source/measuring unit were used.

1.6 Solar Cells Used

The solar cells tested needed to have different characteristics to establish a baseline for experimentation. With a solid baseline, future work can be done for the purpose of discovering better typologies. Given limitations on the research budget, commercially available solar cells were chosen for testing. The selection of commercially available solar cells allowed for the acquisition of cells that were primarily created as photovoltaic (PV) cells by their manufacturers. The solar cells gathered are listed below:

- Polycrystalline Silicon Solar Cell from Velleman
- Amorphous Silicon Solar Cell (A-Si Solar Cell) from Panasonic
- Dye Sensitized Solar Cell (DSSC) Solaronix
- Perovskite Solar Cell from Solaronix

These cells would have proven to be difficult to produce in our lab and buying them allowed us to have a wide assortment of available options that gave us a reasonable variety based on available commercial cells. If more work and resources were allocated this experiment, one could approach companies that would be better suited to manufacture the desired combination of parameters needed to improve on the experimental results gathered. This would be possible as the solar cells would be created for the purpose of maximizing the spectral response of the cell to specific wavelength instead of trying to just improve the overall current production at different wavelengths at a set applied voltage.

2. CHAPTER 2 - LIGHT AND COLOUR

2.1 Behaviour of Light

As stated in the introduction, the visible range of the electromagnetic spectrum is from 380 nm - 700 nm. This visible light encompasses all colours perceived by humans. There are two ways for light to interact when it comes in contact between two mediums, which affects its wavelength composition: Emission and Absorption of light.

The emission from light of an object is caused by a chemical or physical process. All materials above a temperature of 0 Kelvin, radiate energy. Emissivity, ϵ, is defined as the ratio of the radiant exitance or radiance of a given body to that of a blackbody. It has both a spectral and directional property, and is a dimensionless value between 0 and 1. Emittance on the other hand refers to the properties to a single specific sample.

$\epsilon(\lambda)$ is the spectral emittance, $\epsilon(\lambda)$ is the emittance at a given wavelength, (λ). It is the ratio of the radiance of a source at a specific radiance of a blackbody at the same wavelength, this is given by (Palmer, J , 2009):

$$\epsilon(\lambda) = \frac{L_\lambda}{L_{\lambda BB}} \tag{2.1}$$

Where $L_{\lambda BB}$ is the value of the Plank's function at the specific wavelength for a

blackbody.

The opposite of emission is absorption. Absorption is the process by which the incident radiant flux is converted into another form of energy. Absorptance is the fraction of incident flux that is absorbed by an object or surface. Spectral absorptance is defined at a specific wavelength λ as:

$$\alpha(\lambda) = \frac{\phi_{\lambda a}}{\phi_{\lambda i}} \tag{2.2}$$

α (λ) is the spectral absorptance , $\phi_{\lambda a}$ is the absorbed power , and $\phi_{\lambda i}$ is the incident power. Total absorptance is defined as:

$$\alpha = \frac{\phi_a}{\phi_i} \tag{2.3}$$

When light strikes a surface, a fraction of the radiant flux incident on the surface is returned into the hemisphere whose base is the surface containing the incident radiation. This is called a reflection. The reflection of light can be specular, diffusive, or a combination of both. Reflectance is the ratio of reflected power to incident power. Spectral reflectance is defined at a specific wavelength λ as (Palmer, J , 2009):

$$\rho(\lambda) = \frac{\phi_{\lambda r}}{\phi_{\lambda i}} \tag{2.4}$$

Where ρ is total reflectance, $\phi_{\lambda r}$ is reflected flux, and $\phi_{\lambda i}$ is the incident flux.

Transmission is the process by which incident radiant light leaves a surface or medium from a side off the object other than the incident side. The spectral transmittance $\tau(\lambda)$ of a medium is the ratio of the spectral flux ($\phi_{\lambda t}$) to the incident spectral flux ($\phi_{\lambda i}$). This is summarized in the following equation (Palmer, J , 2009):

$$\tau(\lambda) = \frac{\phi_{\lambda t}}{\phi_{\lambda i}} \tag{2.5}$$

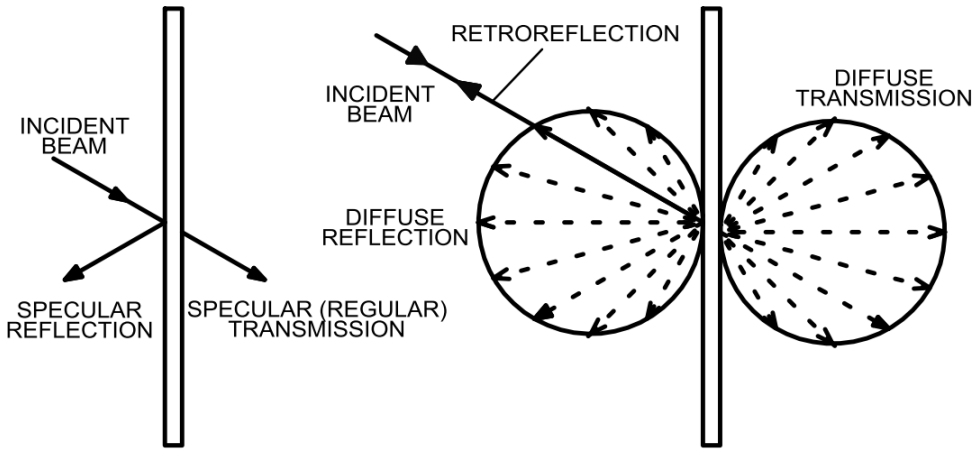

Figure 2.1: Idealized reflection and transmission of incident ray. Reproduced from (Palmer, J , 2009)

In conclusion, when incident light hits a surface at a certain angle, reflection, absorption, and transmission occurs. A fraction of the light beam is reflected of the surface between two mediums, another part is absorbed by the material itself, and the rest is transmitted. These relationships between light and surfaces can be appreciated in figure 2.1, where we can see an incident ray, its different types of reflection, and different types of transmission.

2.2 Colour Communication

In Chapter 1, we introduced the world of colour perception and human limitations; such as human blindness. Even when two people see the same object, differences such a age, illumination, eye fatigue, or even the background behind the object will create discrepancies in the way they describe the colour of said object. Communication, and our inability to be precise and consistent, represents a crucial factor in the determination of the exact colour of an object (Monsen, H , 2005). In the past, before the invention of colour photography, people used examples found in nature in order to

describe a colour. These include minerals, plants, and animals. For example, the tint "Scarlet Red" was compared to the "Scarlet Ibis or Curlew" , the "Large red Oriental poppy", and "light red cinnabar" (Gottlob, A , 1894).

Another problem that arises with communicating colour without a proper guideline is that each person will interpret colours based on personal references. This makes it difficult to be able to easily compare one colour to the other with a high degree of accuracy. When only people are involved, psychological, environmental, and experimental factors will affect the perception of colour.

A colour sensor is a measuring tool that differentiates one colour from all others and assigns it a numerical value. As mentioned in Chapter 1, the most used type of colour sensor are spectrophotometers. The other type are colorimeters.

Spectrophotometers are mainly used in the printing, packaging, and industrial sectors. They can capture colour and sometimes even appearance data of objects. From this, one can get quantitative colour analysis. It is limited by low sensitivity and selectivity. The high cost of spectrophotometers makes it so they are not used by everyday folk. The cheaper alternative are calorimeters. If we would want to create a color sensor, we would go for the cheap and easy route as it would make it more consumer friendly and more widely available.

A colorimeter is a tristimulus device that makes use of Red, Green, and Blue filters. They emulate the response of the human eye to light and colour. They are a much cheaper colour sensor in comparison to spectrophotometers. This does come at a cost, that being an inability to compensate for metamerism, which is the shift in the appearance of a sample due to the light used to illuminate its surface. Since colorime-

ters use a single type of light source, and do not record the spectral reflectance of the object, they are unable to predict the shift in appearance. A spectrophotometer can compensate for the shift, so they are more reliable, and accurate. However, the downside of most spectrophotometers is their size and high cost relative to colorimeters (Monsen, H , 2005).

2.2.1 Colour Description

Colours can then be described by three different elements, hue, chroma(saturation), and value(brightness) of the colour, as follows (see also Fig. 2.2):

Hue: Hue is largely independent of variations in colour intensity such as those coming from changes in colored reagent concentration or sensor membrane thickness (Erenas, M , 2012). The hue is the object's perceived colour. A visual representation of hue is the colour wheel. The wheel is constructed from primary colours (red, blue, yellow) and secondary colours (orange, purple, green). The wheel allows us to see which colours are complementary, such as blue and orange, or purple and lime. Hue aids in distinguishing colours apart from each other.

Chroma (saturation): The chroma is the indication of the strength or weakness of the colour. Another way to describe it is the relative "dullness" or "vividness" or the colour. It is the quality of a colour's saturation. Chroma is the departure degree of a colour from the neutral colour of some value. A high chroma of 30 would depict a fluorescent object, while a low one would be a neutral colour such as grey.

Value: The value is the luminous intensity of a colour. The value indicated the lightness or darkness of the colour. A low saturation would lead to dark colours, while a high saturation leads to a bright colour. If the colour had an extremely low

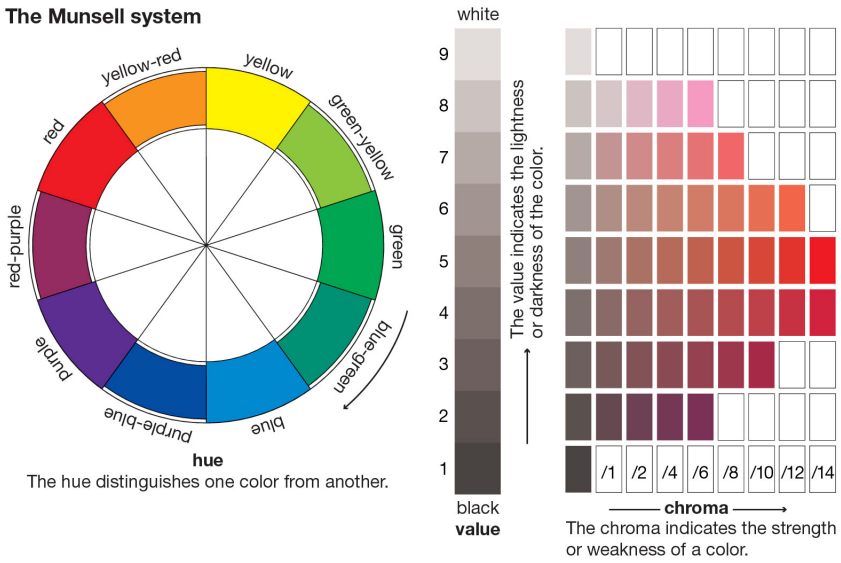

Figure 2.2: The Munsell system, with hue, value and saturation being shown as separate two-dimensional representations.Reproduced from (Augustyn, A , 2018)

saturation, it would appear as black, and with a very high saturation, it would appear as white (Augustyn, A , 2018).

All three of these descriptors are summarized in the Munsell colour system. The system had widespread adoption in the 20th century. Since its inception, the system has been internationally adopted, especially for specifying opaque colours of dyed or pigmented surfaces, making it indispensable for the art world (Augustyn, A , 2018). The Munsell colour system is represented in figure 2.2

Additive colour system: If one shines red light on a white wall, it will reflect off the wall and into the eyes. This will give off the impression of red colour. If one projects green light over the red light, the reflected light will appear yellow. Finally, by adding blue, the reflected light will turn white. This can all be seen in Fig. 2.3(A)

Subtractive colour system: By shining white light onto a yellow pigmented object, most of the white light would be absorbed, except yellow. The yellow wavelength

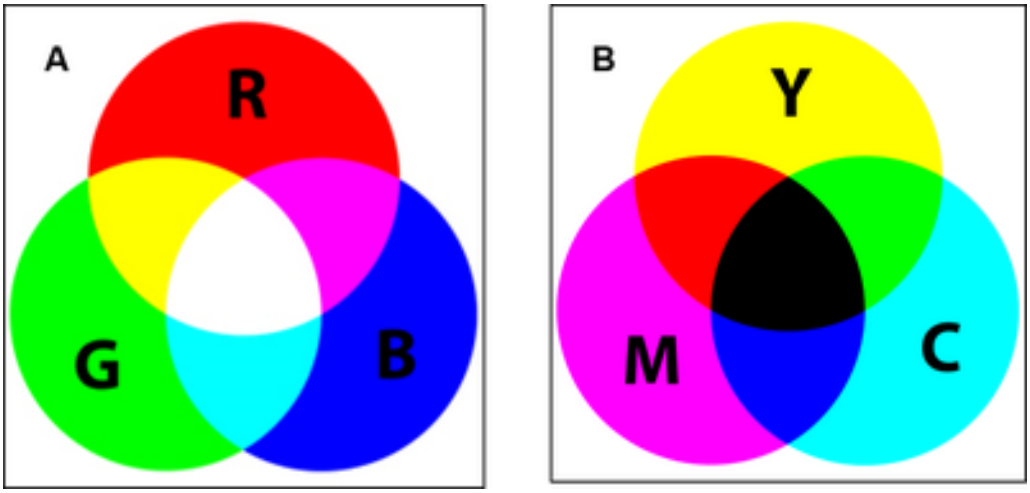

Figure 2.3: Additive colour system (A) and the subtractive colour system (B). Reproduced from Joshua Heafield (https://droso4schools.wordpress.com/l5-vision/)

would be reflected into our eyes, making the object appear yellow. If we added a magenta pigment, a greater absorption of white light would occur. Only red light would be reflected this time, making the object appear red. Now, if all the wavelengths of the white light where absorbed and no light was reflected, then the object would appear black. This can be appreciated in Fig. 2.3(B).

Colour mixing is also described by using Grassmann's Laws. These laws describe the empirical results of how the perception of different mixed coloured lights are composed of different spectral power distributions (concentration, as a function of wavelength, of any photometric quantity, such as radiant flux, illuminance, flux, etc.) (Fairchild, M, 2010).

Grassmann applied mathematical logic into colour mixture and came up with four laws in 1853. These were modernized by Wysdzecki and Stiles, and converted into the following (Hunt, R , 1968):

1) Symmetry law: If colour stimulus **A** matches stimulus **B**, then stimulus **B** matches stimulus **A**.

2) Transitivity law: If **A** matches **B** and **B** matches **C**, then **A** matches **C**.

3) Proportionality law: If **A** matches **B**, then a**A** matches a**B**, where a is a positive factor of the radiant power of the stimulus.
4) Additivity law: If **A** matches **B** and **C** matches **D**, then (**A** + **D**) matches (**B** + **C**) (applicable to additive mixtures).
These laws are fundamental components of trichromatic theory of colour vision. The laws were confirmed by Helmholtz in his colour mixing experiments, and he was able to determine multiple complementary pairs in the spectrum (Brill, M , 2016).

If we were to assume that we had two beams of light, each having a different colour, and the observer chooses (R_1,G_1,B_1) as the strength of the primaries that match the first beam, and then chooses (R_2,G_2,B_2) as the strength of the primaries that relate to the second beam, then if both light beams were combined, the matching values will then be the sum of the components. This can be written as:

$$\begin{aligned} R &= R_1 + R_2 \\ G &= G_1 + G_2 \\ B &= B_1 + B_2 \end{aligned} \tag{2.6}$$

Combining Grassmann's Laws and the spectral power distribution I(λ) into general form with RGB coordinates:

$$\begin{aligned} R &= \int_0^\infty I(\lambda)\ \bar{r}(\lambda)\, d\lambda \\ G &= \int_0^\infty I(\lambda)\ \bar{g}(\lambda)\, d\lambda \\ B &= \int_0^\infty I(\lambda)\ \bar{b}(\lambda)\, d\lambda \end{aligned} \tag{2.7}$$

These matching functions are linear in I(λ). The functions $\bar{r}(\lambda)$, $\bar{g}(\lambda)$, $\bar{b}(\lambda)$ are the

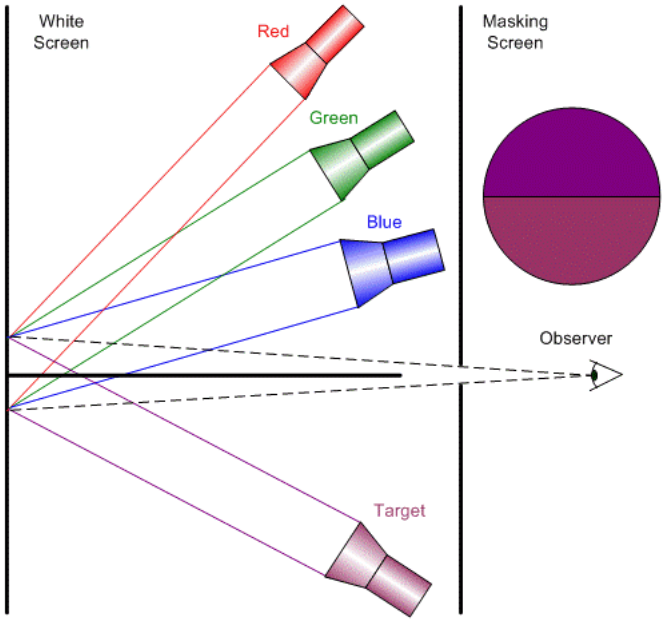

Figure 2.4: Colour Matching Experiment. With 3 primaries, you can get any combination of responses in the 3 cone types, so you can match the appearance of any test light. Reproduced from http://betterphotographytutorials.com

colour matching functions (CMFs) with respect to the red, green, and blue primaries (Schanda, J , 2007).

The RGB coordinates can then be described a colour match by the form:

$$[C] \equiv R[R] + G[G] + B[B] \tag{2.8}$$

Where [C] is the unknown stimulus, "≡" means "matches", [R],[G],[B] are the units of the matching stimuli, and R, G, B are the amounts of each light to be used in order to reach a match. This is all illustrated in the colour matching experiment, seen in figure 2.4. An observer is shown a colour on a white screen. They must then use the addition of three monochromatic lights in order to try to match the target colour.

Once the colour matching experiment is finished, the amounts of the matching stimuli needed for a match of the target colour can be determined by adding the

amounts needed to match the monochromatic components of the test stimulus. The final equation is as follows:

$$[C] = \int_{380nm}^{780nm} \bar{r}\ P(\lambda)\, d\lambda\ [R] + \int_{380nm}^{780nm} \bar{g}\ P(\lambda)\, d\lambda\ [G] + \int_{380nm}^{780nm} \bar{b}\ P(\lambda)\, d\lambda\ [B] \quad (2.9)$$

Where $P(\lambda)$ is the monochromatic test colour stimulus, $\int_{380nm}^{780nm} \bar{r}\ P(\lambda)\, d\lambda\ [R]$, $\int_{380nm}^{780nm} \bar{g}\ P(\lambda)\, d\lambda\ [G]$, and $\int_{380nm}^{780nm} \bar{b}\ P(\lambda)\, d\lambda\ [B]$ are the linear integrals of the tristimulus values. They serve as descriptors of the colour stimulus and the symbols R,G,B are used (Schanda, J , 2007).

2.3 Colour Spaces

2.3.1 Introduction to Colour Spaces

As shown with the Munsell model, it is possible to represent colours quantitatively. For the goal of colour processing, the correct mathematical representation of colour must be selected. This is possible as features in colour can be studied and processed independently, such as chroma and intensity. Different representations of colour are called colour spaces. A colour space is able to represent colours in a three dimensional coordinate system, or form a subspace of the system where every colour is represented from a unique point (Garcia-Lamont, F, 2018). These colour spaces are used for the purpose of colour representation in monitors, printers, visual arts, or other colour dependent works. All colour spaces have their own advantages and limitations. An example being the RGB colour space, which is widely used for image display on monitors, but comes short when it comes to colour processing and analysis, as intensity is not decoupled from the chromaticity (Gonzalez, R , 2009).

RGB as stated before is used for monitors and video cameras. The CMY (Cyan,

Magenta, Yellow) colour space is the standard for television broadcasting. The other colour spaces are:
HSV (Hue, Saturation, Value), HIS (Hue, Saturation, Intensity), L*a*b*, L*u*v*, YUB, and YCbCr (Garcia-Lamont, F, 2018). One can easily go between colour spaces using equations. In the following sections, a detailed description of the colour spaces, their 3D representations, and the equations related to each technique is presented.

2.3.2 RGB Colour Space

This colour space represents visible light using the spectral components of red, green, and blue, hence why it is called RGB. The model itself works by representing a certain colour via the combination of three rays of colour red, green, and blue. The intensity of the different components of colour determines both the hue and the brightness of the resulting colour. The combination of colours is based on the addition of the individual components considering as base the black colour. RGB uses the additive colour system seen in figure 2.3(A).

The three-dimensional representation of the RGB colour space is a cube. The coordinates of the unit cube correspond to the basic colours. The colours red, green, and blue make up the coordinate axis. Different colours are obtained by combining the values of the coordinate axis. All possible colours can be represented by RGB in which each of the rays can go from a value of 0 to 255, this being a subset of real numbers. This can be represented as:

$$[0, 255] \quad \subset \quad \mathbb{R} \tag{2.10}$$

These values can then be normalized to the range [0,1], from which we can get the unit cube representation shown in figure 2.5. Every possible colour can be represented by a coordinate in the cube. One can then go from this unit cube to other colour

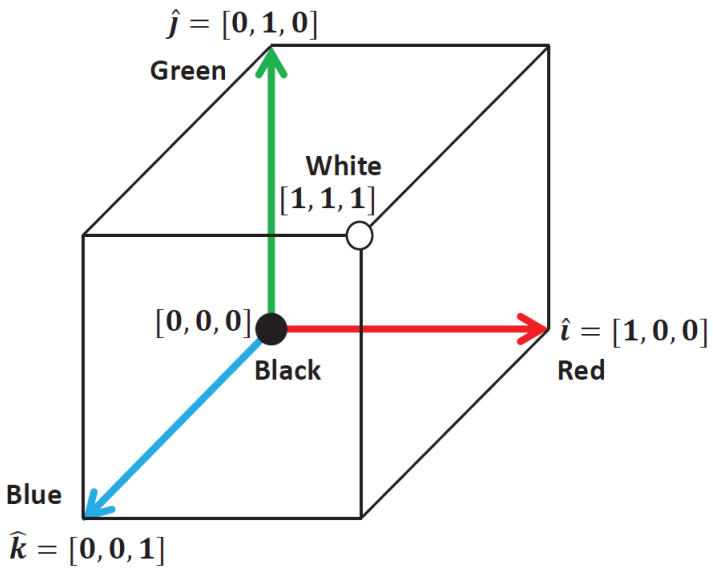

Figure 2.5: RGB space 3D representation. It is a unit cube. Reproduced from (Garcia-Lamont, F, 2018)

spaces by the use of linear transformations (Garcia-Lamont, F, 2018).

The RGB colour space is not suitable for representing and processing colours. The RGB colour space is not suitable for colour segmentation or colour processing, due to the high correlation between the components RGB. Delta E cannot be used for the RGB colour space as colour changes within the colour space are not linear.

The definition and role of Delta E will be further explored in Chapter 3, section 3. The other reason why the RGB space is not used for our purposes is that it is sensitive to illumination. In the RGB colour space, the chromaticity and the intensity are not processed separately. That is there is not an intensity channel. This sensitivity will make two colours with the same chromaticity to be recognized as different if their intensities are not the same (Garcia-Lamont, F, 2018). Figure 2.6 shows two squares with the same chromaticity (green), but with different intensities. In the RGB space, even though the difference intensity between square (a) and (b) is small, both colours would be identified as different. This makes it so many colours would be misclassified due to several colours having the same chromaticity, but a different intensity." The

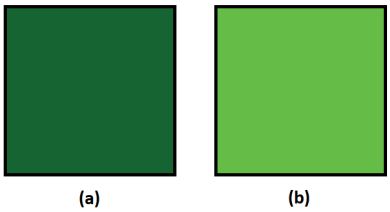

Figure 2.6: Images with the same chromaticity, Green; image (a) darker than image (b)

colour vectors of the squares (a) and (b) have the same orientation in the RGB colour space, but different magnitude.

2.3.3 HSV Space

The HSV colour space uses the components of hue, saturation, and value in order to describe the chromaticity, the light intensity, and brightness of the colour. The HSV has two important features:

1. The intensity component is separated from the hue data
2. The hue and saturation components emulate the human perception of colour

Thanks to these characteristics, the HSV space is a powerful tool used in developing image processing algorithms based on human colour perception. The 3D representation of HSV is a cone. The three parameters have the following ranges:

$$\begin{aligned} &Hue\ in\ the\ range \quad [0, 2\pi] \quad \subset \quad \mathbb{R} \\ &Saturation\ in\ the\ real\ range \quad [0, 1] \\ &Value\ in\ the\ range \quad [0, 255] \quad \subset \quad \mathbb{R} \end{aligned} \tag{2.11}$$

The radius of the cone represents the saturation, and its height is the value com-

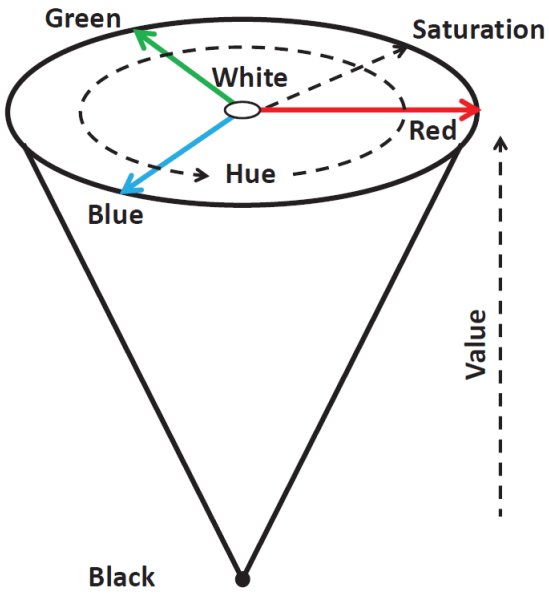

Figure 2.7: HSV colour space. It is in the shape of a cone, with the radius of the cone representing saturation, and the height of the cone being the value. Reproduced from (Garcia-Lamont, F, 2018)

ponent. This can all be summarized in figure 2.7.

A limitation of the HSV space is that the colours black, white and grey have undefined hue parameters. This is due to these colours being considered singularities within the colour space. This comes from them not having a specific chromaticity (Ito, S , 2006).

2.3.4 HSI Space

The HSI space is like the HSV colour space. Instead of value as its third component, it uses intensity. The ranges are almost the same:

$$\begin{aligned} &\textit{Hue in the range} \quad [0, 2\pi] \quad \subset \quad \mathbb{R} \\ &\textit{Saturation in the range} \quad [0, 1] \\ &\textit{Intensity in the range} \quad [0, 255] \quad \subset \quad \mathbb{R} \end{aligned} \tag{2.12}$$

The actual three-dimensional representation of HSI is a double cone, with the bases of each cone touching. The radius of the base of the cones is the saturation component, while now the height in comparison to HSV is the intensity component. HSV and HSI have the same hue and saturation components which are used to represent the desired colours. As stated, the difference is that brightness is the new parameter being used (Garcia-Lamont, F, 2018). The 3D representation can be seen in figure 2.12. HSI is mostly used for colour processing. The model was put forward by Munsell as a colour space suitable for human visual characteristics. In order to use the HSI model, we must use the conversion formula, which is the geometric derivation method (Xiong, N , 2018):

$$H = \begin{cases} \Theta & , \quad G \geq B \\ 2\pi - \theta & , \quad G < B \end{cases} \tag{2.13}$$

$$when\ \theta = \cos^{-1} \frac{(R-G)+(R-G)}{2\sqrt{(R-B)(G-B)+(R-G)^2}} \tag{2.14}$$

$$I = \frac{R+G+B}{3} \tag{2.15}$$

$$S = 1 - \frac{3\ min\ (R,G,B)}{R+G+B} = 1 - \frac{min\ (R,G,B)}{I} \tag{2.16}$$

The equation transforms from the RGB model to the HSI model. One can use the saturation and brightness information of the HSI model to get texture image segmentation. HSV and HSI fail in that they do not effectively separate colour into three value components, which would more closely represent the human perception of colour (Li, H , 2001). The XYZ colour space can then be used for the application of proper human perception of colour.

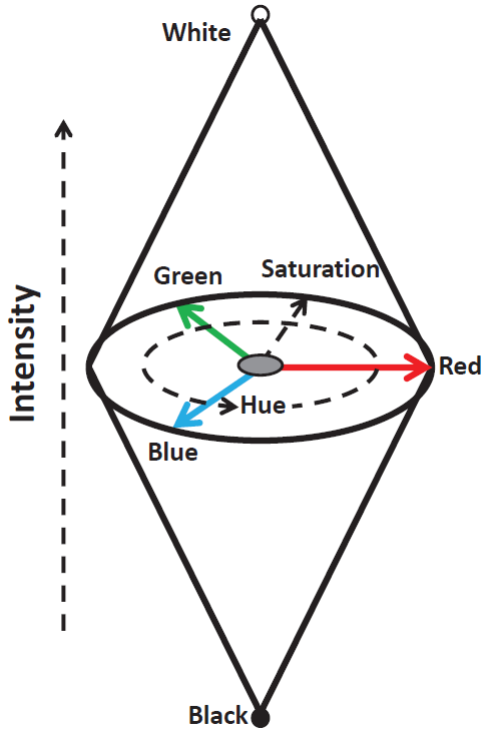

Figure 2.8: HSI colour space.The actual three-dimensional representation of HSI is a double cone, with the bases of each cone touching. The radius of the base of the cones is the saturation component, while now the height in comparison to HSV is the intensity component. Reproduced from (Garcia-Lamont, F, 2018)

2.3.5 CIE XYZ Space

The "Commission Internationale de L'Eclairage" (CIE) or as it is known in English, the International Commission of Illumination is a technical, scientific, and cultural non-profit organization that provides guidance in the application of principles and procedures in the development of international and national standards in the field of light and lightning. These include photometry, colorimetry, involving natural and man made radiation over the ultraviolet, visible, and infra red regions of the spectrum (CIE , 2020).

In 1931, CIE created a colour space in order to link the visible spectrum with the perceived colours of the human eye (Amara, M , 2018). As stated in chapter 1, the human eye has three different types of cones, each attuned to either short, middle or long wavelengths. When performing colour matching with tristimulus of RGB, one gets the colour matching functions as seen in figure 2.9. In figure 2.9 it can be appreciated that the negative parts of the curves refer to the fact that in some parts of the spectrum a colour match can be made only if one of the matching stimuli is added to the test stimulus.

The negative values make calculations unnecessarily more difficult. Therefore, CIE decided to transform the real $[R], [G], [B]$ primaries to a set of imaginary primaries $[X], [Y], [Z]$. After this, when performing colour matching functions, the results no longer give us negative results (Schanda, J , 2007).

The matrix transformation between the R,G,B and the new X,Y,Z tristimulus values is :

$$\begin{vmatrix} X \\ Y \\ Z \end{vmatrix} = \begin{vmatrix} 2.768892 & 1.751748 & 1.130160 \\ 1.000000 & 4.590700 & 0.060100 \\ 0 & 0.056508 & 0.056508 \end{vmatrix} \begin{vmatrix} R \\ G \\ B \end{vmatrix} \tag{2.17}$$

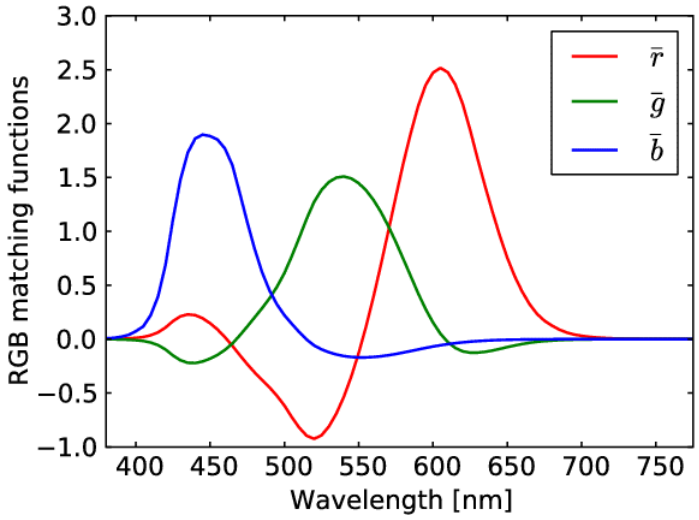

Figure 2.9: CIE 1931 2 degree color-matching functions converted to RGB weighting functions with a D65 illuminant as reference. Reproduced from (Johansen, V , 2014)

The tristimulus values have limited use as colour specifications are they correlate poorly with visual attributes. While Y relates to value, X and Z do not correlate to hue and chroma. As a result, the 1931 CIE standard observer was stablished. The commission recommended using the chromaticity coordinates xyz. These coordinates are used to form the chromaticity diagram. The notation Yxy specifies colour by identifying value (Y) and the colour as viewed in the chromaticity diagram (x,y) (Monsen, H , 2005).

2.3.6 CIE xyY Space

The colour matching functions are the tristimulus of monochromatic radiation, hence why the $\bar{x}(\lambda)$,$\bar{y}(\lambda)$,$\bar{z}(\lambda)$ functions can now be calculated from the $\bar{r}(\lambda)$,$\bar{g}(\lambda)$,$\bar{b}(\lambda)$ colour matching functions using the matrix above. The standard observer colour matching functions can be seen in the spectral sensitivity vs wavelength graph in figure 2.10. These being:

$$\bar{x}(\lambda),\ \bar{y}(\lambda),\ \bar{z}(\lambda) \tag{2.18}$$

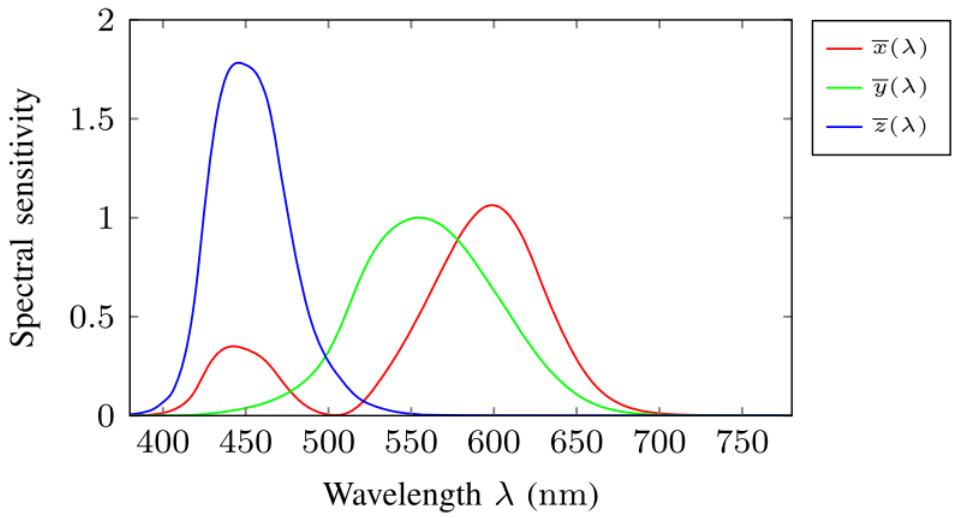

Figure 2.10: The CIE 1931 standard observer colour matching functions. Reproduced from (Amara, M , 2018)

The $\bar{x}(\lambda)$ matching function stands for the red signal (700 nm), the $\bar{y}(\lambda)$ matching function stands for the green signal (546.1 nm), and the $\bar{z}(\lambda)$ matching function represents the blue signal (435.8 nm). These values seen in figure 2.10 are needed in order to calculate the tristimulus values of X,Y, and Z by projection of the optical signal to be converted (S(λ))on the visible light spectrum of the range 380 to 780 nm(Amara, M , 2018)(Schanda, J , 2007).

The optical signal S(λ) is the reflected light (R(λ)) coming from the normalized power density spectrum (AM$_x$ (λ)) when creating a spectral sensitivity vs wavelength graph and colour space chromaticity diagram. The optical signal becomes $S(\lambda) = R(\lambda)AM_x(\lambda)$.

Then the linear integrations for (λ), $\bar{y}(\lambda)$, $\bar{z}(\lambda)$ are written as:

$$\begin{aligned} X &= W^{-1} \int_{380}^{780} \bar{x}(\lambda)\ S(\lambda)\ d\lambda \\ Y &= W^{-1} \int_{380}^{780} \bar{y}(\lambda)\ S(\lambda)\ d\lambda \\ Z &= W^{-1} \int_{380}^{780} \bar{z}(\lambda)\ S(\lambda)\ d\lambda \end{aligned} \tag{2.19}$$

and

$$W = \int_{380}^{780} \bar{y}\ AM_x(\lambda)\, d\lambda \tag{2.20}$$

Y represents the brightness of the signal. This parameter ranges between 0(no light) and 1(all visible light is reflected).

The chromaticity of a colour, which is the balance between each elementary wavelength of the signal, can be described by the parameters x and y, such as:

$$\begin{aligned} x &= \frac{X}{X+Y+Z} \\ y &= \frac{Y}{X+Y+Z} \\ z &= \frac{Z}{X+Y+Z} \end{aligned} \tag{2.21}$$

The x, y, and Y are scalars that correspond to the CIE 1931 xyY colour space, which. is represented by a chromaticity graph. This is known as the gamut or horseshoe diagram. One can describe a colour stimulus by three tristimulus values. It can be difficult to picture the stimulus if only the tristimulus is given, which most of the time are not written in absolute values. Then the chromaticity coordinates can be used instead. This is possible as $x+y+z=1$, which makes it enough to describe the chromaticity with just two numbers, normally being x and y. One must remember,

that if one is to use x, and y as the coordinates for the diagram, Y must be quoted as well. The final CIE chromaticity xyY diagram, otherwise known as the horseshoe diagram, can be seen in figure 2.11.

All colours visible to the average human eye are within the horseshoe diagram. The edge of the diagram, called the spectral locus, represents pure monochromatic light measured by wavelength in nanometres. The monochromatic light is the most saturated colour. The least saturated colours are located at the center, spreading from white. The colours along any line between two points in the graph can be made by mixing the colours at the end point. For example, if one was to mix green $(0.7, 0.2)$ and red $(0.3, 0.65)$, one would get yellow $(0.5, 0.5)$.

2.4 CIE 1964 Transformation

The goal of the thesis is to test out the feasibility of using a solar cell as absolute colour sensor. The basis of the experiment is that the photovoltaic cell will absorb the light that reflects off an object when a light is shined on an object. Once the light is absorbed by the PV cell, a current will be measured for the specific wavelength. These measurements are used to find the spectral response on the individual solar cell.

The spectral response is necessary for identifying if it can distinguish colours when illuminated by monochromatic light, as well as broad light sources. Achieving this would allow for empirically detecting the colour of a beam of light or object. As stated in the previous chapter, colour communication is imperative, and as such, choosing the correct colour space was necessary.

For this experiment we choose the CIE xyY 1964 trichromatic system, as the CIE

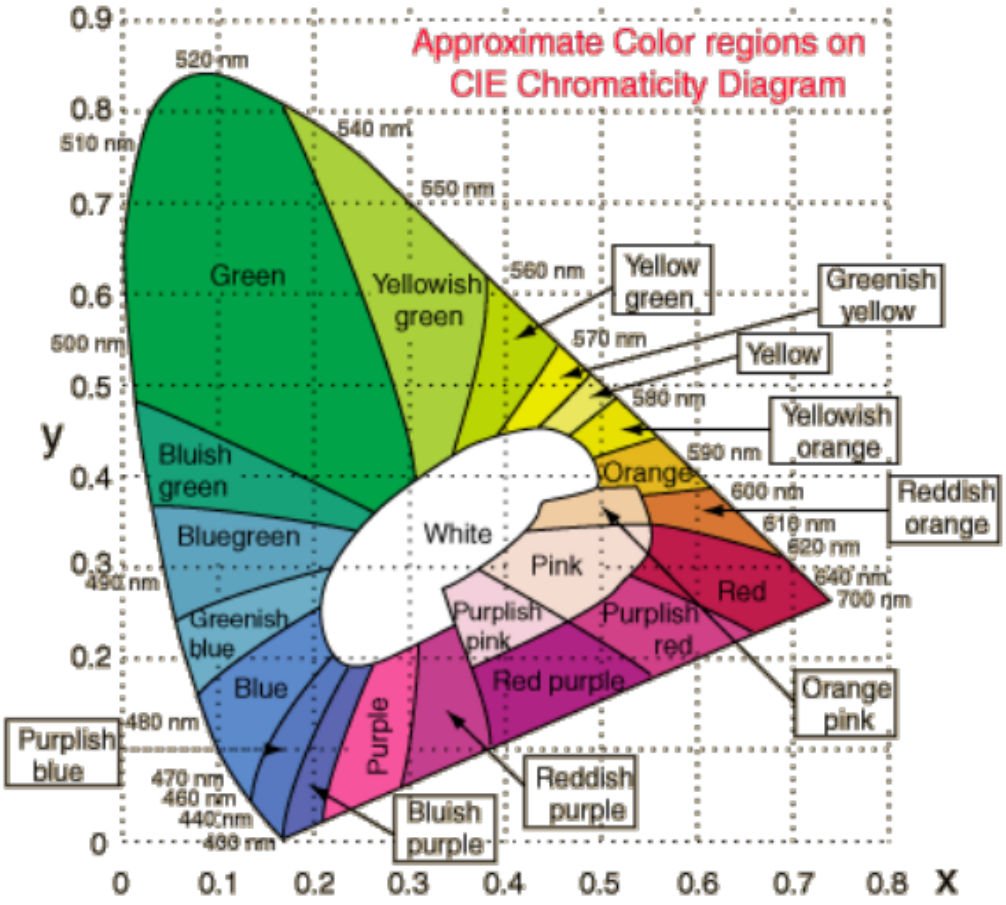

Figure 2.11: CIE 1931 xyY chromaticity graph. Reproduced from http://hyperphysics.phy-astr.gsu.edu/hbase/vision/cie.html

1931 colour space is only recommended for small stimuli, of about 1 degree -4 degrees size. For a larger stimulus, the 1964 system standardized a larger field colorimetric system. It was based on the observations conducted on a 10 degree visual field. This new field represents a diameter of about 90 mm at a viewing distance of 0.5 m (Schanda, J , 2007).

The colour matching functions (CMFs) of the 10 degree system are differentiated from the 2 degrees system by a 10 in the subscript. The standard CMFs values range from 360 nm to 830 nm at 1 nm intervals with six significant figures. The CIE recommendation states "In the case where more coarsely sample data will produce no significant calculation error selected values taken from the standard at 5 nm intervals, rounded to six significant decimals places... will be sufficient. For values between the 1 nm intervals, linear interpolation should be used (Weiss, GR , 1982)."

The tristimulus values are calculated by the following linear interpolations:

$$\begin{aligned} X_{10} &= k_{10} \int_{380nm}^{730nm} \phi(\lambda)\ \bar{x}(\lambda)\, d\lambda \\ Y_{10} &= k_{10} \int_{380nm}^{730nm} \phi(\lambda)\ \bar{y}(\lambda)\, d\lambda \\ Z_{10} &= k_{10} \int_{380nm}^{730nm} \phi(\lambda)\ \bar{z}(\lambda)\, d\lambda \end{aligned} \tag{2.22}$$

The k_{10} in the tristimulus values of self-luminous objects for the 10 degrees observer is 683.6 Lumens per Watt (lm/W).
In the case of non-self-luminous objects, the k_{10} value will be defined by:

$$k_{10} = \frac{100}{\sum S(\lambda)\ \bar{y}_{10}(\lambda)\, d\lambda} \tag{2.23}$$

The chromaticity coordinates for the 10 degrees observer is:

$$
\begin{aligned}
x_{10} &= \frac{X_{10}}{X_{10} + Y_{10} + Z_{10}} \\
y_{10} &= \frac{Y_{10}}{X_{10} + Y_{10} + Z_{10}} \\
z_{10} &= \frac{Z_{10}}{X_{10} + Y_{10} + Z_{10}}
\end{aligned}
\tag{2.24}
$$

2.5 From electrical signal to colour space representation

With a solid understanding of light, colour, colour spaces, and especially the CIE xyY colour space, we can finally broach the connection between solar cells and colour detection. The experiment consists of applying a sweeping voltage on solar cells as they are shined on by monochromatic light. Shining monochromatic light on a solar cell allows the cell to create electron-holes pairs which create a specific current related to the wavelength of the monochromatic light coming from a monochromator.

The current of the solar cell is recorded by a precision source / measuring unit. The multiple current vs wavelength graphs are then linearly transformed into tristimulus signals, $\bar{r}(\lambda)$, $\bar{g}(\lambda)$, $\bar{b}(\lambda)$ by a computer program. The colour matching functions are then transformed from real functions into xyY by a matrix

To test the viability of the results, the xyY chromaticity graphs of each of the tested solar cells is then compared to the actual human eye colour matching response in the form of a horseshoe diagram. In the next chapter, we will describe the experimental setup, equipment and software used. We will then present the data analysis and error analyses. Further improvements on the experiments, obtained by using literature

results and combining it with our experimental results, will also be introduced.

3. CHAPTER 3 - EXPERIMENTAL

3.1 Methodology

The first challenge of this project is represented by the need to establish a bridge between the CIE colour space and the spectral responses gathered from the selected solar cells. In our experiment, the spectral responses for each solar cell was gathered while applying different voltages ranging from -5 to +5 volts. This was done in order to ascertain any unique behavior responses of the solar cells. For example, if different voltages were applied to a solar cell, and its overall SR was a non-fluctuating horizontal line, then that would mean that the cell has an overall high efficiency in terms of energy creation and high energy conversion efficiency.

For normal applications of solar cells, no difference due to voltage or wavelength applied on the cell is what researchers are looking for. No fluctuations and high efficiencies lead to the greatest number of electron-hole pairs on the cells, the normal goal of a functioning solar cell. In the case of our research, we want the absolute opposite of these "positive" traits. For a solar cell to be an acceptable candidate for a colour sensor, it then must have unique and different trends in its spectral response due to specific wavelengths striking its surface and to the different applied biases.

If a solar cell gave out a distinct current response at a particular wavelength and voltage, that could be recorded and classified as a colour with specific colour match-

ing functions in the CIE xyY colour space. Different colours could then be catalogued with inimitable currents so that either a data base can be created, or the response could be converted into an RGB signal.

Having established a clear goal for the experiment, an experimental setup was arranged, gathering of equipment was conducted, the experiment was carried, data for each solar cell was accumulated, interpolation of the spectral responses into xyY colour space, analysis of the results into meaningful conclusion and dive future steps were completed.

3.2 Experimental Setup and Procedure

The experiment was first conducted using a hydrogenated amorphous silicon (a-Si:H) solar cell. The solar cell structure can be appreciated in figure 3.1. The structure begins with the silver front end contacts, beneath them the Indium Tin Oxide (ITO) layer, after that the positively doped layer, the intrinsic a-Si:H layer, then the negatively doped crystalline silicon (c-Si) layer, which makes up a large bulk of the cell, once again an intrinsic layer, a negatively doped a-Si:H layer, ITO, and finally the back-end silver contacts. The arrows in the figure represent the direction of incoming light.

A solar simulator and precision source / measuring unit were used in order to gather the spectral response of the cell over 400 to 800 nm while being applied a voltage. The spectral response of the a-Si:H can be seen in figure 3.2. The response has a directly proportionate correlation with the voltage bias, which can be summarized as: the greater the voltage, the greater the spectral response. When +6V is applied on

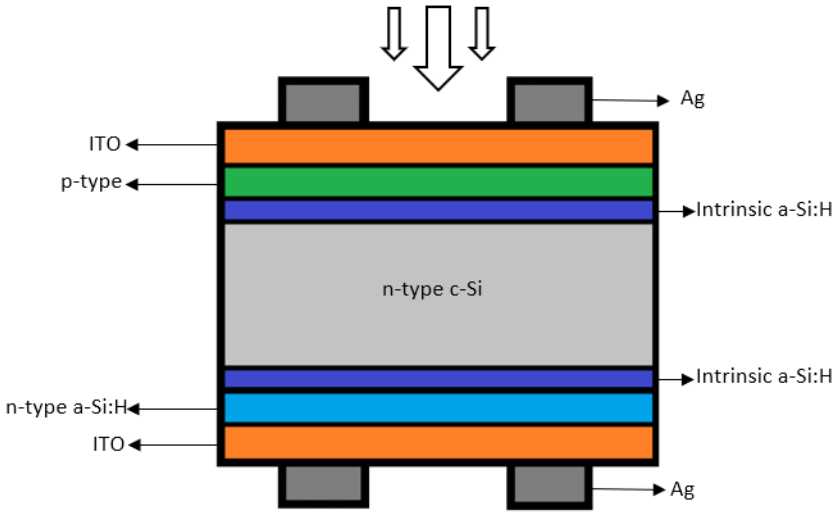

Figure 3.1: Structure of a heterojunction a-Si:H solar cell. The arrows indicate incident light.

the cell, a maximum peak response of 0.12 A/W can be seen, while at -6V, a minimal SR of -0.02 A/W is observed. Both peaks are located around the 600 nm region of the visible spectrum, making it apparent that an a-Si:H has a greater response to wavelength for 600 $\pm$ 50 nm region. After 700 nm, it has close to no difference in the SR when variable voltages bias is applied. Below 500 nm, a varying SR can be seen, yet it is not as great as at the peak of 600nm. All these results make it so that the a-Si:H is the most sensitive to wavelengths from $500 - 700 \pm 50$ nm. Anything outside that range will not give distinct enough responses.

In figure 3.2 one can see that the spectral response not only has a different pattern for each wavelength being shined on the cell, but also that the voltage helps with creating more distinct responses. This preliminary result set the parameters for which the consequent experiments were based and improved upon.

The goal of the experiment is finding other low cost, commercially available solar

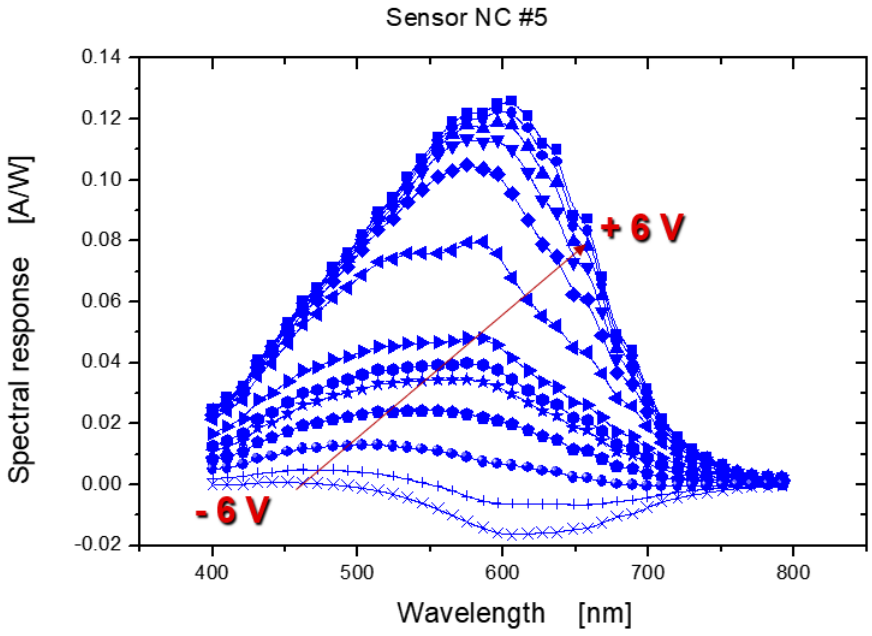

Figure 3.2: Spectral response vs wavelength of a-Si:H.

cells, which will have the desired colour response under variable voltage bias. The data ranging from -6 to 6 V and from 400 to 700 nm of the a-Si:H was linearly interpolated using equation 2.22. This allows for the spectral response to be divided into three colour matching functions, X_{10} Y_{10} Z_{10} using the 1964 CIE colour space guidelines.

The optical signal is converted into the X, Y, and Z. This transformation can be appreciated in figure 3.3. Figure 3.3 can then be compared to figure 2.10 which is the colour matching functions for colour perception of the human eye. A stark difference between the images is the pronounced number of oscillations of each CMF. These oscillations will keep the final colour space from looking like figure 2.10.

Figure 3.4 represents the colour perception of the a-Si:H solar cell in the CIE 1964 colour space. The white (horseshoe shaped) outline is what the human eye can see in terms of visible light. The cell response, when represented in the colour space has

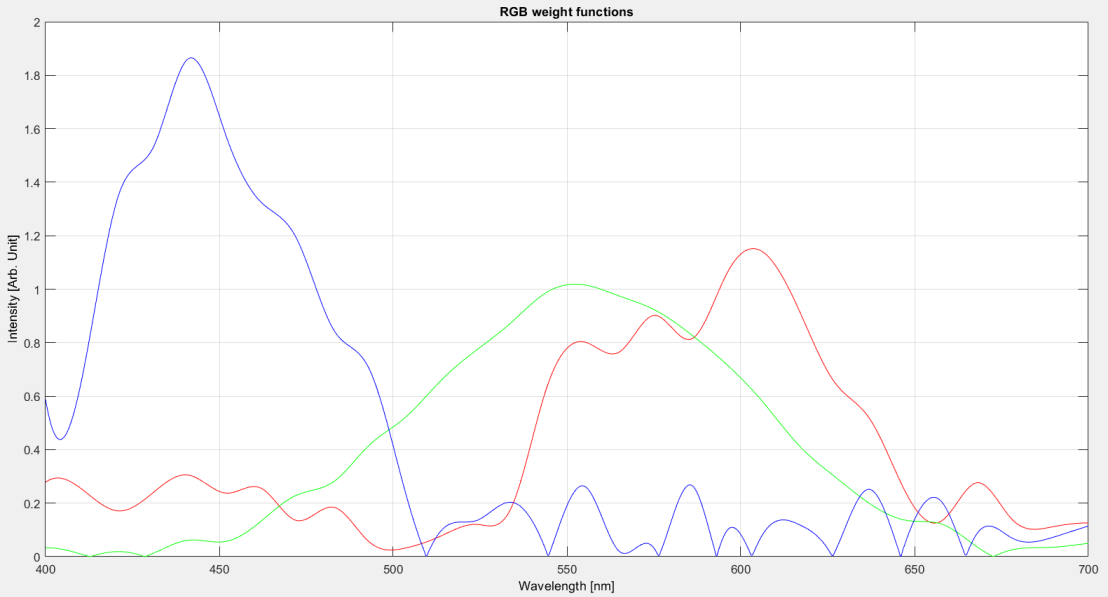

Figure 3.3: a-Si:H -6 to +6 V RGB weight functions.

multiple overlapping folds.

These account for metamers. The metamers will make it so multiple colours collapse upon the same coordinate. The folding and multiple points within the same area could be due to the number of oscillations within figure 3.3. Another feature observed in the graph is the signal being represented outside of the horseshoe diagram, this leads to "impossible colours", which negatively affects the cell's ability to correctly represent the visible spectrum in the CIE colour space.

The "impossible colours" or overall deformation of the horseshoe diagram can be attributed to excess data of the colour matching functions. The perfect CMFs have very smooth responses and a very clear cut off data for the blue, red and green responses. Any alterations to these signals, as seen with the CMF of the a-Si:H solar cell result in an imperfect horseshoe diagram. Great parts of the green, blue and red regions are visible, but a mathematical and empirical way of discerning the colour matching capability of the cell is needed. For that, a Delta E value is used as described

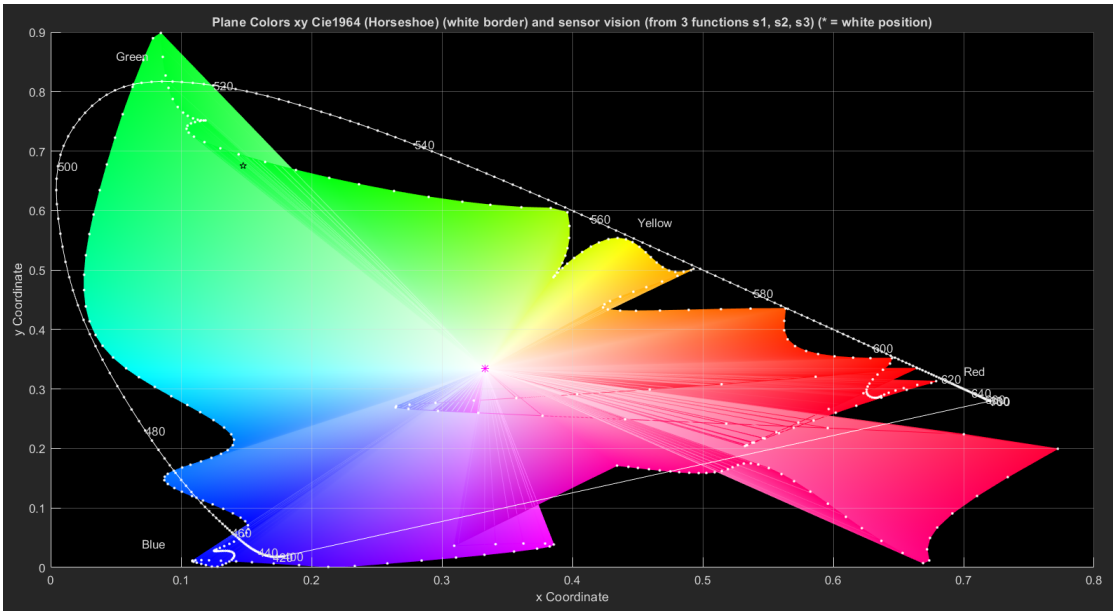

Figure 3.4: a-Si:H -6 V to +6 V xyY colour space

in Delta E section. These linear interpolations were achieved using a written code on Matlab (See Appendix). The code was written by collaborator Massimo Rovere. In the next section, we shall go over the code used found on each appendix.

3.3 Matlab Code

All of the code, and necessary documentation can be found on the google drive link: https://drive.google.com/file/d/1pThGODjUFLTVdGt7nZq_xApSosG39w8f /view?usp=sharing and in Appendices A, B, and C. The following sections illustrate the function of the codes illustrated in the appendices.

3.3.1 Appendix A

The data weights for the r, g, and b are first loaded by using the CIE xyz 64. We then introduce into the program the current vs wavelength responses of each solar cell at specific voltages, from -5V to 5V. With our experimental data in the program, we set the boundaries in our linear interpolation from 400 to 700 nm. After, we use "interp1" to return interpolated values of a 1-D function at specific points using linear interpolation. Vector "x"c contains the sample points (which are the data weights for the r, g, b), and v contains the corresponding values. We use the "spline function" to return a vector of the interpolated values.

We then multiply our interpolated values corresponding to the query points in lambda. Each individual interpolation is then multiplied by the observable structure matrix. We then set "vi" to either "ri", "gi", or bi in for the purpose of fitting the solar cell output into each of the colour matching functions.

The output of the overall code are the coefficients to be used in the linear interpolation, and the x, y and z CMF of the individual solar cell. In the end, we will have from Appendix A the ascii files of the individual colour fit of the current vs wavelength data of the individual solar cells.

3.3.2 Appendix B

In Appendix B, we utilize the three ascii files obtained from Appendix A for an individual solar cell. Each of the ascii files is either the "red", "green" or "blue" response of the solar cell. At the start of Appendix B, the program parameters are set as lambda going from 400 nm to 700 nm. We then load the data weights r, g, b from CIE xyz 64. After, we load the "red", "green", and "blue" CMF of the cell.

This is followed by data interpolation. After, we vector normalize the data weight r, g, b and the CMFs. Then the lambda is introduced into the interpolation. With the interpolations and the correct lambda parameters, it is possible now to plot the combination of the CMFs of the solar cell in the chromaticity diagram, and to then create the outline of the visible spectrum as the boundary of the horseshoe diagram.

We can then change the bandwidth of the virtual source of light, and its location in the visible spectrum. Another output of the code is the colour coordinate with respect to the axis with the origin in white.

3.3.3 Appendix C

Using the colour coordinates with respect of the axis with the origin of white in the horseshoe diagram, we can compare the colour coordinates of a certain colour in the average human response to that of the individual solar cell.

We compare these two-colour coordinates in the L*ab colour space. In the code in Appendix C, we input the xyY coordinates for the solar cell response, and that of the average human colour response. We transform the xyY coordinates into the L*ab colour space using a combination of if statements and specific equations. Once the L*ab transformation has been achieved, we put these coordinates into the Delta E equation. This in the end gives us the Euclidean distance between the two colour coordinates.

3.4 Delta E

The empirical way to know how different the color response of our sensor to the human eye is by calculating the Delta E (Euclidian distance) value. It is a standard

measurement, created by CIE in 1976 in order to address the topic of colour differentiation (CIE , 2020).

Delta E should be used as a helpful metric in order to gauge the difference between two colours. It is defined as the difference between two colours in a L*a*b colour space. The smaller the number, the less noticeable the difference between the two colours in question will be. The main shortcoming of Delta E 1976 is its low accuracy when saturation is at play. It should still be used for its major advantage of being a simple Euclidean distance calculation, which is much faster than other CIE formulas. For performance intensive situations, where simple metrics are required, this method excels. When more in depth and highly accurate recollection of Delta E are required, Delta E 94, or Delta E 2000 should be used. Table 3.1 lists the ranges of Delta E and their meanings (CIE , 2020):

Table 3.1: Meaning of Delta E.

Delta E Value	**Meaning**
0-1	No difference to the human eye
1-2	Very small difference. It is only differentiable to a trained expert
2-10	Perceptible difference at a glance
11-49	Colours are more similar than opposite
100	Colours are exactly the opposite

Figure 3.5 shows different pairs of green shades with each colour RGB values listed at the top of the squares, and the ΔE centered at the bottom of each pair. As it can be seen, The smaller the ΔE, the less pronounced the chromaticity difference between the colors. Once we have a ΔE value higher than 3, it becomes very easy to differentiate between the colored pairs. The ΔE values shown in figure 3.5 range all the way from less than 1 to 45. The figure further illustrates the importance of achieving a low ΔE.

Figure 3.5: Different pairs of shades of green are shown next to each other. Each pair have their RGB values listed at the top of the corresponding shade. A ΔE value is centered at the bottom of each pair. Reproduced from Monovektor. http://monovektor.com/2011/07/colorcolorcolorcolorcolor/

All Delta E values were initially tested at a FWHM of 15 nm at different peaks to represent 8 different colours that are easily recognizable. These colours being violet, blue, cyan, green, yellow, orange, blood orange, and red. We then compare the known locations and xyY values of the known human eye response to these colours to the xyY values we get from the individual solar cells. The smaller the ΔE value between the known human response and the solar cell, the more accurate the solar cells will be as a colour sensor.

To calculate Delta E, one must go from the xyY colour space into the XYZ colour space, and finally into the L*ab colour space. The calculations to transform from xyY to XYZ are as follows (Lindbloom, B, 2017) :

Given an (x, y, Y) colour whose Y component is in the nominal range [0,1]

$$\begin{aligned} X &= \frac{xY}{y} \\ Y &= Y \\ Z &= \frac{(1-x-y)Y}{y} \end{aligned} \tag{3.1}$$

If y=0,then set X=Y=Z=0. To convert from XYZ to L*ab, the following equations are required (Lindbloom, B, 2017):

$$\begin{aligned} L &= 116 f_y - 16 \\ a &= 500(f_x - f_y) \\ b &= 200(f_y - f_z) \end{aligned} \tag{3.2}$$

Where

$$f_x = \begin{cases} \sqrt[3]{x_r} & x_r > \epsilon \\ \frac{kx_r+16}{116} & \text{otherwise} \end{cases} \tag{3.3}$$

$$f_y = \begin{cases} \sqrt[3]{y_r} & y_r > \epsilon \\ \frac{ky_r+16}{116} & \text{otherwise} \end{cases} \tag{3.4}$$

$$f_z = \begin{cases} \sqrt[3]{z_r} & z_r > \epsilon \\ \frac{kz_r+16}{116} & \text{otherwise} \end{cases} \tag{3.5}$$

$$\begin{aligned} x_r &= \frac{X}{X_r} \\ y_r &= \frac{Y}{Y_r} \\ z_r &= \frac{Z}{Z_r} \end{aligned} \tag{3.6}$$

X,Y,Z describes the colour stimulus considered and X_r, Y_r,Z_r describe a specific white achromatic reference illuminant. For CIE 1931, the reference white = Y = 100. For Standard Illuminant D65:

$$\begin{aligned} X_r &= 95.0489 \\ Y_r &= 100 \\ Z_r &= 108.8840 \end{aligned} \tag{3.7}$$

For illuminant D50:

$$\begin{aligned} X_r &= 96.4212 \\ Y_r &= 100 \\ Z_r &= 82.5188 \end{aligned} \tag{3.8}$$

Values for ϵ and κ:

$$\begin{aligned} \epsilon &= 0.008856 \\ k &= 903.3 \end{aligned} \tag{3.9}$$

The equation for Delta E (CIE 1976) is as follows (Lindbloom, B, 2017): The colour difference, or ΔE, between two colours (L_1,a_1,b_1) and (L_2,a_2,b_2) is:

$$\Delta E = \sqrt{(L_1 - L_2)^2 + (a_1 - a_2)^2 + (b_1 - b_2)^2} \tag{3.10}$$

Using the equations above, Table 3.2 was achieved. In it, the Delta E of a-Si:H at 15 nm Light Source was calculated at different wavelength intervals. The highest Delta E value calculated was 53.53, while the lowest being 19.24. On average the

Delta E of the hydrogenated amorphous silicon when a source (almost monochromatic) is shined on our sensor, is 37.8. A Delta E about 30 or above is not acceptable for colour matching functions, as for a correct colour matching, the Delta E should be between 0-10, the closer to zero the better. Another representation of the Delta E of a-Si:H at 15 nm Light Source can be seen in figure 3.6.

Given the Delta E results, it can be concluded that an a-Si:H solar cell by itself could not be used as a colour sensor. The theory behind the experiment is sound, and a solar cell that has a specific spectral response to different wavelengths in the visible spectrum should be found. In the next section the experimental setup will be explained. The equipment used will be highlighted, as well as the quick response data acquired during the first phase of experimental setup and test.

Table 3.2: Delta E of a-Si:H at 15 nm Light Source.

Wavelength (nm)	**Delta E Values**
400	5.35E+01
450	1.92E+01
490	3.08E+01
520	2.26E+01
560	4.84E+01
590	5.26E+01
635	3.17E+01
700	4.33E+01
AVG	3.78E+01

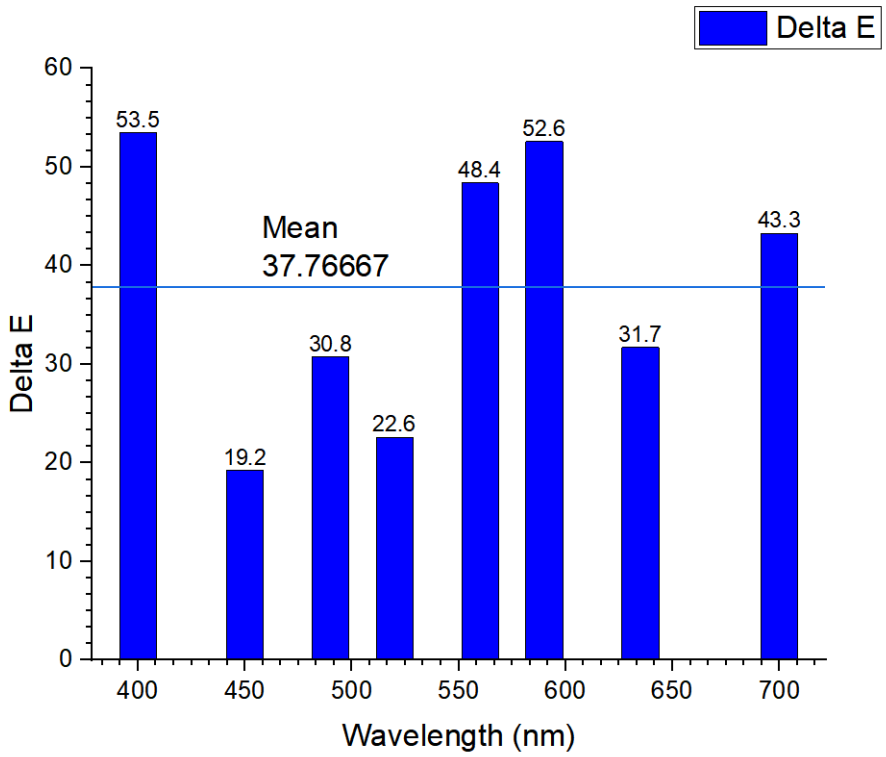

Figure 3.6: Delta E vs Wavelength of a-Si:H at 15 nm Light Source. With a maximum Delta E of 53.53, and a minimum of 19.24

3.5 Equipment

The purpose of this experiment was to measure the wavelength response of a solar cell in association with variations in the current response at different bias with a unique wavelength. If achieved, that would mean the solar cell would create a unique current response to a specific wavelength when applying a voltage bias to the cell. At this point, it was unknown which parameters for which solar cell would yield the best result, hence why different cells were tested under the same experimental conditions in order to determine an optimal current response.

In this study, multiple commercially available lab ready solar cells were purchased and tested for the purpose of confirming their validity as colour sensors. These cells are all illustrated in figure 3.7. The solar cells are as follow:

- Polycrystalline solar cell purchased from Velleman SOL1N
- Amorphous silicon solar cell purchased from Panasonic – BSG AM-145CA
- Dye sensitized solar cell from Solaronix
- Perovskite solar cell from Solaronix

3.5.1 Solar Cell Specifications:

SOL1N Specifications

Polycrystalline

Manufacturer: Velleman

Maximum Power Point (Pm): 0.20 W

Voltage Open circuit (V_{oc}): 0.60 V

Current Open circuit (I_{sc}): 0.44 A

Max Power Volts (V_m): 0.50 V

Max Power Current (I_m): 0.40 A

Connection: Leads

Cable length: 20 cm

Dimensions: 45 × 40 × 2 mm

AM-1456CA Specifications

Amorphous Silicon

Manufacturer: Panasonic – BSG

Power Max Pm: 7.95 μW

Maximum Power Point Current: 5.3 μA

Maximum Power Point Voltage: 1.5 V

Open circuit Voltage Voc: 2.4 V

Short circuit Current: 6 μA

Connection: Leads

Dimensions: 25.00 × 10.00 × 1.10 mm

DSSC Solaronix Specifications

Dye sensitized solar cell

Manufacturer: Solaronix

Dimensions 40 × 40 mm

Aperture 8 × 8 mm

Perovskite Solaronix Solar Cell

Perovskite cell

Manufacturer: Solaronix

Electrode size: 20 × 20 mm

Active area: 6 × 6 mm

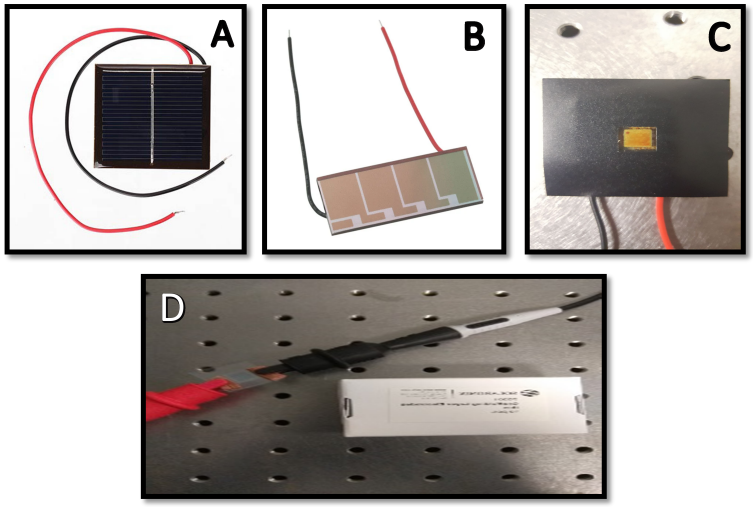

Figure 3.7: SOL1N Polycrystalline Silicon Solar Cell from Velleman (A), Amorphous Silicon Solar Cell (A-Si Solar Cell) from Panasonic(B), Dye Sensitized Solar Cell (DSSC) Solaronix (C), Perovskite Solar Cell from Solaronix (D).

Etched FTO Electrodes, allowing for any sort of build-up.

Blocking Layer Titania Electrodes (etched FTO plus a titania blocking layer

Scaffolding Titania Electrodes (etched FTO, blocking layer, plus a 500 nm thick mesoporous layer)

After the solar cells were acquired and prepped with the appropriate contacts, a solar simulator, a monochromator, a flexible liquid light guide, and a precision source/ measuring unit were used in an optical bench for the purpose of the experiment. An illustration of the equipment used for the experiment can be appreciated in figure 3.8. The experiment was conducted in the dark, with the Solar simulator and monochromator providing the necessary monochromatic illumination. The list and description of each equipment is detailed below:

3.5.2 Equipment and Instruments

150-300W Air Mass 16S-Series Solar Simulators: Solar Light Company's 16S-Series Solar Simulators produce Class A Air Mass 0 and Air Mass 1.5 Emission

Spectra to accurately replicate full spectrum sunlight, with 1 sun output intensity. They can be quickly and easily configured by the user to provide UVA only, UVB only, UVA+B, Visible Only, or custom spectra.

Light guide UV-Visible 2 meters: The standard light guide is designed specifically to transmit large amounts of radiation in the Ultra-Violet and Visible regions. The output end of the light guide is designed for a snug fitting focusing optics piece, called the focusing lens. The focusing lens can slide in and out of the light guide. This enables the optical beam to be sharply focused to a spot. A liquid light guide is an alternative to a light guide made of silica or glass fiber bundle. They provide excellent light transmission and are highly flexible. The liquid light transmitting media results in a higher uniformity and optical transmission in comparison to traditional waveguides.

Digital Monochromator, 200 – 800 nm: The Digital Mini-Chrom (DMC) is a manually operated monochromator that utilizes a digital counter for wavelength selection. Rotation of the dial causes, via a precision lead screw/ sine bar mechanism, rotation of the diffraction grating which positions the selected wavelength at the exit slit. The resolution with the 300 μ slits is 2.18 nm. Wavelength reproducibility is $\pm$ 0.15 %. The wavelength readability is 0.2 nm, and the wavelength accuracy is $\pm$ 0.2 % of λ.

The Keysight B2901A Precision Source / Measure Unit (SMU): The Keysight B2901A Precision Source / Measure Unit (SMU) is a 1-channel, compact and cost-effective bench-top SMU with the capability to source and measure both voltage and current. It is versatile to perform I/V (current vs. voltage) measurement easily with high accuracy. Integration of 4 quadrant source and measurement capabilities

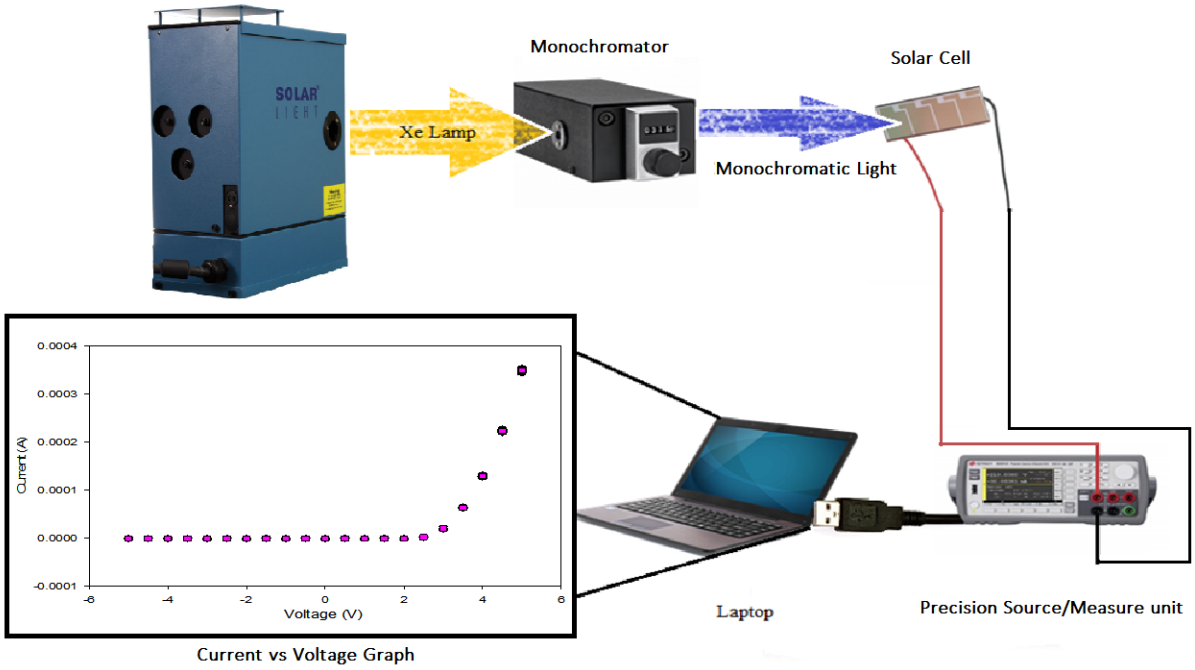

Figure 3.8: Schematic of the equipment and preliminary results of IV characteristic of the solar cells under specific illumination.

enables I/V measurement simply and easily without configuring multiple instruments.

Keysight B2900A Quick IV Measurement Software: The Keysight B2900A series includes PC-based Keysight B2900A Quick I/V Measurement Software. This powerful software makes it easy to quickly setup and perform I/V measurements and to display the measurement data in a table or graph without the need to perform any programming. The software allows one to control up to four SMU channels over a GPIB or LAN connection, or one B2900A series unit via a USB connection.

The equipment was assembled on top of an optical bench. For the experiment, a controlled illumination source was required. An AM 1.5 solar simulator was chosen. The 150-300 W Air Mass 16S-Series Solar simulator was used for its ability to accurately replicate the full spectrum of sunlight, with a 1 sun output intensity.

The solar cells were placed on a 1.0 m magnetic bench. A monochromator was placed between the cells and a solar simulator. An optical waveguide of 2.0 m in length was attached between the solar simulator and monochromator as to guide the light from one opening to the other with minimal losses.

The monochromator allowed for an easily reproducible and mechanically selected narrow band of wavelength of light as an input on the tested solar cells. The white light was manipulated into the visible spectrum in order to illuminate the solar cell with light from 400 to 800 nanometres (nm). The first wavelength used was 400 nm, and that reading was increased by 5 nm every time a new reading was necessary until a reading of 800 nm was reached. The experiment could have been done by increasing by 1 nm increment, but it was found that a 5 nm increase would still give the same overall response, so it was used as the step function. The increments of wavelengths were manually operated, so finding an efficient step function was imperative. If the experiment was to be repeated with a digitally operated monochromator, then it would be recommended that every wavelength be tested in order to get an even more precise reading at a possible faster measuring time.

When using the solar simulator, the illumination at different distances away from the monochromator was tested to see if enough light was present at a greater distance. For the graph at 8 cm, the new peak was found at 6.5 lux, as seen in figure 3.9. For the rest of the experiments, the solar cell was placed at exactly 8 cm away from the solar cell, as at that distance, the output from the monochromator illuminated the whole surface area of the cell and retained high illumination. The higher illumination and surface coverage a solar cell have, the more efficient its output current will be.

Once the distance at which the solar cells should be placed to get full coverage was determined, data gathering commenced for the current created by the individual

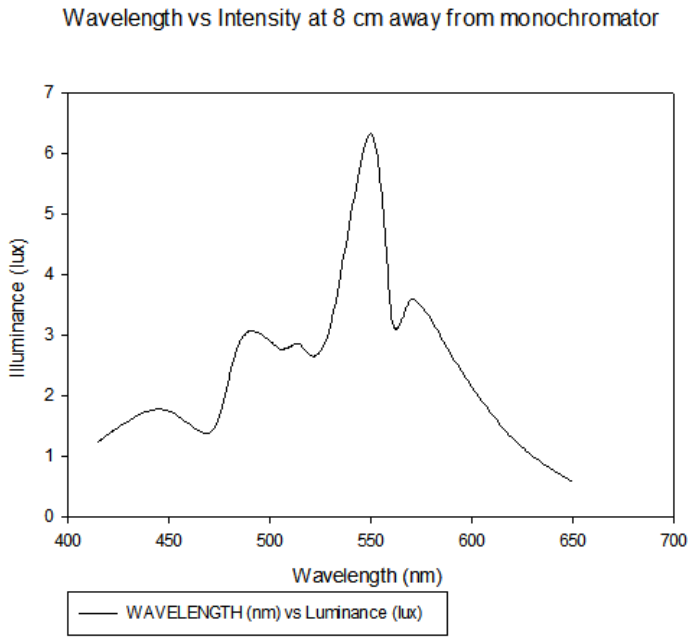

Figure 3.9: Illumination of a solar cell at 8 cm away from the monochromator.

wavelengths. A Keysight B2901A was used as the interface between the cells and the laptop in which the data was stored. The Keysight B2901A is a precision source/measuring unit, allowed for voltages to be applied, which ramped up from -5 Volts to 5 V. This step up was done with 5000 steps in between.

The data fed into Origin Pro and Sigma Plot 14 allowed for the analysis of the current vs voltage, and current response vs wavelength of the solar cells. The different graphical results are shown in figure 3.10, and figure 3.11.

Figure 3.10, shows the different voltage bias represented as different colours. The graph depicts +5V as the set of data at the top of the graph, and -5V as the lower set of data. The same pattern is being repeated for each set of data, the only difference being the voltage being applied to the solar cell. The relationship that can be obtained from the graph is proportional, as in that in an amorphous silicon cell, the

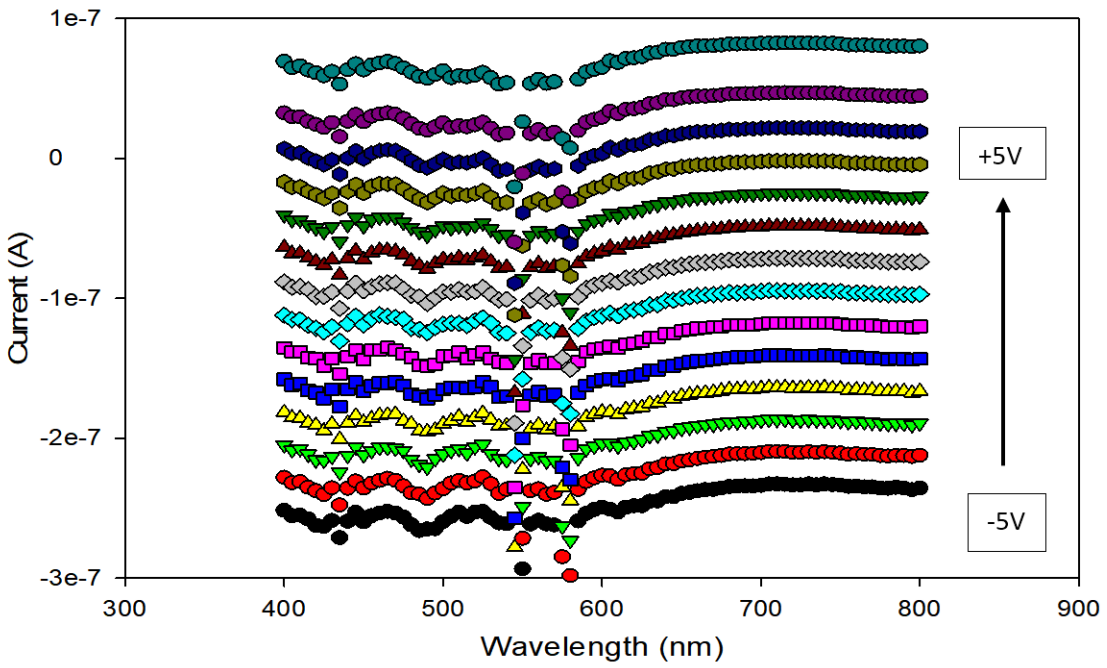

Figure 3.10: The Current vs Wavelength of A-Si AM1456Ca solar cell. The solar cell has a bias from -5 to +5 V.

lower the voltage, the smaller the current response of the cell. This comes without an overall change to the pattern for different voltages being applied.

Figure 3.10 puts into view that the overall pattern on the current vs wavelength graph for A-Si is simply repeated at lower currents. This produces figure 3.11., the current vs voltage graph of A-Si. In the graph, there are multiple sets of data being shown, but every single one of the data sets sits on top of each other. This produces a I-V graph that has no distinct and unique readings for the specific wavelengths. Therefore, the A-Si solar cell may not be the best suited for colour recognition, but it gives a repeatable maximum current output at different wavelengths, which is ideal for a photovoltaic cell when maximum power creation is the only goal.

The next step is to further analyse the current response from each of the solar cells and transform those responses into colour matching functions that can then be made into a three-dimensional colour space. That 3D colours space is then sliced and we

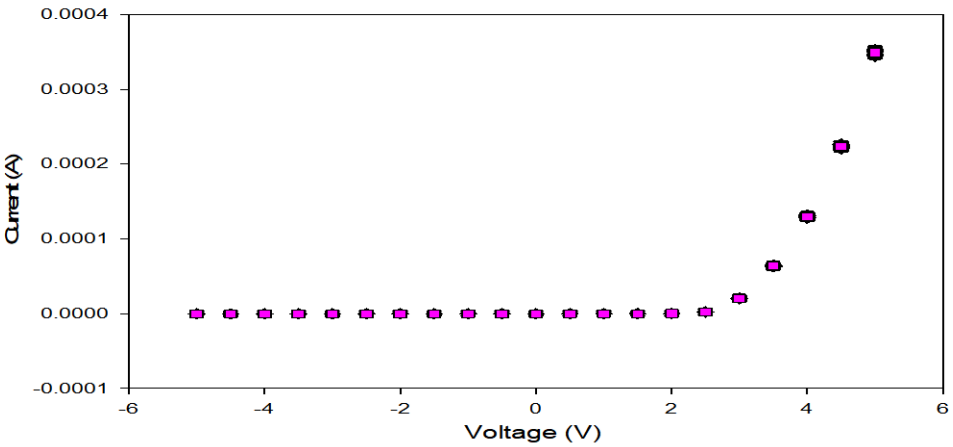

Figure 3.11: The Current vs Voltage of A-Si AM1456Ca solar cell.

are shown a two-dimensional projection of the colour space with x and y coordinates for a more coherent visual representation of the colour space seen by the human eye.

4. CHAPTER 4 - EXPERIMENTAL RESULTS

4.1 Optimal Response

In this chapter, the results from the empirical experiments outlined in section 3.3 onwards are presented and examined in detail. The effects of different voltage bias and wavelengths on the performance of the solar cells are explained, and various implications of their colour matching functions and finally colour spaces are discussed. The code used to go from current vs wavelength graphs to colour matching functions to, lastly, horseshoe diagrams, may be found in Appendix A and Appendix B respectively. The code used to calculate Delta E may be found in Appendix C The code in Appendix A is called EMRS5 and was developed at POLITO. It allows the user to interpolate multiple current vs wavelength signals from specific solar cells, and fit them into one of the three required colour matching signals. The final product is a x, y, and z signal, each one representing the red, green, and blue signal respectively. Figure 4.1 shows the colour matching functions using the CIE 1964 model for the human eye response.

In figure 4.2, an example of such an interpolation can be seen. The figure shows the interpolation for the $\bar{y}(\lambda)$ colour matching function (green response). The Yellow line is the optimal colour fitting response of the human eye for green. The green line in figure 4.2 is the interpolation of the data gathered from the solar cell using the experimental setup described in Chapter 4. If the interpolation strays from the

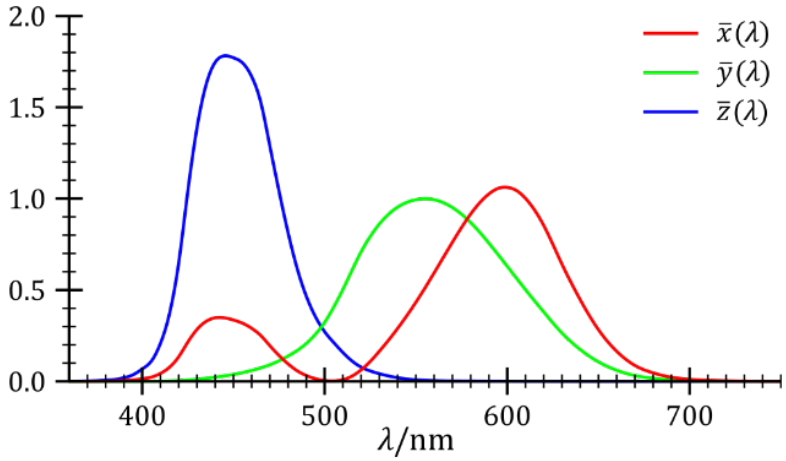

Figure 4.1: Colour fitting of CIE 1964 human eye response. Reproduced from http://cvrl.ioo.ucl.ac.uk/database/text/cmfs/ciexyz31.htm

optimal response, this will create folding and metamers in the chromaticity diagram.

If the final product of the interpolation for each colour matching function was exactly like a human colour response, then the colour matching functions would resemble the CIE XYZ standard observer colour matching functions. Figure 4.3 shows the CIE XYZ standard observer CMFs using the aforementioned code. Note how there are no values below 0 on the y axis, and how the CMFs cross each other at multiple points in the x axis.

The $\bar{x}$ CMF has two peaks, one at around 430 nm with intensity of 0.4, and a second peak at 590 nm with an intensity of 1.1. The intensity units are arbitrary. The $\bar{y}$ CMF has one peak at around 560 nm, with a half intensity maximum of 0.5. The CMF hasvalues ranging from 400 to 700 nm. Each one of the CMF represents one of the tristimulus values.

Figure 4.3 can then be made into a 3-dimensional space based on three primary colours, called XYZ. For clarity and for easier understanding, the colour space is sliced in a 2-dimensional representation; this is the chromaticity diagram. Figure 4.4 shows the chromaticity diagram produced from the CIE XYZ standard observer CMFs. The

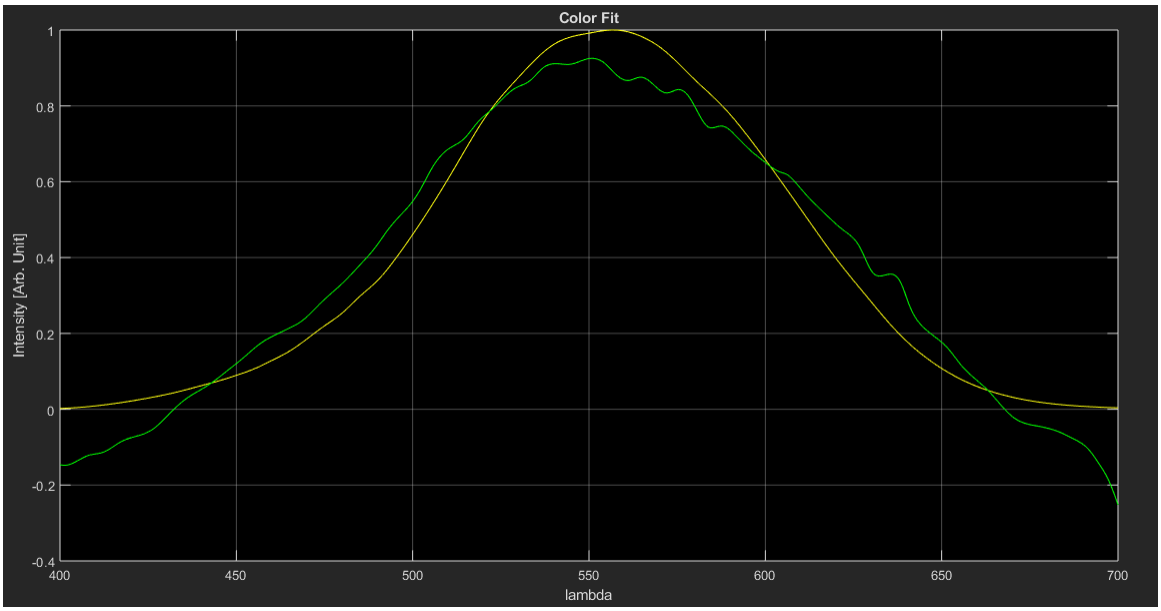

Figure 4.2: EMRS5 colour fitting function for $\bar{y}(\lambda)$. The Interpolation is the green signal, and the optimal response is the yellow signal.

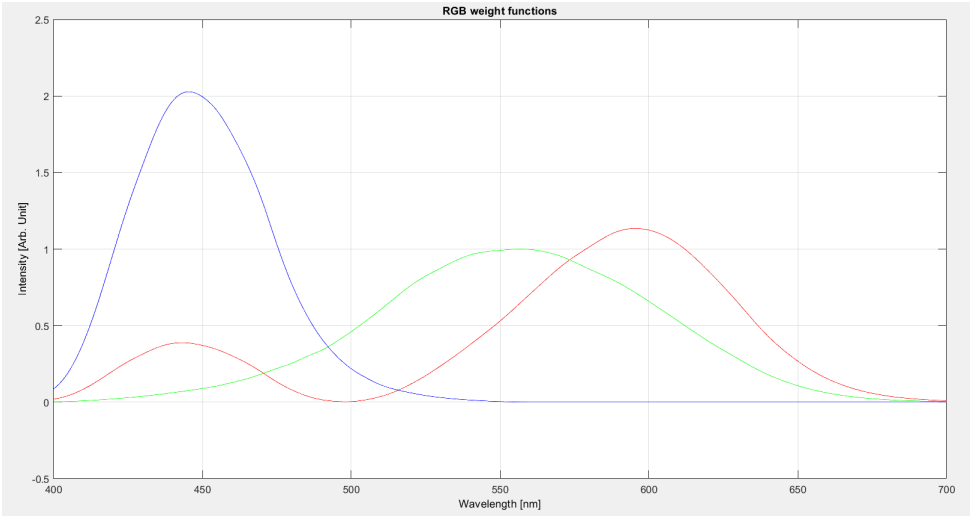

Figure 4.3: The CIE XYZ standard observer color matching functions using EMRS5.

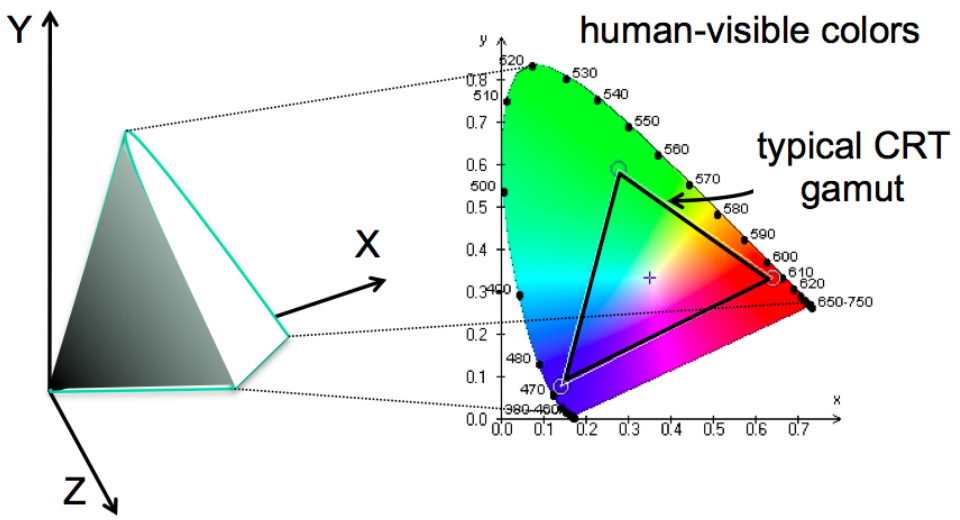

Figure 4.4: Three-dimensional colour space on the left side of the figure. Plane colours xy CIE 64 chromaticity diagram. The white outline of the diagram represents monochromatic light. All colours available to the human eye are within the outline. Reproduced from http://web.mit.edu/6.813/www/sp16/classes/16-color/

outline of the horseshoe diagram represents monochromatic light. Within the outline, all of the colours in the visible spectrum are represented. With the representations of the CIE 1964 standard observer CMFs and chromaticity diagrams shown in figure 4.2, and figure 4.3 respectively, one can see the deviations that each solar cell tested will have from the average human eye response. When showing colour matching function graphs, all values are taken in their absolute form for the purpose of not having any negative intensities. The CMF graphs for the solar cells can properly represent the CIE, once only absolute intensities are present in the 1964 chromaticity graph.

In the next section, the CMF graphs are shown to display very sharp change in the minimum points in the data. These are locations where the intensity would have been negative, but has been corrected. The trade-off is that now the chromaticity diagram is either missing data points or has an abundance of intensity at certain points. That will only distort the horseshoe diagram, and will leave us with high Delta E values. This abundance of sharp pivots in the data can be more readily seen in solar cells

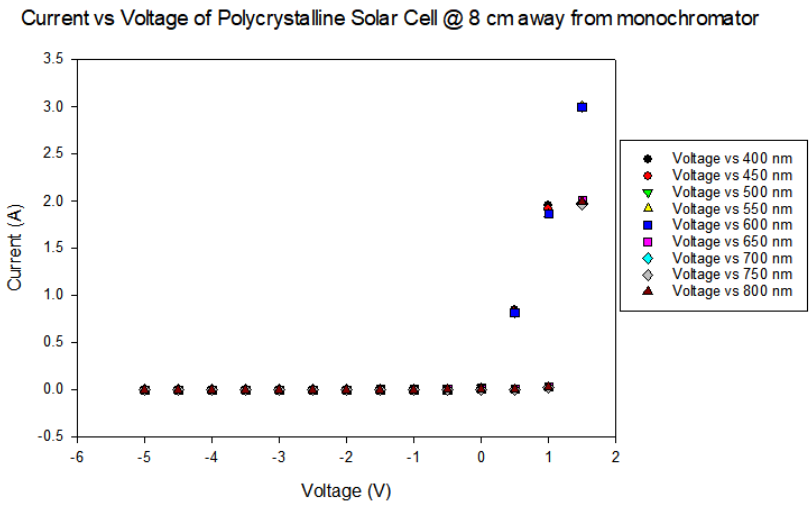

Figure 4.5: The Current vs voltage of the Polycrystalline solar cell.

that do not have a unique response to either voltage or wavelength, thus decreasing the likelihood of the cell being a good candidate for colour sensing applications.

In the next section, the current vs voltage, current vs wavelength, colour matching functions, and finally chromaticity diagram of every tested solar cell will be presented.

4.2 Results

4.2.1 Poly-crystalline Silicon SOL1N from Velleman

In figure 4.5, the current vs voltage graph of the polycrystalline solar cell can be seen. While the graph has multiple wavelengths being shown, most of them are overlapping each other. The response is akin to a diode under illumination. The overall lack of distinction for different wavelength makes it so no one wavelength will create a unique current response for the solar cell. No unique response to different wavelengths is great for overall photoelectric current creation, but it is detrimental to the application being examined here.

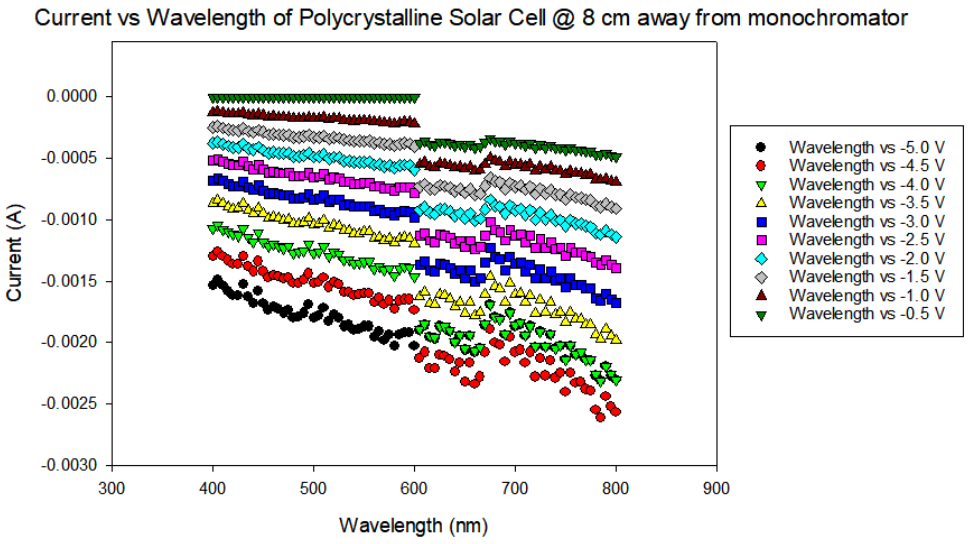

Figure 4.6: The Current vs wavelength of the Polycrystalline solar cell.

Figure 4.6 shows the current vs wavelength graph of the polycrystalline solar cell. In the figure, for wavelengths under 600 nm, there is simply a repeating pattern for each voltage. The only major difference being the position of the signal, which is dictated by the voltage bias on the cell. After 600 nm, there was a sharp decrease in the signal, yet with this change, the same repeating pattern was appreciated. Once again, no unique response to either voltage or wavelength decreases the likelihood of the cell being a good candidate for colour sensing applications.

Figure 4.7 transformed the current vs wavelength graph shown in figure 4.4 into colour matching functions. The interpolations results have multiple oscillations, and the characteristics and locations of the peaks of the CMF are extremely difficult to make out.

Figure 4.8 shows the horseshoe diagram of the polycrystalline solar cell. In the figure, a great amount of the chromaticity diagram is covered, yet a great number of folding is present. Any point on the white outline is a spectral (monochromatic) colour. Every point inside of the outline is a non-spectral colour. Every point outside of the curve is an imaginary colour, which is meaningless and has no true colour

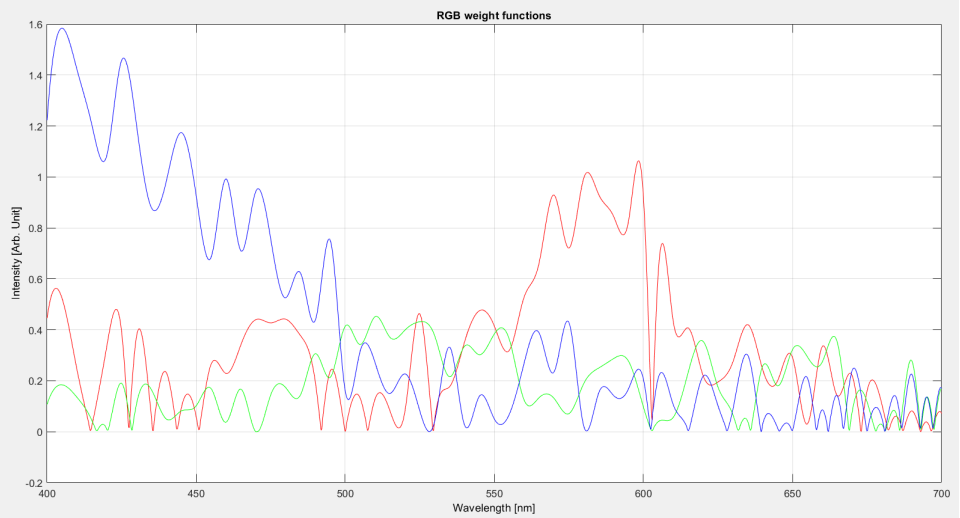

Figure 4.7: Polycrystalline solar cell colour matching functions.

parallel. The greater amount of data leaked outside of the outline, the greater the Delta E value will be.

In figure 4.9, the Delta E values for the polycrystalline cell are presented. The highest Delta E value is 222 at 560 nm, while the lowest is 29 at 400 nm. In table 4.1 one can see that the average value for Delta E for the polycrystalline solar cell is of 119, an extremely high value. All of these results show that a commercially polycrystalline solar cell should not be used for the purpose of colour sensing due to its lack of unique responses for both current vs voltage graphs and current vs wavelength graphs. The high number of oscillations in the CMF creates disturbances within the horseshoe diagram as well as a high number of metamers.

4.2.2 AM145 Amorphous Silicon (A-Si) Solar Cell from Panasonic

Figure 4.10 shows the current vs voltage of the AM1456Ca amorphous silicon solar cell. Within the graph, multiple responses to different wavelengths are present, yet no one response deviates from the overall pattern. All of the wavelengths are producing

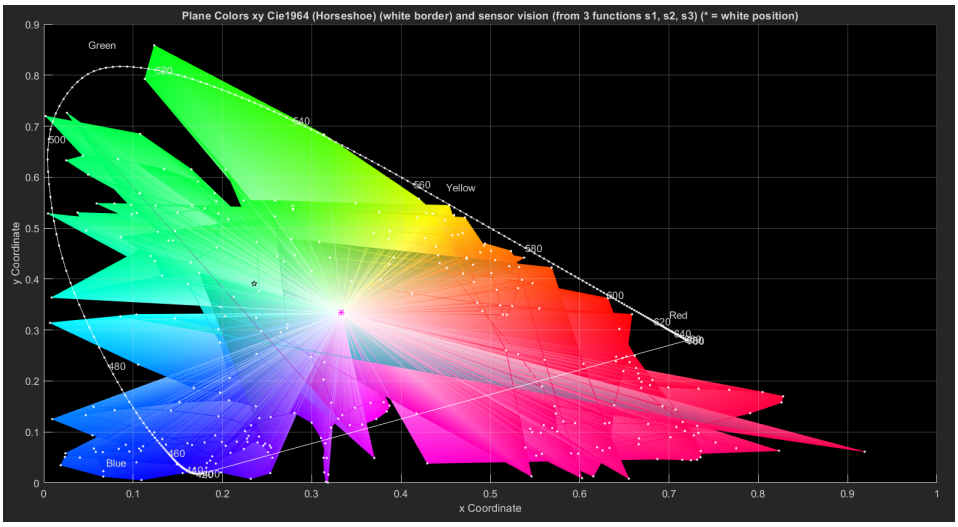

Figure 4.8: Polycrystalline solar cell chromaticity diagram.

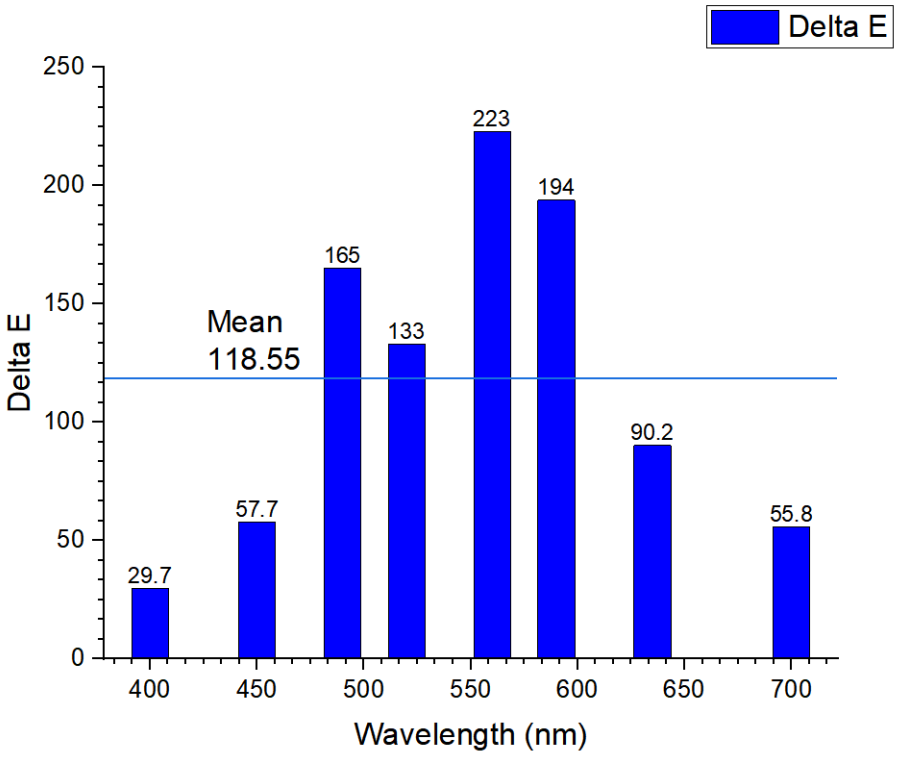

Figure 4.9: Delta E vs Wavelength of Polycrystalline Silicon at 15 nm Light Source

Table 4.1: Delta E of Polycrystalline solar cell at 15 nm Light Source.

Wavelength (nm)	**Delta E Values**
400	2.97E+01
450	5.77E+01
490	1.65E+02
520	1.33E+02
560	2.23E+02
590	1.94E+02
635	9.02E+01
700	5.58E+01
AVG	1.19E+02

the same current response. This figure shows that no matter the illumination, the solar cell produces close to the same optimal current response. This is ideal for power creation. For this thesis, absolutely no deviation in the current vs voltage graph lets one know that the cell will not have a unique current response to a specific wavelength. That by itself can lead one to believe that a-Si solar cells are not a viable candidate for colour sensing applications.

Figure 4.11 shows the current vs wavelength of the amorphous silicon solar cell. In the graph, it can be seen that at any one point, for example at 800 nm, the current response is linearly proportionate to the voltage. As the voltage increases, the current response increases at a regular interval.

Figure 4.12 is very similar to figure 4.7. They both display a great number of oscillations in the long colour matching functions. In figure 4.12, there is no distinction of a defined peak for the $\bar{z}$ colour matching function, and there is an excess of data after 550 nm. This will only hinder the transformation from weight functions to the colour space.

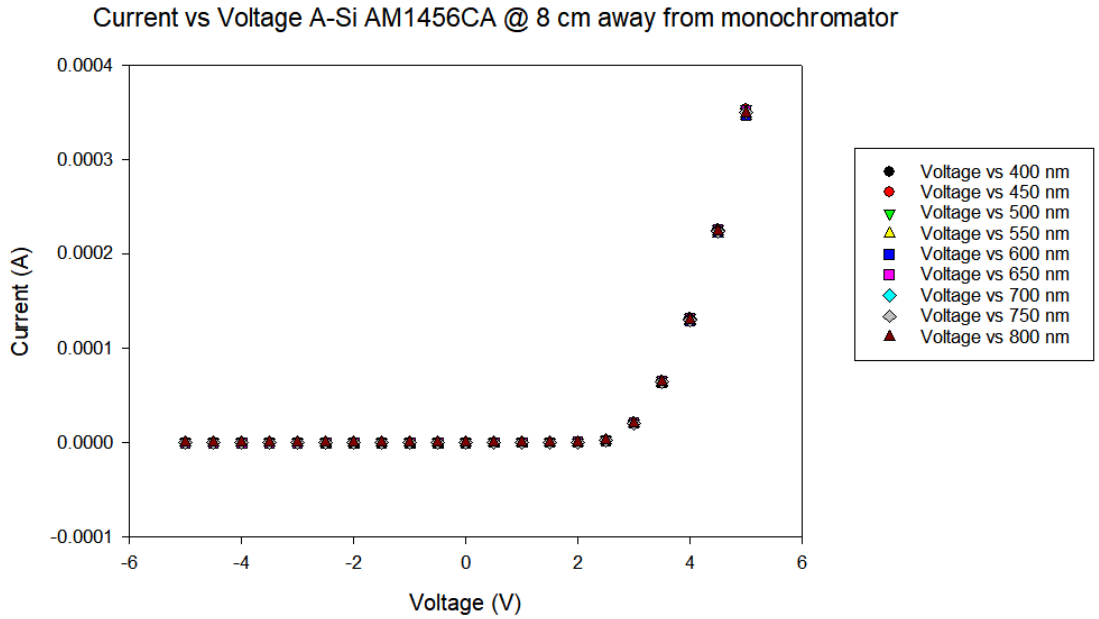

Figure 4.10: The Current vs voltage of the Amorphous Silicon solar cell.

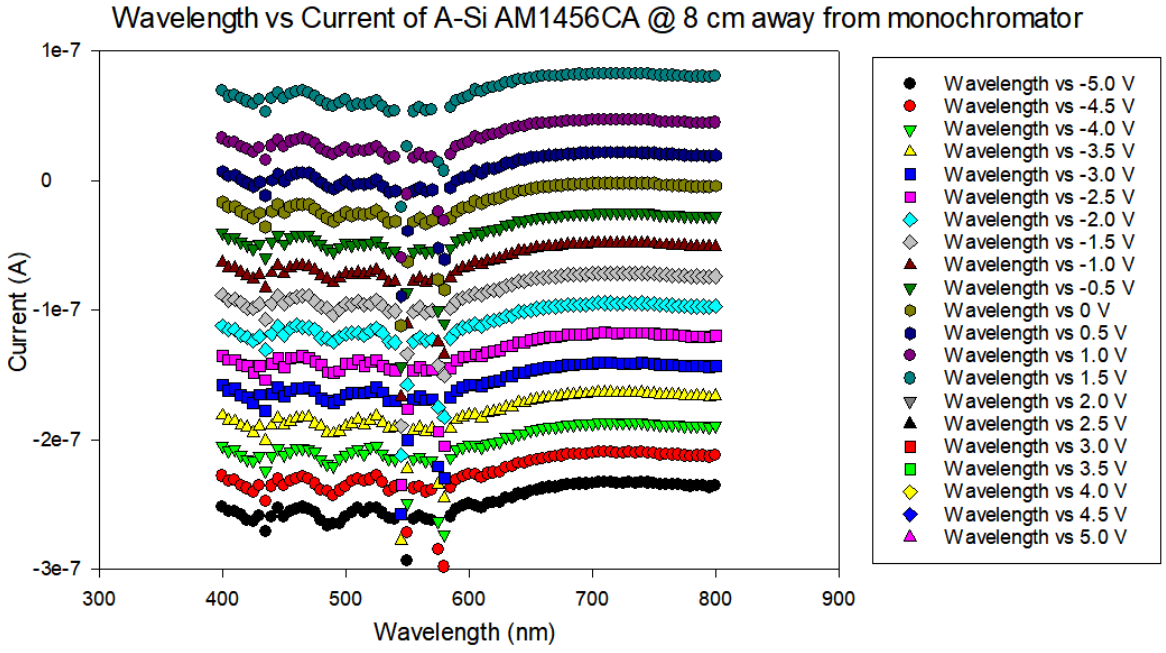

Figure 4.11: The Current vs wavelength of the Amorphous Silicon solar cell.

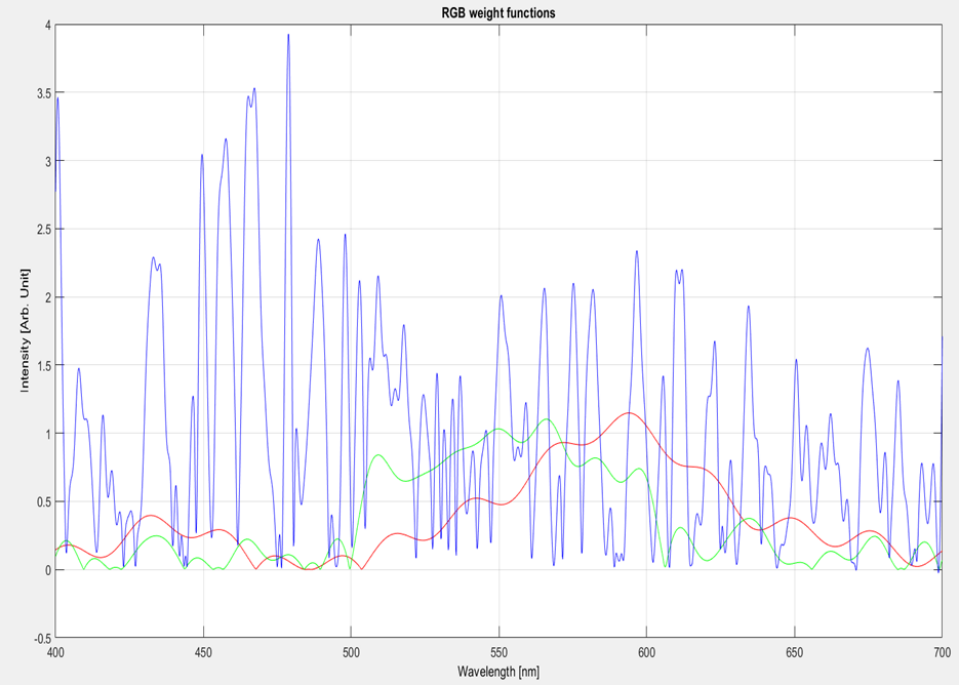

Figure 4.12: Amorphous Silicon solar cell colour matching functions.

Figure 4.13 shows the chromaticity diagram of the amorphous silicon solar cell. In the figure, a high number of folding and a great amount of data outside of the monochromatic outline can be seen. Additionally, one can see that a smaller amount of space is being filled up by the data within the white outline in comparison to figure 4.8.

Table 4.2 shows the delta E values for the amorphous silicon solar cell when illuminated with a 15 nm light source. The data was then graphed, as shown in figure 4.14. Figure 4.14 shows that the overall distribution of Delta E for the solar cell. The max Delta E value is 167, and its lowest is 31.3. On average, the delta E for the amorphous solar cell is of 110. A lower average than the polycrystalline solar cell, yet both are extremely high. As a reminder, an acceptable value should be lower than ten. From the analysis of figure 4.10 to figure 4.14, one can summarize that a single amorphous silicon solar cell is also not a viable solution for the purpose of colour sensing.

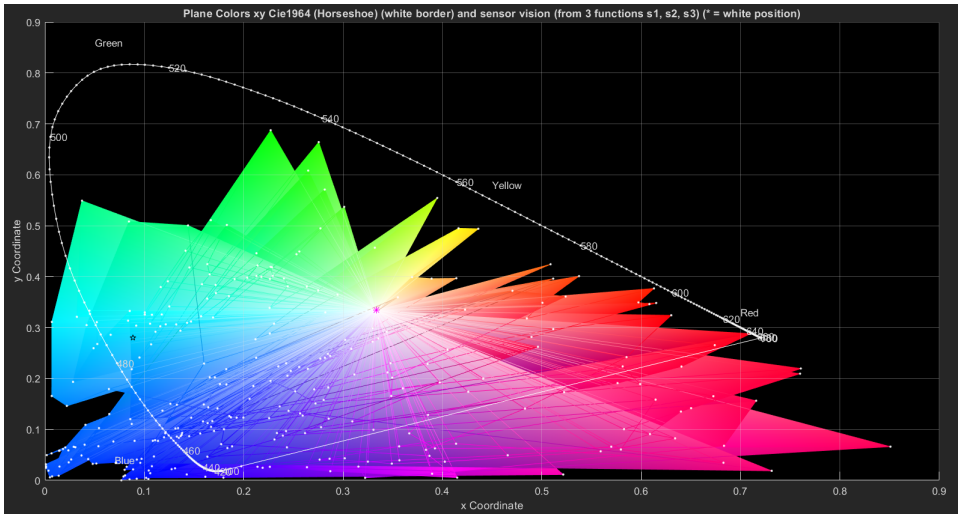

Figure 4.13: Amorphous Silicon solar cell chromaticity diagram.

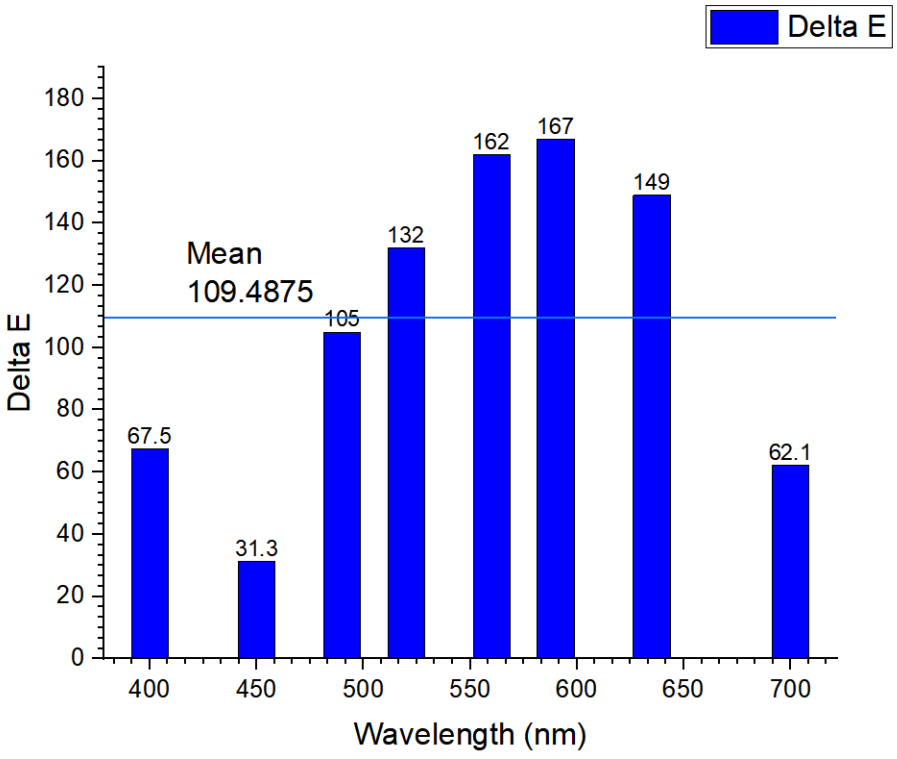

Figure 4.14: Delta E vs Wavelength of the Amorphous Silicon at 15 nm Light Source.

Table 4.2: Delta E of the Amorphous Silicon solar cell at 15 nm Light Source.

Wavelength (nm)	**Delta E Values**
400	6.75E+01
450	3.13E+01
490	1.05E+02
520	1.32E+02
560	1.62E+02
590	1.67E+02
635	1.49E+02
700	6.21E+01
AVG	1.10E+02

4.2.3 Perovskite Solar Cell from Solaronix:

Figure 4.15 shows the current/voltage graph for the Perovskite solar cell, with a different behavior than that observed in figures 4.5 and 4.10. In figure 4.15, we can see that different wavelengths create distinct current response. The response is very akin to an odd-number power function. The more unique the current response, then the current vs wavelength will be much different to an ideal diode solar cell when illuminated.

In figure 4.16 we observe very defined current responses at specific voltages. As the current vs wavelength graph of perovskite no longer has straight repeating patters, in comparison to figure 4.6 or figure 4.11, the linear interpolation will have more defined points. The more different defined points, the closer the colour matching function will be to the CIE XYZ standard observer colour matching function.

Figure 4.17 shows a much clearer x, y and z CMF. We can see the two defined peaks for the red signal. There is a clearly defined peak for the blue signal. The green signal has a peak at 590 nm. The drawback is the presence of remaining oscillations

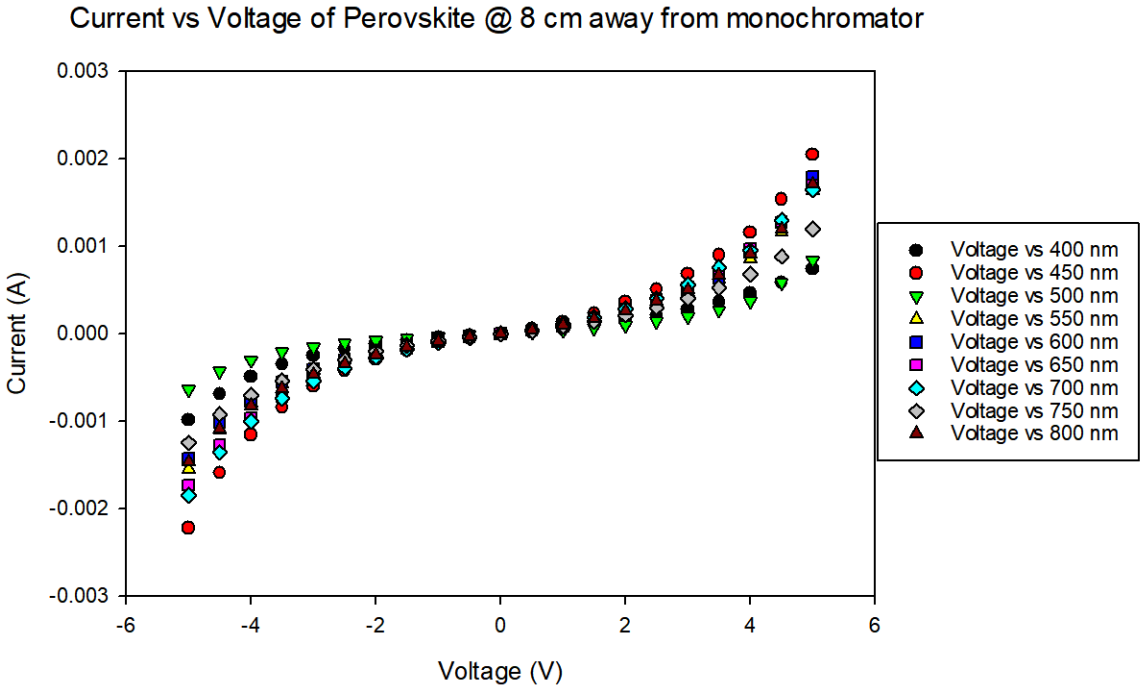

Figure 4.15: The Current vs voltage of the Perovskite solar cell.

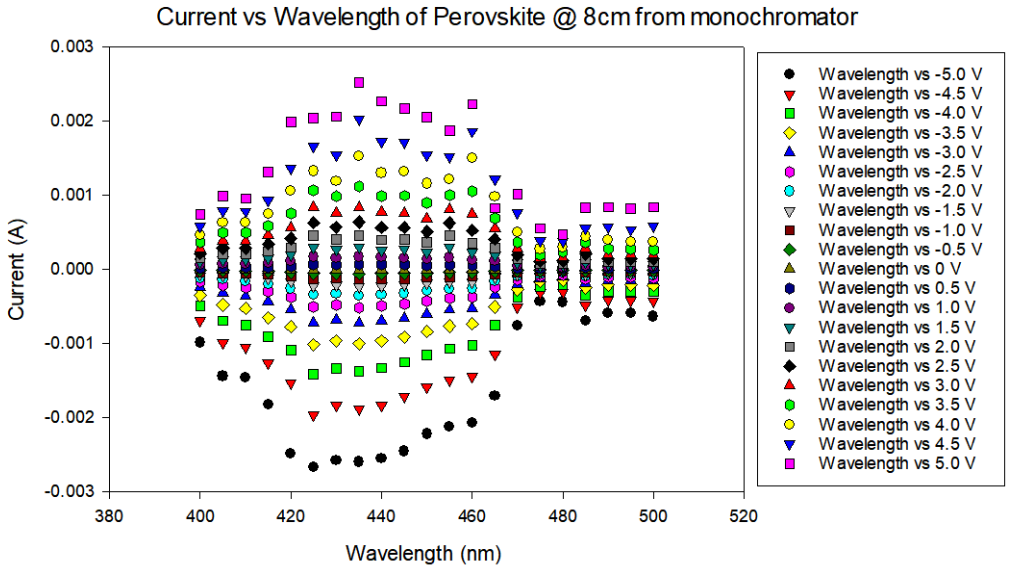

Figure 4.16: The Current vs wavelength of the Perovskite solar cell.

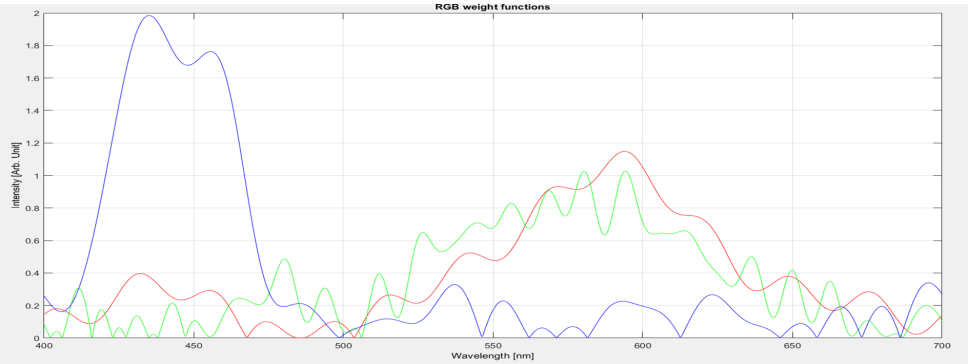

Figure 4.17: Perovskite solar cell colour matching functions.

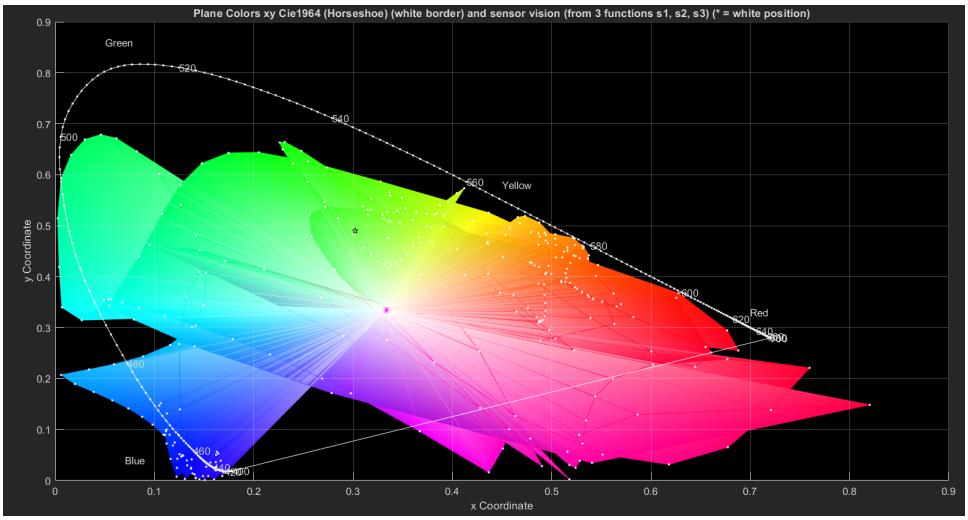

Figure 4.18: Perovskite solar cell chromaticity diagram.

in the intensity vs wavelength graph which leads to the presence of metamers in the chromaticity diagram.

Figure 4.18 shows a smaller number of imaginary colours, a great amount of space being covered in the chromaticity diagram in comparison to figure 4.13, yet many metamers are still present. Figure 4.17 has the most defined peaks of the three cells shown so far.

The Delta E for the Perovskite cell are shown in figure 4.19, with a maximum delta E of 146 at 520 nm, and a minimum of 35 at 700 nm, with an average value of 72.2. On average, this is a much smaller delta E than A-Si or polycrystalline,

yet too high for colour sensing applications. We can see that the data coming from the perovskite solar cell has more defined current responses, yet its high amount of oscillation translates into folding, and once again, distortions of the horseshoe diagram. The extra peaks in the signals cause overlaps and folding in the horseshoe diagram. This makes our sensor create impossible colours and metameres. However, the "blue" and "red" signals seem rather promising, so a perovskite solar cell could be improved and used for the purpose of sensing either red or blue colour signals, and their combinations. From the results, we conclude that a single commercially available perovskite solar cell is not suited for monochromatic colour sensing.

Table 4.3: Delta E of the Perovskite solar cell at 15 nm Light Source.

Wavelength (nm)	**Delta E Values**
400	8.15E+01
450	5.03E+01
490	6.80E+01
520	1.47E+02
560	8.47E+01
590	6.77E+01
635	8.35E+01
700	3.51E+01
AVG	7.72E+01

4.2.4 Dye Sensitized Solar Cell (DSSC) Solaronix

Figure 4.20 shows a similar odd number power function response in the current vs voltage graph, yet we no longer observe a steady rise in current as the voltage increases past 2 volts. In comparison to figure 4.15, figure 4.20 has a more pronounced oscillating current response. In terms of maximum current creation, that is not great,

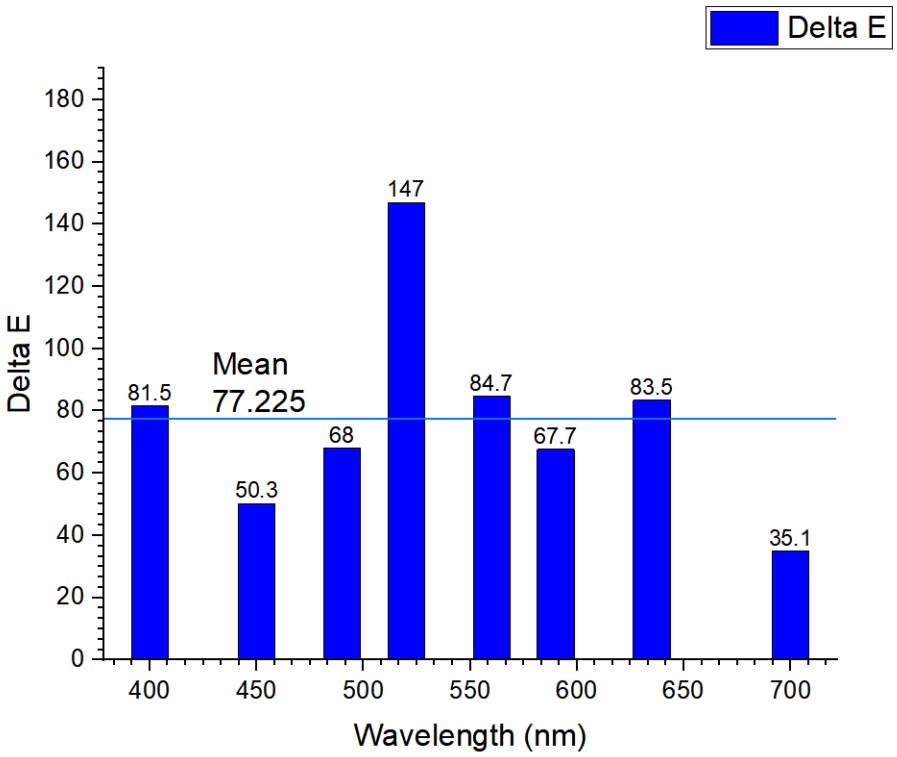

Figure 4.19: Delta E vs Wavelength of Perovskite solar cell at 15 nm Light Source.

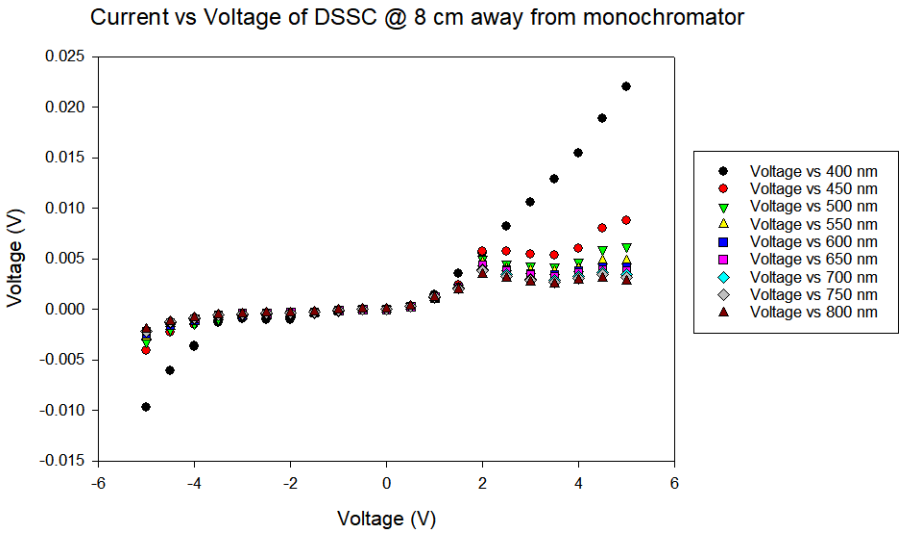

Figure 4.20: The Current vs voltage of the DSSC.

as there is a great dependence on not only the voltage being applied, but also on the wavelength used on the solar cell. For our purposes, this "fault" in the eyes of commercial applications is a positive characteristic that can be exploited for colour sensing applications.

Figure 4.21 shows the current vs wavelength of the DSSC. We have a maximum response around 400 nm. We then see an almost exponential decay for the data, which is mirrored for negative voltage values.

Figure 4.22 shows the intensity vs wavelength graph for the DSSC. The green signal of the graph is the one with the least number of oscillations out of all tested solar cells. The red signal has a low number, but very big oscillations. The blue signal has a low number of oscillations, but it covers a very big area, much bigger than the optimal signal response.

Figure 4.23 shows the chromaticity diagram for the DSSC. The diagram has the least amount of impossible colours, and has some very linear contour from 400 to 490 nm, We see an almost straight line from 480 nm to 560 nm. This graph has the least amount of metamers and folding present out of any of the solar cells tested.

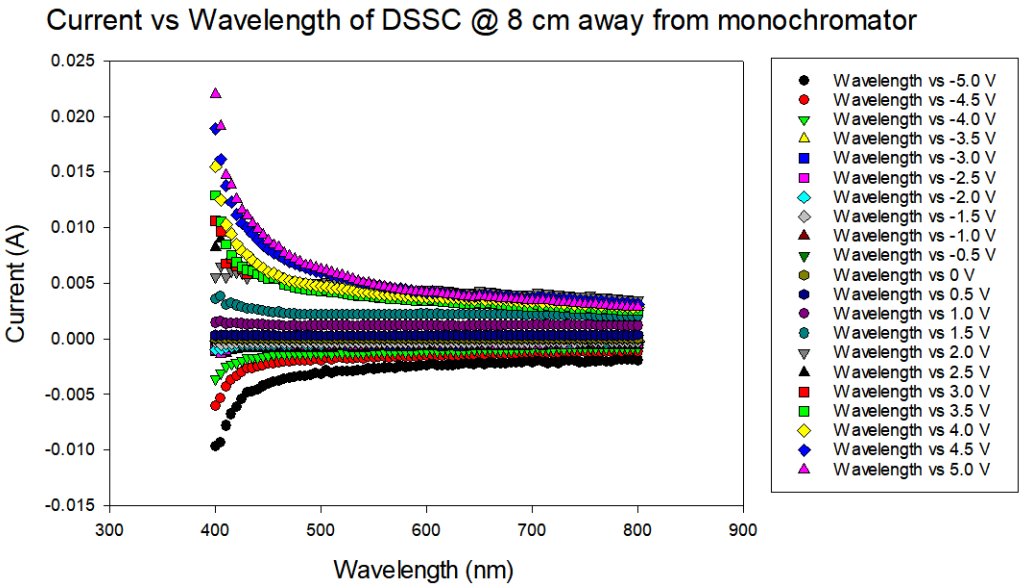

Figure 4.21: The Current vs wavelength of the DSSC.

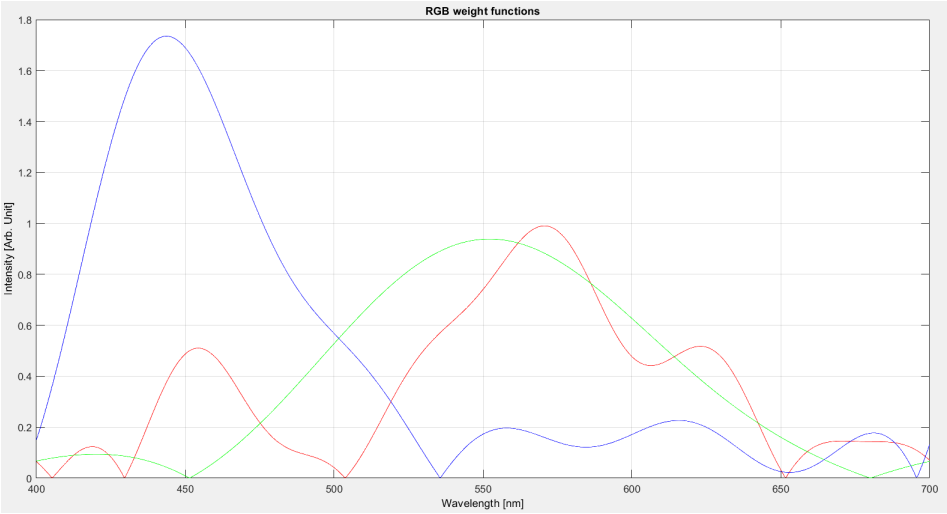

Figure 4.22: DSSC colour matching functions.

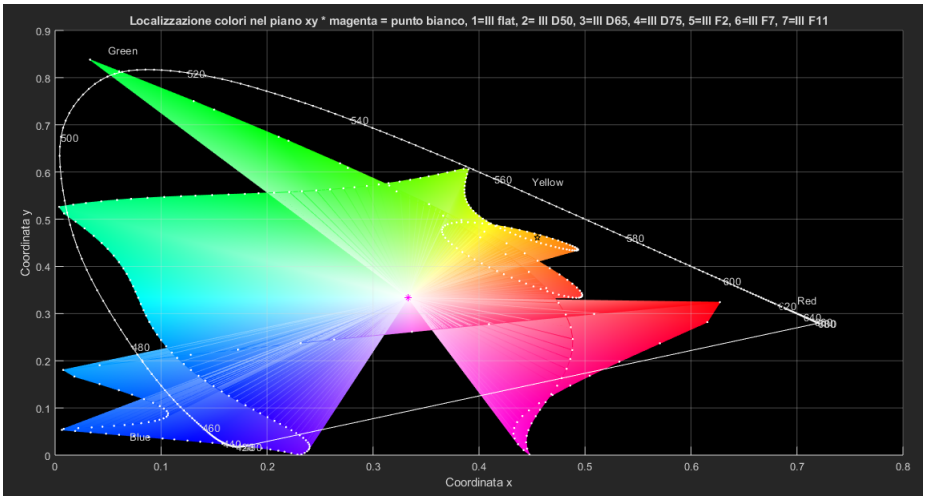

Figure 4.23: DSSC chromaticity diagram.

From figure 4.24, we get a maximum Delta E value of 110 at 400 nm, and a minimum value of 43 at both 450 and 700 nm. The average Delta E value for the DSSC was 76. The DSSC colour fitting had some of the lowest number of oscillations in all of our experiments. This reduced the number of folds dramatically, but we still see that the chromaticity diagram to the right is not able to cover the whole spectrum. The dye sensitized solar cell (DSSC) exhibited a very unique response from the 400 to the 500 nm range. After that range, its response became more a plateau. The early response could be linked to the cell having high sensitivity to blue light. High sensitivity could mean that the cell would have more distinct current responses at different wavelengths. All of these characteristics make a DSSC a promising candidate for colour sensing, yet a few modifications must be made in order to specialize for our purposes. At the moment, a commercially available DSSC as is can not be used for reliable colour sensing applications.

4.2.5 DSSC "Virtual Band Pass"

The DSSC had the least number of oscillations in the intensity vs wavelength graph, as seen in Figure 4.25. As a test, we examined the possibility of eliminating unwanted

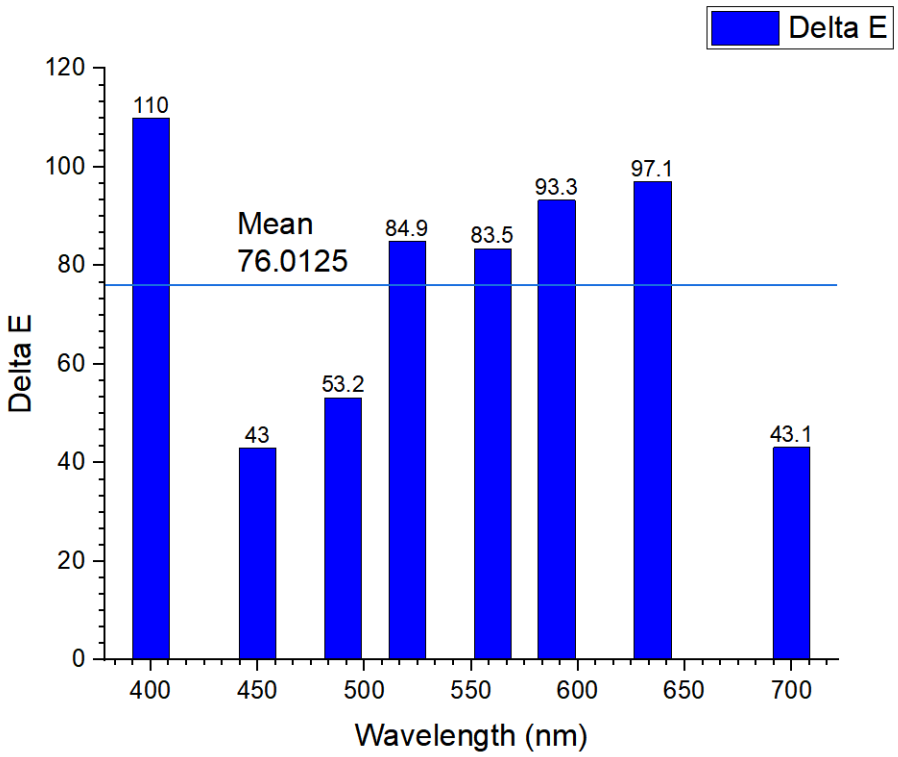

Figure 4.24: Delta E vs Wavelength of DSSC at 15 nm Light Source.

Table 4.4: Delta E of the DSSC solar cell at 15 nm Light Source.

Wavelength (nm)	**Delta E Values**
400	1.10E+02
450	4.30E+01
490	5.32E+01
520	8.49E+01
560	8.35E+01
590	9.33E+01
635	9.71E+01
700	4.31E+01
AVG	7.61E+01

portions of the spectral response, by making everything after 540 nm equal to zero for the "blue" signal, and by choosing only the data from 450 to 670 nm for the "green" signal. We left the "red" signal as it was. This was done in order to simulate a high band pass filter being applied on the solar cell. This implementation of the "virtual" band pass allows us to see a much lower number of oscillations in figure 4.25. From that new data, a new chromaticity diagram was created, as shown in figure 4.26. In the new horseshoe diagram, we see the least amount of folding yet. The main drawback is the great number of impossible colours.

Figure 4.27 shows the Delta E of the DSSC being applied a band pass. We have a max Delta E of 85.8 at 635 nm, a minimum of 3.57 at 700 nm, and an average of 50.6. Not only does it give out the lowest of averages for Delta E average, but we get a Delta E of 3.57, the lowest value yet, and within acceptable colour sensing parameters. The result is only theoretical, and at this point we are only selecting a very restrictive section of the data. Even if the results were all much lower, and withing the acceptable colour sensing parameters, one could not say that a DSSC

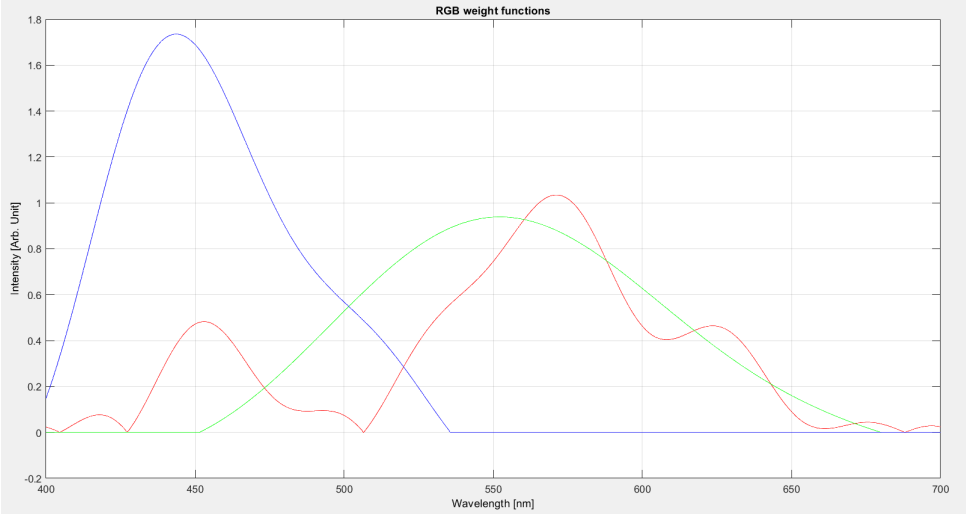

Figure 4.25: Dye sensitised solar cell colour weight functions Band pass.

can be used as is for colour sensing applications. What can be concluded is that if a DSSC was made specifically for the purpose of colour sensing, and we used some kind of band pass for discrimination of wavelength ranges, the final Delta E ranges will lower overall, as the CMF from the DSSC will more closely resemble the CMF of the CIE XYZ standard observer.

4.3 Discussion

In section 4.2, the results and analysis of graphs surrounding each solar cell was conducted. From the results, we can draw the following conclusions: Getting a constant current is ideal for normal uses of solar cells. For many high to medium efficiency solar cells, their quantum efficiency ranges are either plateaus or their parabolic peaks are outside of the visible spectrum, making them incompatible with our goals in this experiment.

The current difference due to different wavelengths on the polycrystalline and the A-Si cell were minimal to non-existent. The consistent plateau behavior of silicon

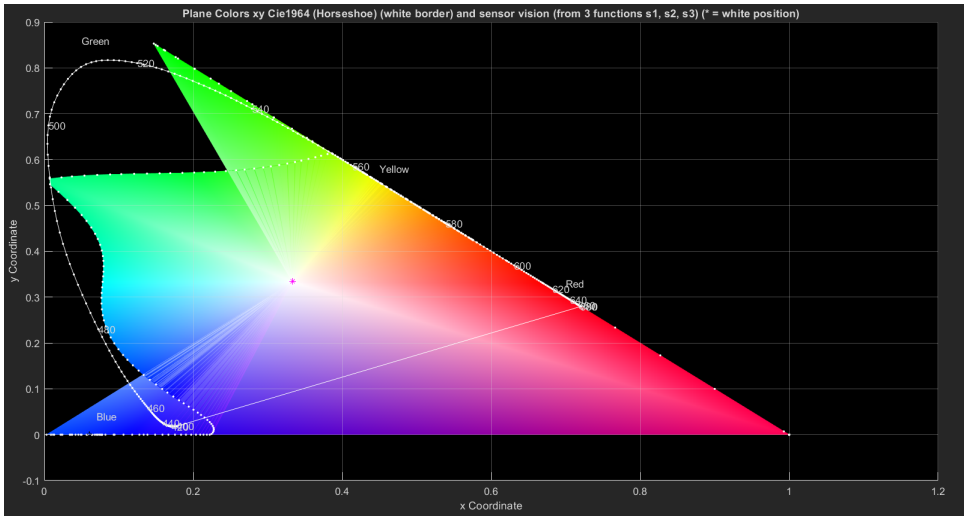

Figure 4.26: Chromaticity diagram of DSSC Virtual Band Pass.

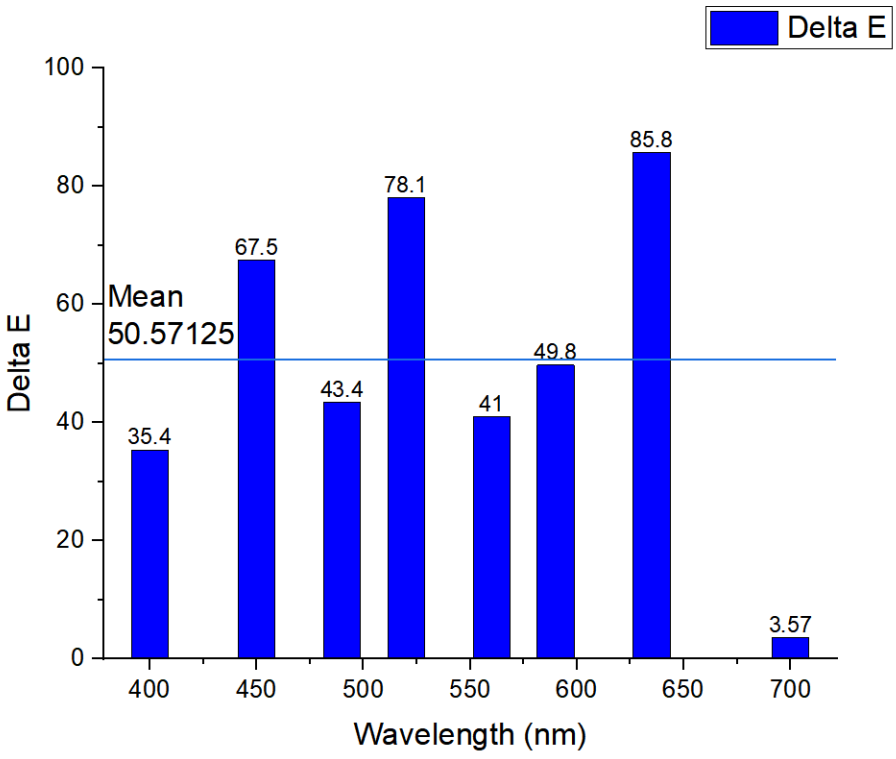

Figure 4.27: Delta E vs Wavelength of DSSC Band Pass at 15 nm Light Source.

Table 4.5: Delta E of the DSSC Virtual Band Pass solar cell at 15 nm Light Source.

Wavelength (nm)	**Delta E Values**
400	3.54E+01
450	6.75E+01
490	4.34E+01
520	7.81E+01
560	4.10E+01
590	4.98E+01
635	8.58E+01
700	3.57E+00
AVG	5.06E+01

cells under monochromatic illumination makes them not suited for monochromatic colour sensing. This also suggested that non-ideal solar cells, with a more varied current response to wavelength and voltage, would be a better choice for this application.

The Delta E values for DSSC and Perovskite were lower than the polycrystalline or the A-Si cell, yet the Delta E values were still above 10, the upper limit for an acceptable value, making them not suited for monochromatic colour sensing at their present configuration. Most tested solar cells displayed a great number of oscillations in their colour weight functions graphs. The great number of oscillations distorted the chromaticity diagrams, leading to high values for Delta E.

The solar cell with the lowest Delta E average was the DSSC with Delta E avg = 50. The lowest Delta E of the DSSC was 3.57 at 700 nm. Out of all the tested cells, that was the most promising result. However, a single DSSC would not be able to be used for the purpose of colour sensing on its own.

We can conclude that the use of a single solar cell cannot provide a feasible colour sensor due to high Delta E values. The use of multiple solar cells working in unison for the purpose of colour sensing applications is therefore proposed as the next step. The main conditions required for an effective solar cell-based colour sensor are:

1) That they be not necessarily, high quality, efficient solar cells but can exhibit unique responses to specific wavelengths
2) The quantum efficiency in the visible spectrum should exhibit a parabolic peak

A type of cell that can be considered for this purpose is the tandem cell. As we did not have access to physical tandem cells, literature data was used instead. In the next chapter, the tandem cell data is explored, and finally analysed with the DSSC data in order to test out their possible work in combination

5. CHAPTER 5 - COMPLEMENTARY ANALYSIS

5.1 Micromorph structure

A micromorph is a tandem solar cell made of a MICROcrystalline cell and an aMORPHous cell. A tandem structure is designed to capture more of the solar spectrum than a single-junction thin-film cell. Figure 6.1 shows the spectral response for a typical Micromorph solar cell. The high band-gap a-Si layer that is closest to the sun (top cell) absorbs the short wavelengths while the narrower band-gap μc-Si layer that is farther from the sun (bottom cell) absorbs the longer wavelengths. For comparison, a tandem cell structure with a double layer a-Si stack is also shown, these being the dash lines on figure 5.1. This cell structure is unable to capture light in the near IR region, which significantly reduces the efficiency potential of this structure (Shea, J , 2005).

The spectral response of the Micromorph and the tandem cell structure with a double layer of amorphous silicon resemble parabolic peaks within the visible spectrum. This is the kind of response that better fits the necessary parameters for colour sensing. We were not able to purchase laboratory ready tandem cells for our experiments. Instead, we had access to software which is able extract data points from graphs.

That data was then fed into EMRS5 in order to create CMFs from the tandem cells.

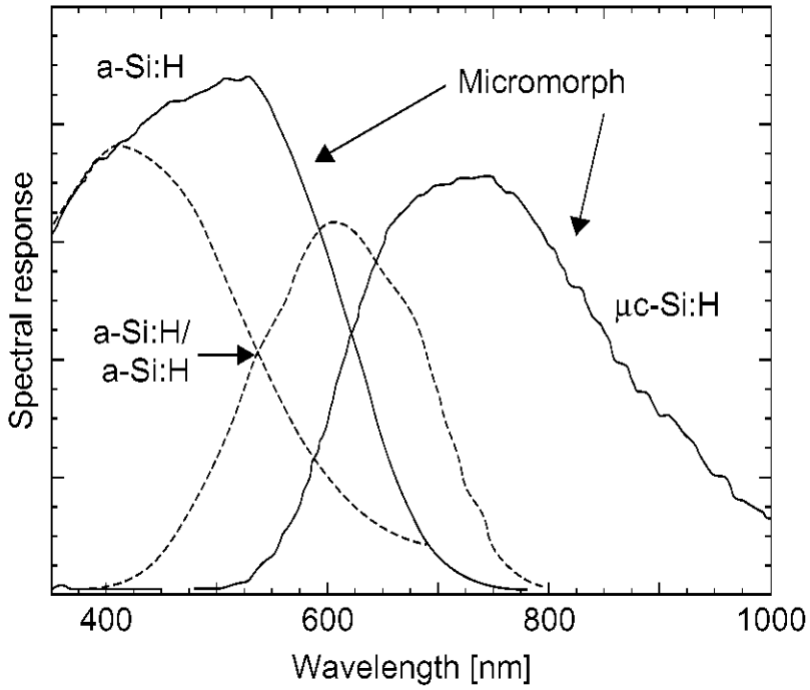

Figure 5.1: Spectral response of an $a-Si:H/\mu c-Si:H$ tandem (micromorph) structure compared to an a-Si:H/a-Si:H tandem structure.

The final interpolations are shown in figure 5.2. The signals very strongly resemble the CMFs of the CIE XYZ standard observer. However, they are not without flaw. The blue signal extends past the 400 nm mark towards lower wavelengths. The green and red signals have very defined peaks with a very small number of oscillations. As always, the lower the number of oscillations in the CMFs, the closer the chromaticity diagram of the cell will be to the standard observer.

Figure 5.3 shows the chromaticity diagram of the micromorph and tandem cells. The diagram boasts a great area of the horseshoe diagram being filled up, as well as a rather low number of folding of the colours and a small region of impossible colours.

Figure 5.4 shows the Delta E values of the Micromorph and tandem cells. The maximum value for Delta E is of 62.96 at 450 nm. The minimum value of 17.57 at 490 nm, and an average value of 42.1, the lowest value in comparison to the experimental data. Even with such low results, even its lowest value is not acceptable for colour

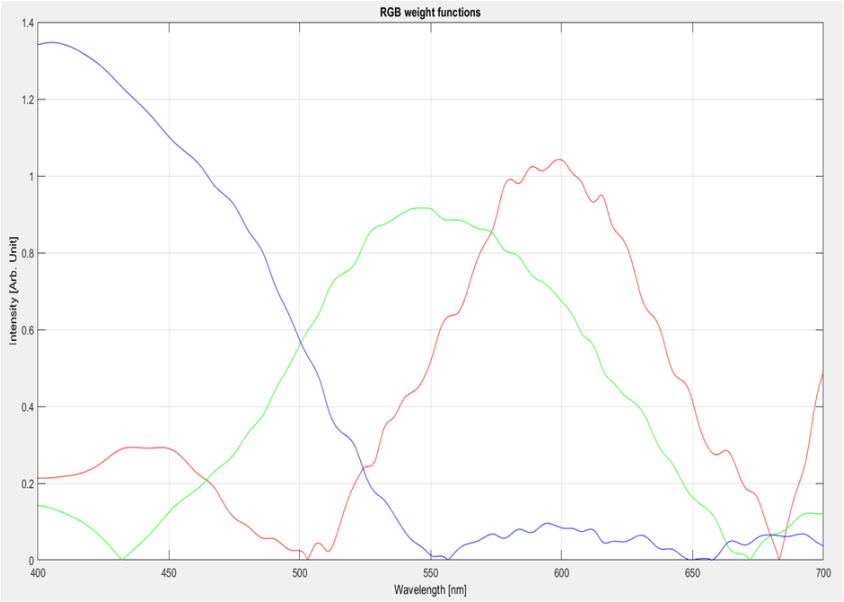

Figure 5.2: Micromorph colour fitting weight functions. Reproduced from (Shea, J , 2005)

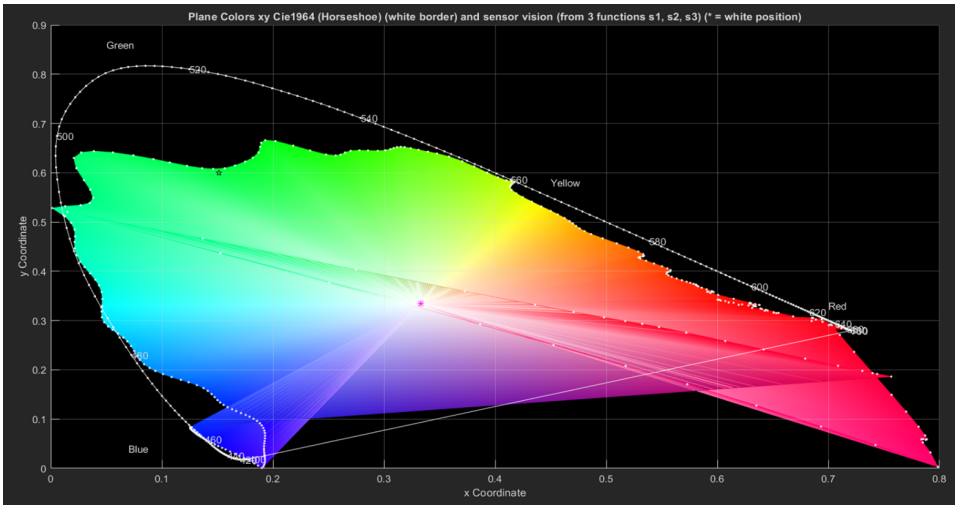

Figure 5.3: Micromorph solar cell chromaticity diagram.

Table 5.1: Delta E of the Micromorph solar cell at 15 nm Light Source.

Wavelength (nm)	**Delta E Values**
400	5.00E+01
450	6.30E+01
490	1.76E+01
520	4.41E+01
560	4.47E+01
590	5.37E+01
635	2.72E+01
700	3.62E+01
AVG	4.21E+01

sensing applications.

However, these results open the possibility of not only using tandem solar cells for further research, but allows for future research to gather significant data points from graphs in literature and tests them using the aforementioned EMRS5 software needed for the transformation of spectral response of a solar cell into CMFs.

5.2 Combination of literature and experimental data

The next iteration in the development of solar cell-based color sensors was to investigate the combination of different solar cells, not necessarily in a standard "Tandem" configuration. We begun by combining the Micromorph and the DSSC cells. After analysing both experimental data, and data from literature, we wanted to try out and see what would be the theoretical CMFs for the purpose of colour sensing.

The spectral response for this combination where combined into one intensity vs wave-

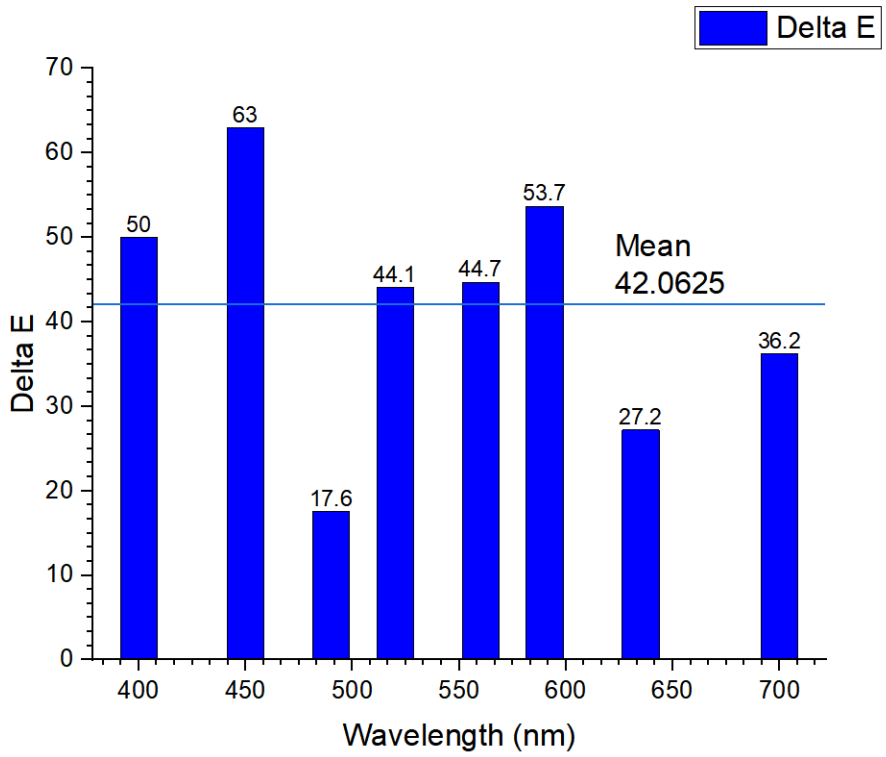

Figure 5.4: Delta E vs Wavelength of Micromorph solar cell at 15 nm Light Source

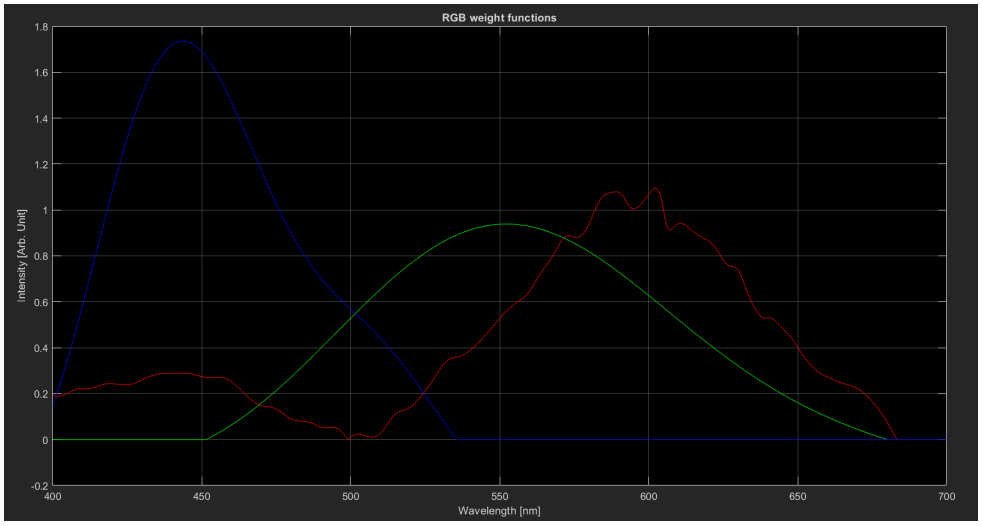

Figure 5.5: Micromorphs and DSSC colour matching functions.

length graph. Figure 5.5 shows both the DSSC and the tandem solar cells CMFs. The data has the smallest number of oscillations and thanks to applying a virtual bandpass filter to each CMF, we are now without sharp turning points at the minimums of the data points. For the "blue" signal, we made all data after 540 nm be equal to zero. For the "green" signal, we only took data from 450nm to 660 nm, every else was set to zero. For the "red" signal, after 660 nm, we set the data equal to zero Micromorph and DSSC data cleaned up and combined:

Figure 5.6 shows the chromaticity diagram of the combination of a DSSC and tandem solar cells. This chromaticity diagram is the one out of all created so far that resembles the CIE chromaticity diagram the most. Most of the area within the white outline is covered, there is a lack of folding of data, yet there is a great area of impossible colours.

Table 5.2 shows the Delta E values for the combination of the Micromorph and the DSSC signal at an illuminant bandwidth of 15 nm. Figure 5.7 shows the Delta E values for table 5.2 in graph form. The maximum value for Delta E is of 74.97 at 450 nm. A minimum value of 4.08 at 590 nm, follow by 6.27 and 8.49 at 635 nm and 560 nm respectively. The average value of 29.4 is much lower than the best result from

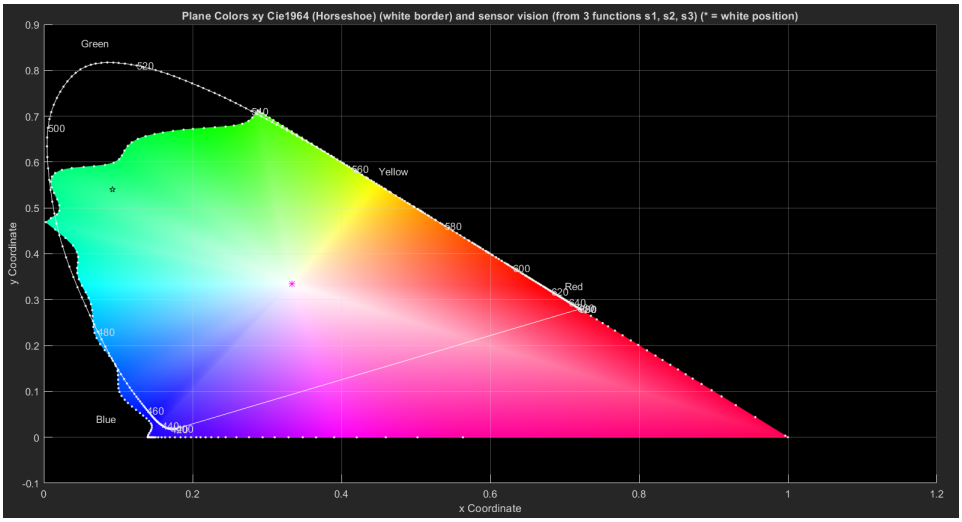

Figure 5.6: Micromorphs and DSSC chromaticity diagram.

the single solar cells, or the tandem cell. With Delta E values below 10, this suggests that more work should be pursued on this cell.

Even though this combination improves on the chromaticity diagram, the Delta E values at near monochromatic light are still too high for our application, as it still fails to achieve a low Delta E of the order of 3 or less. However, bandwidths up to 40 nm are commonly used as monochromatic light sources for microscopy and other optical applications. In the next section, we examine the effect of changing bandwidth of the simulated light sources.

5.3 Bandwidths of Light sources

One of the most important components of solar simulators are light sources. The standard light source for solar simulators is short arc and long arc xenon lamps. Metal halide arc lamps, carbon arc lights, and quartz tungsten halogen lamps (Riedel, N , 2015). Arc lamps can provide powerful and broad spectrum light, yet they are difficult to spectrally alter for the light biasing of multijunction solar cells and the realistic modelling of air mass Dennis, T (2017).

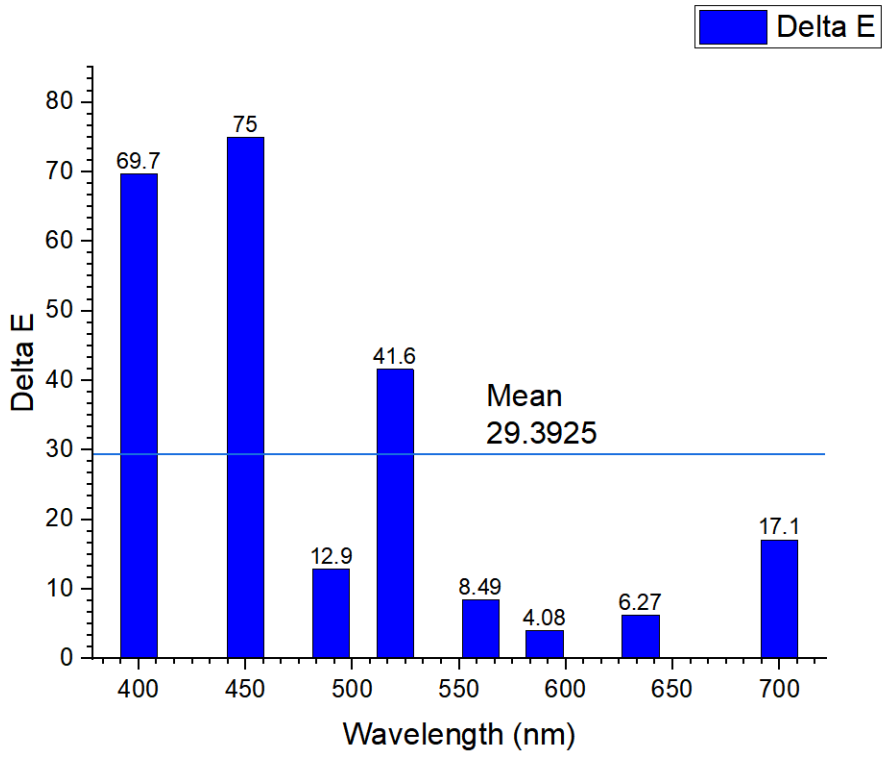

Figure 5.7: Delta E vs Wavelength of Microomorph and DSSC at 15 nm Light Source

Table 5.2: Delta E of the Micromorph and DSSC at 15 nm Light Source.

Wavelength (nm)	**Delta E Values**
400	6.97E+01
450	7.50E+01
490	1.29E+01
520	4.16E+01
560	8.49E+00
590	4.08E+00
635	6.27E+00
700	1.71E+01
AVG	2.94E+01

A super continuum laser is a high power, broadband light source that provides optical compatibility for photovoltaic materials and devices. Then a high-power continuum laser, can be used as a light source ranging from visible to the infrared spectrum (Dudley, J , 2006). These kinds of lasers are powerful, and easy to concentrate, yet they have unrealistic narrow spectra.

Light emitting diodes (LEDs) are the preferred light source in research compared to these other sources as they are less costly, are compact, have low power consumption, and can simulate AM 1.5 (Chawla, M , 2006) . LEDs have a long-life cycle, and can be easily calibrated. LEDs can radiate to a larger angled area compared to super continuum lasers, but they are insufficient in UV and IR wavelengths of the solar spectrum (Hamadani, B , 2013).

In recent years, highly intensive compact, and cheap LEDs have become available for the whole UV/Visible wavelength range in the commercial market. This makes the implementation of another type of light coupling techniques possible, which results in a very compact, low-cost measurement equipment (Rodríguez, J , 2013).

LEDs can be used for the purpose of chromaticity experimentation. Some commercial array spectroradiometers do not allow negative values of measured spectral distribution. In the spectral region where there is no source emission (for example the blue region for a red LED), the noise signal would produce positive and negative values. This negative noise is then removed and turned to zero. The remaining positive noise would cause similar effects to stray light, and cause significant error in the chromaticity graph.

Yet for typical LEDs having a spectral half width of 20 nm to 30 nm, a mismatch condition will not affect the results at 5 nm scanning intervals or less. If an LED has a narrower spectral width, problems may arise (Schanda, J , 2007).

In our simulation, we can easily reproduce a light source with one peak either as a line or a bell shape curve. As such, we were able to reproduce the illumination of an LED and impose different bandwidths. In figure 5.8 shows the spectral power distribution (SPD) of a single wavelength blue LED light (A) with a peak at 460 nm. A white LED light (B) which first peaks at 460 nm, and a second one at 560 nm. Then a white compact fluorescent lamp (CFL) (C) and a yellow CFL (D), both of which have multiple peaks in their own SPD graphs (Shang, Y , 2014).

Figure 5.9 shows the spectral profiles of light emitting diodes for the purpose of optical microscopy. These LEDs have peaks at 365 nm, 400 nm, 455 nm, 470 nm, 505 nm, 530 nm, 590 nm, and 625 nm. The spectral width (FWHM) of a typical quasi-monochromatic LED vary from 20 to 40 nm (Gustafsson, M , 2013). These widths are similar to the width of standard fluorophores used in microscopy.

To expand upon figure 5.9 , Table 5.3 show the peak wavelengths and FWHM of some example LEDs, such as red, wide green, blue, and narrow green (Liu, A , 2015). The table shows that truly the FWHM of LEDs vary from around 20 to 40 nm. For a narrow band green, its bandwidth is 7 nm, and for a wide green bandwidth, its 31 nm. Figure 5.10 shows the SPD of the wide and narrow green shown in table 5.3.

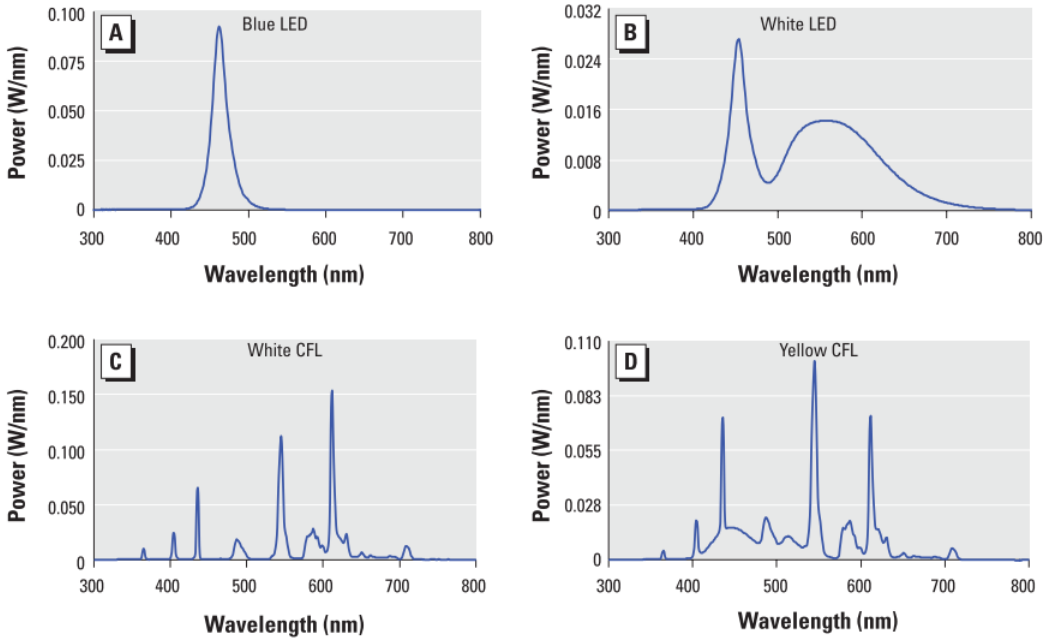

Figure 5.8: Light source SPD curves for (A) blue LED, (B) white LED, (C) white CFL, and (D) yellow CFL. Reproduced from (Shang, Y , 2014)

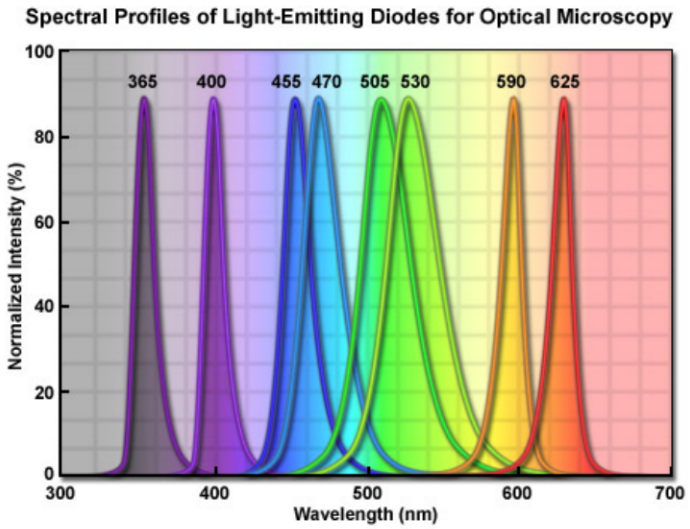

Figure 5.9: Spectral profile of LED used for optical microscopy. Reproduced from (Gustafsson, M , 2013)

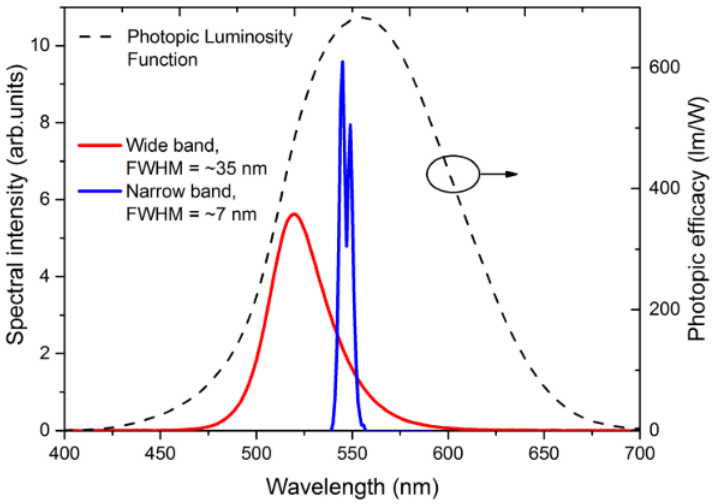

Figure 5.10: Spectral power distribution (SPD) of wide band and narrow line green phosphors. The data for the wide band phosphor is from CREE XP-E Green LED. Reproduced from (Liu, A , 2015)

They are both green LEDs, yet they have a very different FWHM. The narrow band is very similar to a line width monochromatic light source.

Table 5.3: Peak wavelength and FWHM of LEDs.

LED Type	**Peak wavelength (nm)**	**FWHM (nm)**
Red	625	16
Wide Green	520	31
Blue	477	22
Narrow Green	550	7

With the given range of FWHM of LEDs given in figure 5.10 and Table 5.3, we were able to recreate light sources with different FWHM in our simulation. By increasing the FWHM, we will be able to simulate more realistic light sources. For this thesis, we have limited our sources to LEDs for ease of recreation with our current code.

In the tables and figures below, we present the results at different FWHM for the same combination of the Tandem and DSSC data. In Table 5.4, and subsequently figure 5.11, we show the results for a FWHM of 30 nm. The average Delta E value for this test was 18.7. The highest Delta E was 59.9, and its lowest value was 3.88. At 30 nm FWHM, the average Delta E values show an improvement with respect to the 15 nm FWHM case. Also, the Delta E values for 450 nm, 490 nm, 590 nm, and 635 nm are less than 10. Still not acceptable values for colour sensing applications, but already much better than those at the bandwidth of 15 nm.

Table 5.4: Delta E of the Micromorph and DSSC at 30 nm Light Source.

Wavelength (nm)	**Delta E Values**
400	5.98E+01
450	9.23E+00
490	7.15E+00
520	2.02E+01
560	2.26E+01
590	9.18E+00
635	3.88E+00
700	1.73E+01
AVG	1.87E+01

At the upper limit of the average of bandwidths for LEDs, we tested a 45 nm FWHM. The Delta E values for the combination of the tandem and DSSC signal are shown in the table and figure below. Table5.5 shows an average value of Delta E of 16.1. In figure 5.12 we note that the 3 values at 450 nm, 490 nm, and 635 nm have Delta E below 5.65. The highest Delta E value being 26.2, and the lowest Delta E being 5.10. The overall average value of Delta E for the 45 nm bandwidth is lower than the 30 nm one, even though the 30 nm bandwidth showed very low Delta E

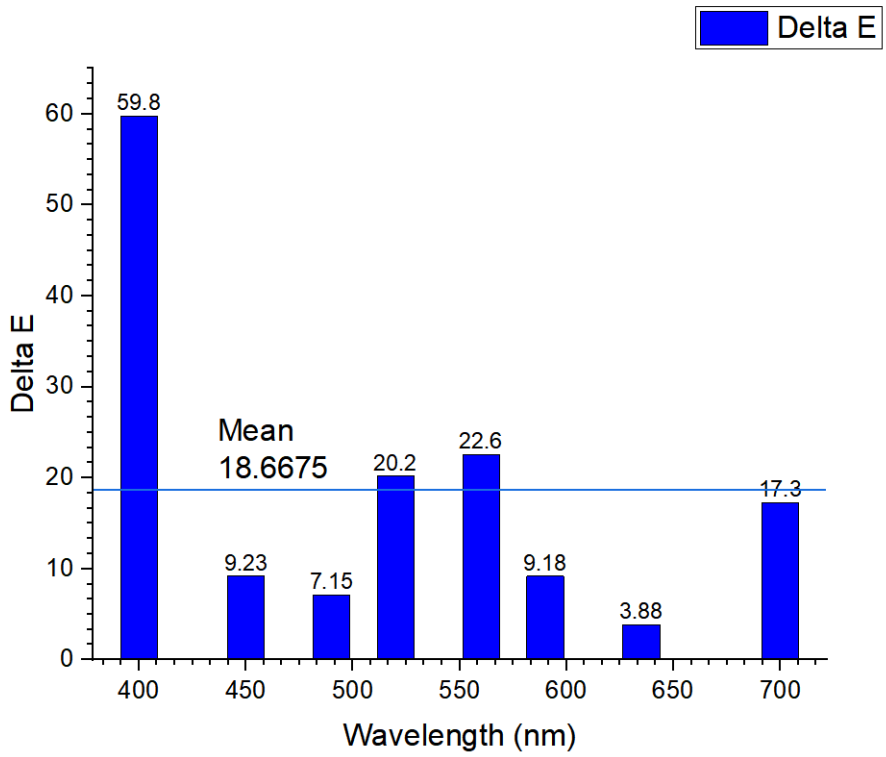

Figure 5.11: Delta E vs Wavelength of Micromorph and DSSC at 30 nm Light Source

value at specific wavelengths.

Table 5.5: Delta E of the Micromorph and DSSC at 45 nm Light Source.

Wavelength (nm)	**Delta E Values**
400	2.62E+01
450	5.33E+00
490	5.62E+00
520	1.08E+01
560	1.55E+01
590	1.43E+01
635	5.10E+00
700	1.02E+01
AVG	1.16E+01

From figure 6.9, we show that the average bandwidth for an LED is around 20-40 nm. We have shown simulated FWHM from 15 nm to 45 nm. As a test, a FWHM of 60 nm was tested as well. The results can be seen in table 5.6, and figure 5.13. Table 5.6 shows an average Delta E of 8.67, the lowest average out of any result. Figure 5.13 has a maximum Delta E value of 13.1 at 400 nm, and a minimum value of 5.34 at 450 nm. All other values are less than 11.

In table 5.7, all Delta E values at each simulated FWHM for the combined tandem and DSSC signal are shown. The table is then made into a graph. This graph is figure 5.14.

In figure 5.14, Series 1 represent Delta E for a light source with a bandwidth of 15 nm. Series 2 represent Delta E for a light source with a bandwidth of 30 nm. Series 3 represent Delta E for a light source with a bandwidth of 45 nm. Series 4 represent Delta E for a light source with a bandwidth of 60 nm. On average, the Delta E values are inversely proportionate with the bandwidth, the greater the bandwidth,

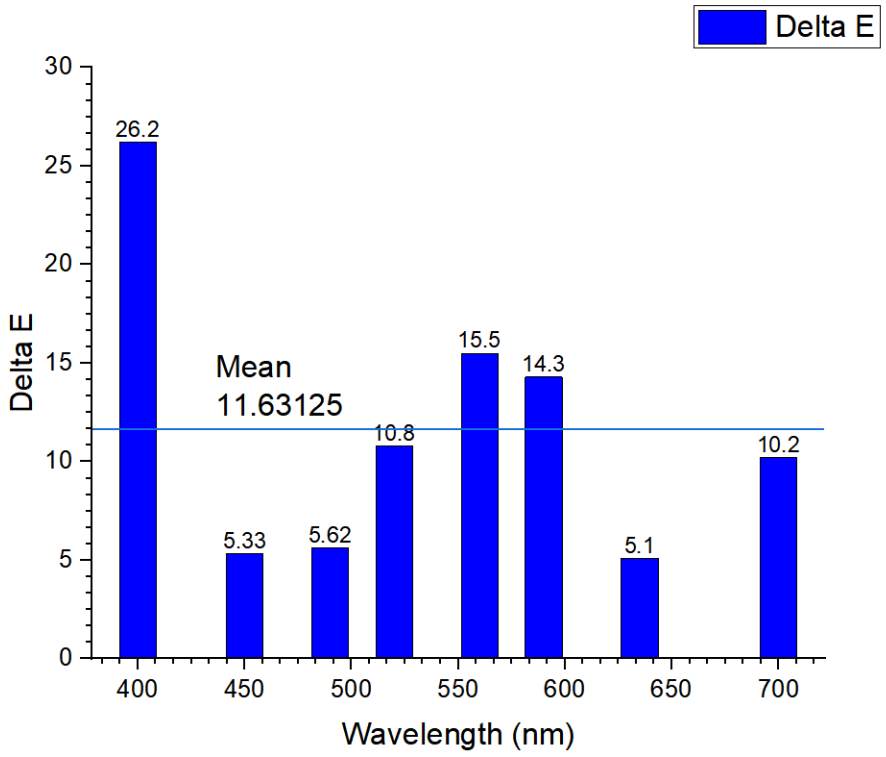

Figure 5.12: Delta E vs Wavelength of Micromorph and DSSC at 45 nm Light Source

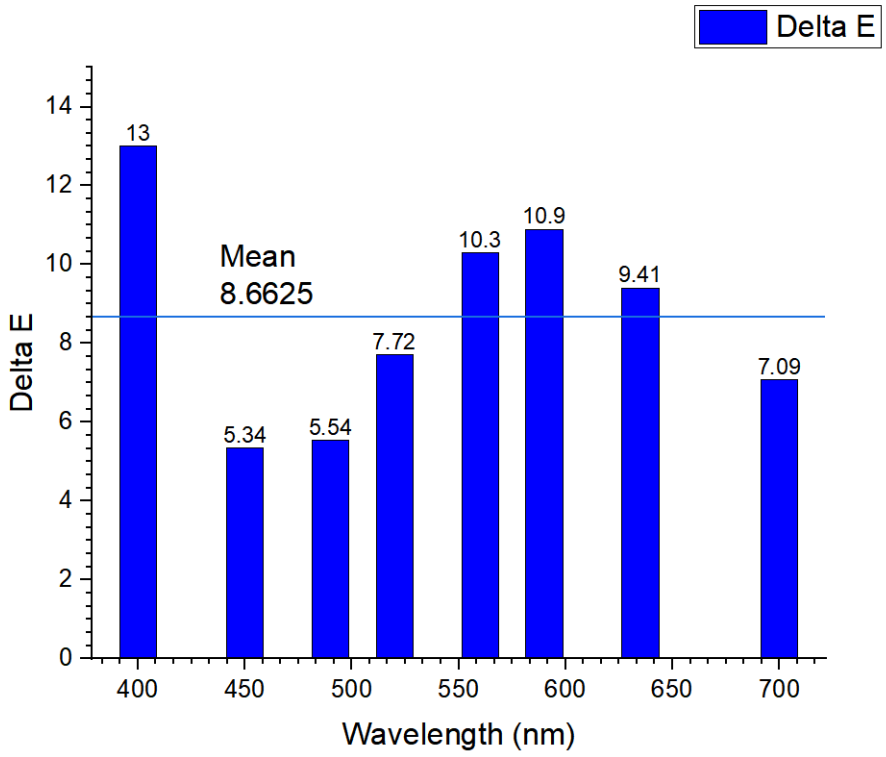

Figure 5.13: Delta E vs Wavelength of Micromorph and DSSC at 60 nm Light Source

Table 5.6: Delta E of the Micromorph and DSSC at 60 nm Light Source.

Wavelength (nm)	**Delta E Values**
400	1.30E+01
450	5.34E+00
490	5.54E+00
520	7.72E+00
560	1.03E+01
590	1.09E+01
635	9.41E+00
700	7.09E+00
AVG	8.67E+00

the smaller the average Delta E value.

Even though we did not achieve the desirable value of Delta E $\leq$ 3, our tests and simulations strongly suggest that with a proper choice of multiple solar cells combinations we can improve from the current best values. When multiple solar cells were used in unison (Tandem and DSSC), an average of 8.67 was achieved when shined with a light source of a bandwidth of 60 nm. The next step would be to get the average Delta E value lower than 3, and exploring different solar cell combinations under different illuminant bandwidths.

Table 5.7: Delta E of Micromorph and DSSC at multiple Light Source Bandwidths

	Delta E			
Wavelength (nm)	**15 nm**	**30 nm**	**45 nm**	**60 nm**
400	6.97E+01	5.98E+01	2.62E+01	1.30E+01
450	7.50E+01	9.23E+00	5.33E+00	5.34E+00
490	1.29E+01	7.15E+00	5.62E+00	5.54E+00
520	4.16E+01	2.02E+01	1.08E+01	7.72E+00
560	8.49E+00	2.26E+01	1.55E+01	1.03E+01
590	4.08E+00	9.18E+00	1.43E+01	1.09E+01
635	6.27E+00	3.88E+00	5.10E+00	9.41E+00
700	1.71E+01	1.73E+01	1.02E+01	7.09E+00
AVG	2.94E+01	1.87E+01	1.16E+01	8.67E+00

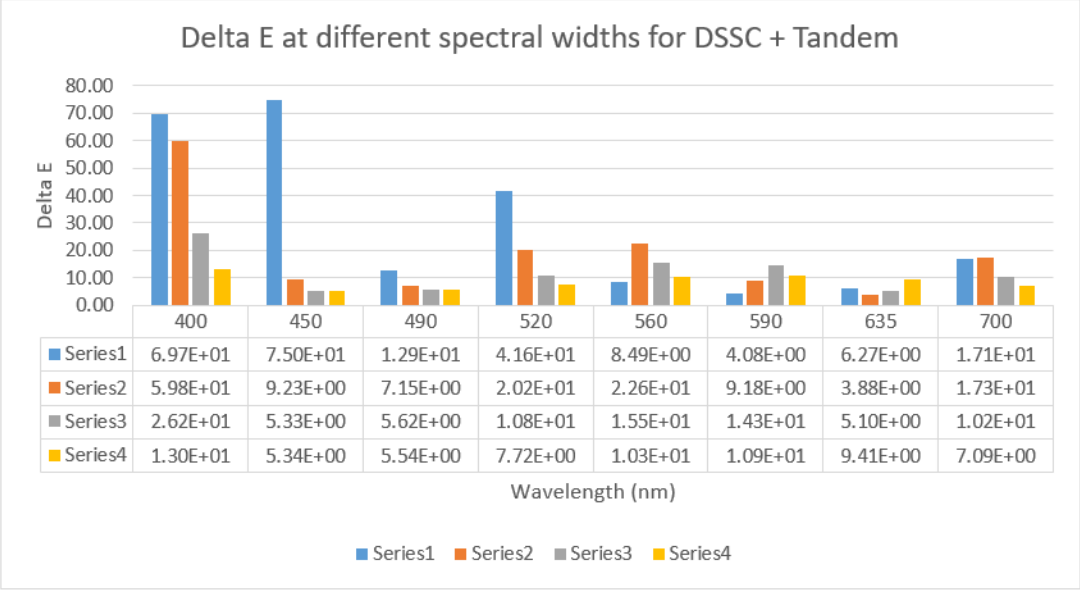

Figure 5.14: Delta E vs Wavelength of Micromorph and DSSC at different bandwidths. Series 1 is 15 nm, Series 2 is 30 nm, Series 3 is 45 nm, and Series 4 is 60 nm.

6. CONCLUSION AND FUTURE STEPS

The purpose of this thesis was to explore the possibility of using solar cells as a colour sensor. Colour sensors already exist, yet they are either costly or fail at correctly sensing monochromatic light. Our experiment was set up in order to see if a solar cell would create a unique current response to a specific monochromatic wavelength.

The more unique the current response was to a specific wavelength, the better the transformation of the current vs wavelength at different voltages could be properly transformed into colour matching functions. The XYZ values are then converted into the chromaticity diagram for the purpose of representing the colour perception of the solar cell in comparison to human vision.

A polycrystalline silicon solar cell from Velleman, an amorphous silicon solar cell (A-Si Solar Cell) from Panasonic, a perovskite Solar Cell from Solaronix, and a dye sensitized solar cell (DSSC) from Solaronix were tested in the laboratory by measuring the spectral response of the cells to varying voltages. A CMFs code was developed and used to obtain the chromaticity diagrams. Subsequently, the Euclidian distance (Delta E) was used to determine the difference in the solar cells' response with respect to the human eye.

Delta E allows for measuring colour differentiation, as it gauges the difference be-

tween two perceived colours. The smaller the Delta E value, the less noticeable the difference between the two colours in question (Delta E below 10 being acceptable, and Delta E < 3 being optimal). Our experimental results established that single solar cells do not provide the required response over the visible spectrum range. Among the single solar cells, the DSSC was able to cover a much greater area of the chromaticity diagram in comparison to the other cells, making it a promising candidate for colour sensing in a different setting.

The main source of error for these single cells was the high number of oscillations in their respective CMFs due to the lack of distinct current response to different wavelengths. These oscillations translated into folding and distortion of the chromaticity diagram. The more distorted the diagram, the higher the Delta E value. A possible way of solving these oscillations is to use filters in order to clean out the data.

Another conclusion is that the main conditions required for an effective solar cell based colour sensor are that they are not necessarily high quality, efficient solar cells but rather they can exhibit unique responses to specific wavelengths, and that the quantum efficiency in the visible spectrum should exhibit a parabolic peak.

Finally, we examined the impact of the light source. At a simulated Full Width Half Maximum (FWHM) of 15 nm, the Delta E for the combination of the Tandem and DSSC is too high for usable colour sensing applications. At a simulated light source bandwidth of 60 nm, an average Delta E of 8.67 was observed, the lowest of all Delta E averages and an acceptable value for color sensing. The next step will be to achieve an average Delta E value lower than 3, by exploring different solar cell combinations under different illuminant bandwidths.

Further research should focus on quantum efficiency graphs from solar cells gathered from literature. These graphs can then be extrapolated and studied using our provided code in order to create chromaticity diagrams. If these cells from literature give out positive results, such as a low amount of distortion of the horseshoe diagram, and low Delta E values, they should then become the focus of experimental modification to better tailor their characteristics to color sensing.

Multijunction or hydrogenated amorphous silicon cells should be some of the first to be tested. DSSC cells with different colour dyes should be tested independently and then together. The addition of some kind of physical or simulated filter could prove useful for the purpose of gathering data without a high number of oscillations for CMFs.

A solar simulator and a monochromator were used as the experimental light sources, but using different light sources, such as LEDs, fluorescent lightbulbs, or other controlled light sources should also be explored.

REFERENCES

[1] Albrecht, M, Correspondence Color blindness Rapid readout detector captures protein time-resolved WAXS, *Nature Publishing Group*, **7**, 10, (2010), DOI:10.1038/nmeth1010-775a

[2] Bosch, S, Cama, R, Edelstein, E, & Malkin, J, The Application of Color in Healthcare Settings, *The center for health design*, **1** October, 1–78, (2012)

[3] Monsen, H, Understanding Color, *Printwear*, **18**, 32-36 , (2005), DOI:10.1007/978-1-349-16373-1

[4] Alaya, M, Tóth, Z,& Géczy, A, Applied color sensor based solution for sorting in food industry processing, *Periodica polytechnica Electrical engineering and computer science*, **63**, 1, 16-22 , (2019), DOI:10.3311/PPee.13058

[5] Wong, B, Color blindness, *Nature Methods*, **8**, 6, 441 , (2019), DOI:10.1038/nmeth.1618

[6] Udd, E, & Spillman, W, Field Guide to Fiber Optic Sensors, *SPIE*, **1** , (2014), DOI:10.1117/3.1002803

[7] Letterle, B, The next generation of color sensors, *Sensors (Peterborough, NH)*, **23**, 28–30 , (2006), ISBN:07469462

[8] Bube, R, Photovoltaic materials, *Sensors (Handbook of Ecomaterials)*, **1**, 1-277 , (1998), ISBN:9781860940651

[9] Lan, D, & Green, M, A new look at silicon solar cell performance, *Energy Convers*, **11**, 63–73, (1971), ISBN:9780123869647

[10] Palmer, J , & Grant, B, Radiometric Properties of Materials, *Art Radiom*, **1**, 61–81, 2009, DOI:10.1117/3.798237.ch3.

[11] Gottlob, A,& Syme, P, Werner's Nomenclature of Colour, with additions, arranged so as to render it highly useful to the arts and sciences, *Oxford University*, **XXXX**, 61–81, (1894), ISBN: 3663537137

[12] Erenas, M, Cantrell, K, Ballesta-Claver, J, De Orbe-Payá, I, & Capitán-Vallvey, L, Use of digital reflection devices for measurement using hue-based optical sensors. Sensors Actuator, *Sensors and Actuators, B: Chemical*, **174**, 10-17, (2012),DOI: 10.1016/j.snb.2012.07.100

[13] Augustyn, A, Munsell colour system, *Britannica Online Encyclopedia*, **February 01**, 1-2, (2018), https://www.britannica.com/science/Munsell-color-system

[14] Fairchild, M, Color appearance models and complex visual stimuli, *Journal of Dentistry*, **38**,SUPPL. 2, 25-33, (2010), DOI: 10.1016/j.jdent.2010.05.008

[15] Hunt, R, Concepts and Methods, Quantitative Data and Formulas, *Optica Acta: International Journal of Optics*, **15**, 2, 197, (1968), DOI: 10.1080/713818072

[16] Brill, M, Encyclopedia of Color Science and Technology, *Encyclopedia of Color Science and Technology*, **1**, (2016), DOI: 10.1007/978-1-4419-8071-7

[17] Shanda, J, Colorimetry Understanding CIE System, *WILEY-INTERSCIENCE*, 1, 2007, ISBN: 9780470049044

[18] Garcia-Lamont, F, Cervantes, J, López, A, & Rodriguez, L, Segmentation of images by color features: A survey, *Neurocomputing*, **292**, October, 1-27, (2018), DOI: 10.1016/j.neucom.2018.01.091

[19] Gonzalez, R, & Woods, R. & Eddins, S, Digital Image Processing Using MATLAB, *Gatesmark*, **1**, 1, 1–303, (2009), ISBN: 9781259084072

[20] V. E. Johansen, J. Andkjær, & O. Sigmund, Design of structurally colored surfaces based on scalar diffraction theory, *Journal of the Optical Society of America B*, **31**, 2, 207, (2014), DOI: 10.1364/josab.31.000207.

[21] Ito, S, Yoshioka, M, Omatu, S, Kita, K, & Kugo, K, An image segmentation method using histograms and the human characteristics of HSI color space for a scene image, *Artificial Life and Robotics*, **10**, 1, 6-10, (2006), ISBN: 14335298

[22] Xiong, N, Shen, Y, Yang, K, Lee, C, & Wu, K, Color sensors and their applications based on real-time color image segmentation for cyber physical systems, *EURASIP Journal on Image andVideo*, **23**, 1-16, (2018), DOI: 10.1186/s13640-018-0258-x EURASIP

[23] Li, H, Liu, Z, & Zhan, S, A segmentation method of color texture image, *CHINESE JOURNAL OF COMPUTERS*, **9** ,965-971, (2001)

[24] CIE's Objectives, *CIE*, 1, 2020, http://cie.co.at/about-cie/cie-s-objectives

[25] Amara, M, & Mandorlo, F, Couderc, R, Gerenton, Félix, & Lemiti, M, Temperature and color management of silicon solar cells for building integrated photovoltaic, *EPJ Photovoltaics*, **9**, 1, (2018), DOI:10.1051/epjpv/2017008

[26] GR, Weiss , & AM, Bruce, Luminosity "Y" vs 457 nm brightness interrelationship, *Pulp Paper Canada*, **83** ,T50–T57, (1982)

[27] Price, M, 3 color sensor gadgets to take the pain out of paint matching, *C-NET*, **1**, 1-10, (2018)

[28] Lindbloom, B, xyY to XYZ, *online*, (2017), available at: http://www.brucelindbloom.com/index.html?EqnxyYtoXYZ.html

[29] Lindbloom, B, XYZ to LAB, *online*, (2017), available at: http://www.brucelindbloom.com/index.html?Equations.html

[30] Lindbloom, B, Delta E (CIE 1976), *online*, (2017), available at: http://brucelindbloom.com/EqnDeltaECIE76.html

[31] Shea, J, Handbook of thin film deposition - processes and technologies, *IEEE Electrical Insulation Magazine*, **18**,4, (2005), ISBN:9781437778731

[32] Riedel, N, Pratt, L, Edler, A, & Haas, F, Effects of a neutral density filter in measuring low-light performance with a pulsed light Xe arc solar simulator, *IEEE 42nd Photovolt. Spec. Conf*, **2015**, 1, 21–24, (2015), DOI: 10.1109/PVSC.2015.7355835

[33] Dennis, T, A programmable solar simulator for realistic seasonal, diurnal, and air-mass testing of multi-junction concentrator photovoltaics, *IEEE 44th Photovolt. Spec. Conf*, **2017**, 1, 1–6, (2017), DOI: 10.1109/PVSC.2017.8366534

[34] Dennis, T, Saturation in solar cells from ultra-fast pulsed-laser illumination, *IEEE 44th Photovolt. Spec. Conf*, **2017**, 1, 1–4, (2017), DOI: 10.1109/PVSC.2017.8366716

[35] Dudley, J, Genty, G, & Coen, S, Supercontinuum generation in photonic crystal fiber, *Reviews of Modern Physics*, **78**, 4, 1135-1184, (2006), DOI: 10.1103/RevModPhys.78.1135

[36] Chawla, M, A Step by Step Guide to Selecting the "Right" Solar Simulator for Your Solar Cell Testing Application, *Photo Emission Tech*, **1**, (2006)

[37] Hamadani, B, Roller, J, Dougherty, B, & Yoon, H, Fast and reliable spectral response measurements of PV cells using light emitting diodes, *Conference Record of the IEEE Photovoltaic Specialists Conference*, **1**, 73-75, (2013), DOI: 10.1109/PVSC.2013.6744102.

[38] Rodríguez, J, Fortes, M, Alberte, C, Vetter, M, & Andreu, J, Development of a very fast spectral response measurement system for analysis of hydrogenated

amorphous silicon solar cells and modules, *Materials Science and Engineering B: Solid-State Materials for Advanced Technology*, **178**, 1, 94-98, (2013), DOI: 10.1016/j.mseb.2012.10.009

[39] Shang, Y. M., & Wang, G. S., & Sliney, D., & Yang, C. H., & Lee, L. L, White light-emitting diodes (LEDs) at domestic lighting levels and retinal injury in a rat model, *Environmental Health Perspectives*, **122**, 3, 269-276, (2014), DOI: 10.1289/ehp.1307294

[40] Gustafsson, M, Patterson, G, Lippincott-Schwartz, J, & Davidson, M, Education in Microscopy and Digital Imaging, *Zeiss*, **1**, 1-18, (2013)

[41] Liu, A, Khanna, A, Dutta, P, & Shur, Red-blue-green solid state light sources using a narrow line-width green phosphor, *Optics Express*, **23**, 7, A309, (2015), DOI: 10.1364/oe.23.00a309

A. APPENDIX A

Appendix A

EMRS5: Current vs Voltage graphs to Colour matching Functions

```
colordef black;
clear;
clc;
close all;
% caricamento dati pesi r,g,b
rc=load('C:\Users\sergi\Desktop\Masters 15-07-19 Sergio Majluf
\Matlab Work\Colori\ciexyz64red.dat');
gc=load('C:\Users\sergi\Desktop\Masters 15-07-19 Sergio Majluf
\Matlab Work\Colori\ciexyz64green.dat');
bc=load('C:\Users\sergi\Desktop\Masters 15-07-19 Sergio Majluf
\Matlab Work\Colori\ciexyz64blue.dat');

s1=load('C:\Users\sergi\Desktop\Masters 15-07-19 Sergio Majluf
\Matlab Work\Colori\emrs\NC5m6V.dat');
s2=load('C:\Users\sergi\Desktop\Masters 15-07-19 Sergio Majluf
\Matlab Work\Colori\emrs\NC5m5V.dat');
s3=load('C:\Users\sergi\Desktop\Masters 15-07-19 Sergio Majluf
\Matlab Work\Colori\emrs\NC5m4V.dat');
```

```
s4=load('C:\Users\sergi\Desktop\Masters 15-07-19 Sergio Majluf
\Matlab Work\Colori\emrs\NC5m3V.dat');
s5=load('C:\Users\sergi\Desktop\Masters 15-07-19 Sergio Majluf
\Matlab Work\Colori\emrs\NC5m2V.dat');
s6=load('C:\Users\sergi\Desktop\Masters 15-07-19 Sergio Majluf
\Matlab Work\Colori\emrs\NC5m1V.dat');
s7=load('C:\Users\sergi\Desktop\Masters 15-07-19 Sergio Majluf
\Matlab Work\Colori\emrs\NC50V.dat');
s8=load('C:\Users\sergi\Desktop\Masters 15-07-19 Sergio Majluf
\Matlab Work\Colori\emrs\NC5p1V.dat');
s9=load('C:\Users\sergi\Desktop\Masters 15-07-19 Sergio Majluf
\Matlab Work\Colori\emrs\NC5p2V.dat');
s10=load('C:\Users\sergi\Desktop\Masters 15-07-19 Sergio Majluf
\Matlab Work\Colori\emrs\NC5p3V.dat');
s11=load('C:\Users\sergi\Desktop\Masters 15-07-19 Sergio Majluf
\Matlab Work\Colori\emrs\NC5p4V.dat');
s12=load('C:\Users\sergi\Desktop\Masters 15-07-19 Sergio Majluf
\Matlab Work\Colori\emrs\NC5p5V.dat');
s13=load('C:\Users\sergi\Desktop\Masters 15-07-19 Sergio Majluf
\Matlab Work\Colori\emrs\NC5p6V.dat');


lambda=400:0.5:700;
ri=interp1(rc(:,1),rc(:,2),lambda,'spline');
gi=interp1(gc(:,1),gc(:,2),lambda,'spline');
bi=interp1(bc(:,1),bc(:,2),lambda,'spline');
si1=interp1(s1(:,1),s1(:,2),lambda,'spline');
si2=interp1(s2(:,1),s2(:,2),lambda,'spline');
```

```
si3=interp1(s3(:,1),s3(:,2),lambda,'spline');
si4=interp1(s4(:,1),s4(:,2),lambda,'spline');
si5=interp1(s5(:,1),s5(:,2),lambda,'spline');
si6=interp1(s6(:,1),s6(:,2),lambda,'spline');
si7=interp1(s7(:,1),s7(:,2),lambda,'spline');
si8=interp1(s8(:,1),s8(:,2),lambda,'spline');
si9=interp1(s9(:,1),s9(:,2),lambda,'spline');
si10=interp1(s10(:,1),s10(:,2),lambda,'spline');
si11=interp1(s11(:,1),s11(:,2),lambda,'spline');
si12=interp1(s12(:,1),s12(:,2),lambda,'spline');
si13=interp1(s13(:,1),s13(:,2),lambda,'spline');

vi=ri; % change to either r g or b to fit into the 3 main colours
scof=ones(1,length(lambda));
si1p=si1.*scof;
si2p=si2.*scof;
si3p=si3.*scof;
si4p=si4.*scof;
si5p=si5.*scof;
si6p=si6.*scof;
si7p=si7.*scof;
si8p=si8.*scof;
si9p=si9.*scof;
si10p=si10.*scof;
si11p=si11.*scof;
si12p=si12.*scof;
si13p=si13.*scof;
```

```
figure;

plot(lambda,vi,'y',lambda,si1,'r',lambda,si2,'g',lambda,si3,'b',
lambda,si4,'c',lambda,si5,'m',lambda,si6,'w',lambda,scof,'w',
lambda,si7,'r:',lambda,si8,'g:',lambda,si9,'b-.',lambda,si10,
'c-.',lambda,si11,'m-.',lambda,si12,'w-.',lambda,si13,'.');
grid;
a=1;
b=1;
c=1;
d=1;
e=1;
f=1;
g=1;
h=1;
i=1;
l=1;
m=1;
n=1;
o=1;
global Plothandle
hold on;
Plothandle=plot(lambda,vi,'Erasemode','xor');
options = optimset('TolX',1e-16,'MaxIter',39500,
'MaxFunEvals',109500,'Tolfun',1e-16);
p=[a b c d e f g h i l m n o];
```

```
yf=0;
a = coef(1);
b = coef(2);
c = coef(3);
d = coef(4);
e = coef(5);
f= coef(6);
g= coef(7);
h = coef(8);
i = coef(9);
l= coef(10);
m = coef(11);
n= coef(12);
o= coef(13);
yf=(a.*si1)+(b.*si2)+(c.*si3)+(d.*si4)+(e.*si5)
+(f.*si6)+(g.*si7)+(h.*si8)+(i.*si9)+(l.*si10)+
(m.*si11)+(n.*si12)+(o.*si13);
colourFit=[lambda' yf'];
save('NC5Red.dat', 'colourFit','-ascii');
figure;
plot(lambda,vi,lambda,yf,'b');
xlabel('lambda');
ylabel('Intensity [Arb. Unit]');
title('Color Fit');
grid;
hold;
coef
```

B. APPENDIX B

Appendix B

Colour matching function to colour space

```
colordef black;
clear;
clc;
close all;
% settaggio parametri programma
lambdain=400;
passo=1;
lambdafin=700;
% caricamento dati pesi r,g,b
%r=load('C:\Users\sergi\Desktop\Masters 15-07-19
Sergio Majluf\Horseshoe\ciexyz64red.dat');
%g=load('C:\Users\sergi\Desktop\Masters 15-07-19
Sergio Majluf\Horseshoe\ciexyz64green.dat');
% b=load('C:\Users\sergi\Desktop\Masters 15-07-19
Sergio Majluf\Horseshoe\ciexyz64blue.dat');
r=load('C:\Users\sergi\Desktop\Masters 15-07-19
Sergio Majluf\Horseshoe\NC5Red.dat');
g=load('C:\Users\sergi\Desktop\Masters 15-07-19
```

```
Sergio Majluf\Horseshoe\NC5Green.dat');
b=load('C:\Users\sergi\Desktop\Masters 15-07-19
Sergio Majluf\Horseshoe\NC5Blue.dat');
Mrgb=load('C:\Users\sergi\Desktop\Masters
15-07-19 Sergio Majluf\Horseshoe\Madobe98.dat');
r=abs(r);
g=abs(g);
b=abs(b);
%Mrgb=load('J:\Onedrive\OneDrive -
Politecnico di Torino\work\Colori\MatriciRgb\Mprophoto.dat');
%s1=load('D:\programmi\MATLAB\R2007a\work
\Colori\emrs\result\rosso1.dat');
%s2=load('D:\programmi\MATLAB\R2007a\work
\Colori\emrs\result\verde1.dat');
%s3=load('D:\programmi\MATLAB\R2007a\work
\Colori\emrs\result\blu1.dat');
s1=load('C:\Users\sergi\Desktop
\Masters 15-07-19 Sergio Majluf\Horseshoe\ciexyz64red.dat');
s2=load('C:\Users\sergi\Desktop
\Masters 15-07-19 Sergio Majluf\Horseshoe\ciexyz64green.dat');
s3=load('C:\Users\sergi\Desktop
\Masters 15-07-19 Sergio Majluf\Horseshoe\ciexyz64blue.dat');
% interpolazioni dei dati // data interpolations
Mrgb=Mrgb';
lambda=linspace(lambdain,lambdafin,2017);
ri=interp1(r(:,1),r(:,2),lambda,'spline');
gi=interp1(g(:,1),g(:,2),lambda,'spline');
```

```
bi=interp1(b(:,1),b(:,2),lambda,'spline');
si1=interp1(s1(:,1),s1(:,2),lambda,'spline');
si2=interp1(s2(:,1),s2(:,2),lambda,'spline');
si3=interp1(s3(:,1),s3(:,2),lambda,'spline');
% normalizzazione vettori si // vector normalization if
%ri=ri./max(ri);
%gi=gi./max(gi);
%bi=bi./max(bi);
%si1=si1./max(si1);
%si2=si2./max(si2);
%si3=si3./max(si3);
% introduzione della P(lambda)

% introduzione della P(lambda)
%Rsogg1=si3;
%Rsogg1=50*gauss(lambda,632,18,0)
+50*gauss(lambda,540,18,0);
%Ill1=50*gauss(lambda,460,5,0);
rgbsample=[243 243 242]./255;
%zz=load('J:\Onedrive\OneDrive -
Politecnico di Torino\work\Colori\Canada\Data\Bimetal\CoOs4Sim.dat');
%The line below shows a star in the horseshoe diagram. We can move
the star
%by changing the source, so we can make it green, blue, red, or any
%combination of the three of them
zz(:,1)=lambda;
%for the line below, whats inside the parenthesis after labda is as
```

```
%follows:The wavelength, and how broad the source is, and zero so it
%remains in the xy plane.
zz(:,2)=10000*gauss(lambda,400,15,0); %violet
%zz(:,2)=10000*gauss(lambda,450,15,0); %Blue
%zz(:,2)=10000*gauss(lambda,490,15,0); %Cyan
%zz(:,2)=10000*gauss(lambda,520,15,0); %Green
%zz(:,2)=10000*gauss(lambda,560,15,0); %Yellow
%zz(:,2)=10000*gauss(lambda,590,15,0); %Orange
%zz(:,2)=10000*gauss(lambda,635,15,0); %Blood Orange
%zz(:,2)=10000*gauss(lambda,700,15,0); %Red
illu=load('C:\Users\sergi\Desktop\Masters 15-07-19
Sergio Majluf\Horseshoe\D65.dat');
iln='D65';
if strcmp(iln,'flat')
nor=[ 1.165542332532506e+02 1.166505679842604e+02
1.162557392029152e+02];
end
if strcmp(iln,'D50')
nor=[1.102347953277927e+02 1.140092109700676e+02
92.663139821210251];
end
if strcmp(iln,'D65')
nor=[1.101061436728935e+02 1.161948653480489e+02
1.243928229942044e+02];
end
if strcmp(iln,'D75')
nor=[1.11861066128224e+02 1.178416301898311e+02
```

```
1.418009138026290e+02];
end
if strcmp(iln,'F2')
nor=[15.991826447130618 15.483177020847545
10.692139677478895];
end
if strcmp(iln,'F7')
nor=[15.296100308323496 15.969118100675999
17.191833933434225];
end
if strcmp(iln,'F11')
nor=[16.062900655896350 15.463221682767776
10.156036489263158];
end
inl=find(illu(:,1)>=lambdain&illu(:,1)<=lambdafin);
%illu(:,2)=illu(:,2)./285;
Ill1=interp1(illu(inl,1),illu(inl,2),lambda,'spline');
in=find(zz(:,1)>=lambdain&zz(:,1)<=lambdafin);
%zz=[ zz(in(end:-1:1),1) zz(in,2)];
zz=[ zz(in,1) zz(in,2)];
zint=interp1(zz(:,1),zz(:,2),lambda,'spline');
%Rsogg1=max(zint)-zint;

Rsogg1=zint/100;
%Rsogg1=zz(:,2)';
%Ill1=100*ones(1,length(lambda));
%Rsogg1=ones(1,length(lambda));
```

```
Ill1=Ill1/100;
P1=Rsogg1.*Ill1;
%P1=Ill1;
%P=0.92973912.*ones(1,length(lambda)); %sorgente
bianca a spettro uniforme!
% definizione funzioni integrande
irp1=trapz(lambda,ri.*P1);
igp1=trapz(lambda,gi.*P1);
ibp1=trapz(lambda,bi.*P1);
N=trapz(lambda,gi.*Ill1);
%plot risultati
plot(lambda,P1,'w',lambda,Rsogg1,'y',lambda,Ill1,'c');
xlabel('Wavelength [nm]');
ylabel('intensity [Arb. Unit]');
%title('Emissivita sorgente (Giallo),
Illuminazione (Cyan), Emissivita Totale (Bianco)');
title('Source emissivity (Yellow), Illumination
(Cyan), Total Emissivity (White) ');
grid
figure;
plot(lambda,ri,'r',lambda,gi,'g',lambda,bi,'b');
xlabel('Wavelength [nm]');
ylabel('Intensity [Arb. Unit]');
title('RGB weight functions');
grid
figure;
plot(lambda,ri.*P1,'r',lambda,gi.*P1,'g',
```

```
lambda,bi.*P1,'b',lambda,P1,'k');
xlabel('Wavelength [nm]');
ylabel('Intensity [Arb. Unit]');
title('(RGB Weight Functions) * Total spectral
emissivity, Total emissivity');
grid
% normalizzazione risultati // normalization result
format long;
disp('Illuminated Object Color Coordinates');
disp('x Coordinate');
irxc=irp1./(irp1+igp1+ibp1);
disp(irxc);
disp('y Coordinate');
igxc=igp1./(irp1+igp1+ibp1);
disp(igxc);
disp('z Coordinate');
ibxc=ibp1./(irp1+igp1+ibp1);
disp(ibxc);
disp('Y luminance / Luminanza Y');
disp(igp1);
disp('X Coordinate');
disp(irp1);
disp('Y coordinate');
disp(igp1);
disp('Z Coordinate');
disp(ibp1);
disp('XYZ coordinate according to new calculation');
```

```
cxyz=[irp1 igp1 ibp1]/N;


cXYZ=cxyz./sum(cxyz);
disp('Colour Lab Coordinate');
%curcol=convXYZ2Lab(irp1,igp1,ibp1,nor)'
% gammacorr=1.418;
% rgbpure=double(xyz2rgb(cXYZ,'OutputType','uint8'));
% rgbcorr=rgbpure.^(1./gammacorr)
% rgbcorr1=rgbcorr/255; %rescale 0 1
% CoCalc=rgb2lab(rgbcorr1,'WhitePoint','d50');
% Cosample=rgb2lab(rgbsample,'WhitePoint','d50');
% disp('Differenza Colore Calcolata');
% cd=deltaE00(Cosample',CoCalc')
%coordinate bianco puro e colori primari vertici del
triangolo rgb
%xw=0.317919;
xw=0.33309939076606;
yw=0.33336518213157;
%yw=0.336595;
xr=0.640007;
yr=0.32997;
xg=0.3;
yg=0.6;
xb=0.15002;
yb=0.06001;
% ricavo coordinate colore rispetto asse con
origine nel bianco
```

```
% Get color coordinates with respect to axis
with origin in white
irxw=irxc-xw;
igxw=igxc-yw;
a=atan(igxw./irxw);
% ricavo angolo colore (in gradi) e quadrante
di appartenenza
% color angle (in degrees) and quadrant it's
part of
if irxw>0 && igxw>0
quad=1;
ad=a.*(180./pi);
end
if irxw<0 && igxw>0
quad=2;
ad=(a.*(180./pi))+180;
end
if irxw<0 && igxw<0
quad=3;
ad=(a.*(180./pi))+180;
end
if irxw>0 && igxw<0
quad=4;
ad=360+(a.*(180./pi));
end
% disp(strcat('Quadrante Colore rispetto
punto Bianco = ',num2str(quad)));
```

```
% disp(strcat('Angolo Colore rispetto
punto Bianco = ',num2str(ad)));
% calcolo angoli colori primari e
conversione in gradi
ar=atan((yr-yw)./(xr-xw));
ag=atan((yg-yw)./(xg-xw));
ab=atan((yb-yw)./(xb-xw));
adr=ar.*(180./pi);
adg=ag.*(180./pi)+180;
adb=ab.*(180./pi)+180;
% Stabilisco retta intersezione corretta
% I establish straight correct intersection
if ad>0 && ad<0.15230427963168

retta=3;
end
if ad>0.15230427963168 &&
ad<92.68832564678937
retta=1;
end
if ad>92.68832564678937 &&
ad<2.388415657483586e+002
retta=2;
end
if ad>2.388415657483586e+002 && ad<360
retta=3;
end
```

```
% calcolo retta passante per le coordinate
(irx,igx) ---(xw,yw)
% straight line calculation through the
coordinates (irx,igx) ---(xw,yw)
mc=(igxc-yw)./(irxc-xw);
qc=det([irxc xw; igxc yw])./(irxc-xw);
% assegnazione retta intersezione corretta
% correct intersection correct assignment
if retta==1
ml=(yg-yr)./(xg-xr);
ql=det([xg xr; yg yr])./(xg-xr);
end
if retta==2
ml=(yg-yb)./(xg-xb);
ql=det([xg xb; yg yb])./(xg-xb);
end
if retta==3
ml=(yb-yr)./(xb-xr);
ql=det([xb xr; yb yr])./(xb-xr);
end
% calcolo colore intersezione
% intersection color calculation
xint=(ql-qc)./(mc-ml);
yint=mc.*xint+qc;
zint=1-(xint+yint);
disp('Colore Intersezione');
disp(strcat('Coordinata x= ',num2str(xint)));
```

```
disp(strcat('Coordinata y= ',num2str(yint)));
% generazione grafico correzione colore
% color correction chart generation
mbr=(yb-yr)./(xb-xr);
qbr=det([xb xr; yb yr])./(xb-xr);
mgb=(yg-yb)./(xg-xb);
qgb=det([xg xb; yg yb])./(xg-xb);
mgr=(yg-yr)./(xg-xr);
qgr=det([xg xr; yg yr])./(xg-xr);
% generazione retta br
% straight generation br
xbr=xb:0.001:xr;
ybr=polyval([mbr qbr],xbr);
% generazione retta gb
% straight generation gb
xgb=xb:0.001:xg;
ygb=polyval([mgb qgb],xgb);
% generazione retta gr
% straight generation gr
xgr=xg:0.001:xr;
ygr=polyval([mgr qgr],xgr);
% generazione retta colore - punto bianco
% straight color - white point generation
if irxc<xw
xcr=irxc:0.001:xw;
else
xcr=xw:0.001:irxc;
```

```
end
ycr=polyval([mc qc],xcr);
%creazione grafico // graphic creation
% definizioni costanti varie utili * plot
% various useful constant definitions * plot
% xw=0.31272;
% yw=0.3291;
mbr=(yb-yr)./(xb-xr);
qbr=det([xb xr; yb yr])./(xb-xr);
mgb=(yg-yb)./(xg-xb);
qgb=det([xg xb; yg yb])./(xg-xb);
mgr=(yg-yr)./(xg-xr);
qgr=det([xg xr; yg yr])./(xg-xr);
% generazione retta br
xbr=xb:0.001:xr;
ybr=polyval([mbr qbr],xbr);
% generazione retta gb
xgb=xb:0.001:xg;
ygb=polyval([mgb qgb],xgb);
% generazione retta gr
xgr=xg:0.001:xr;
ygr=polyval([mgr qgr],xgr);
ind=1;
ccx=[];
ccy=[];
ccsx=[];
ccsy=[];
```

```
Cnew=[];
fb=0;
Rsoggbianco=1.*ones(1,length(lambda));
Ill=1.*ones(1,length(lambda));
for jk=lambdain:passo:lambdafin;
Rsogg=10*gauss(lambda,jk,0.01,0);
P=Rsogg.*Ill;
if fb==0
Pbianco=Rsoggbianco.*Ill;
irs=trapz(lambda,Pbianco.*si1);
igs=trapz(lambda,Pbianco.*si2);
ibs=trapz(lambda,Pbianco.*si3);
irsx=irs./(irs+igs+ibs);
igsx=igs./(irs+igs+ibs);
ibsx=ibs./(irs+igs+ibs);
xwn=irsx;
ywn=igsx;
fb=1;
end
%P=0.92973912.*ones(1,length(lambda));
%sorgente bianca a spettro uniforme!
% uniform spectrum white source!
% definizione funzioni integrande
% definition of integrated functions
irs=trapz(lambda,si1.*P);
igs=trapz(lambda,si2.*P);
ibs=trapz(lambda,si3.*P);
```

```
ir=trapz(lambda,ri.*P);
ig=trapz(lambda,gi.*P);
ib=trapz(lambda,bi.*P);
irx=ir./(ir+ig+ib);
igx=ig./(ir+ig+ib);
ibx=ib./(ir+ig+ib);
irsx=irs./(irs+igs+ibs);
igsx=igs./(irs+igs+ibs);
ibsx=ibs./(irs+igs+ibs);
Xc=[ir;ig;ib];
sRgb=Mrgb*Xc;
flag=0;
for i=1:length(sRgb)
if sRgb(i)<0
flag=1;
end
end
if flag==1
%disp('Tripletta RGB Approssimata (x Rescaling)');
%RGB approximation
mn=min(sRgb);
sRgb=sRgb-mn;
sRgb=sRgb./max(sRgb);
%pause;
else
%disp('Tripletta RGB');
sRgb=sRgb./max(sRgb);
```

```
%pause;
end
Cnew=[Cnew;sRgb'];
ccx(ind)=irx;
ccy(ind)=igx;
ccsx(ind)=irsx;
ccsy(ind)=igsx;
ind=ind+1;
%plot(irx,igx,'w.');
end
%tracciamento // tracing
figure;
%x=h(:,1);
%y=h(:,2);
x=[ccx';ccx(1)];
y=[ccy';ccy(1)];
for i=1:length(x)-1
faces(i,1)=i;
faces(i,2)=i+1;
faces(i,3)=length(x)+1;
end
for i=1:length(x)
vertx(i,1)=x(i);
vertx(i,2)=y(i);
vertx(i,3)=0;
end
vertx(length(x)+1,1)=xw;
```

```
vertx(length(x)+1,2)=yw;
vertx(length(x)+1,3)=0;
C=[Cnew;Cnew(1,:);1 1 1];
patch('Vertices',vertx,'Faces',faces,'FaceVertexCdata'
,C,'Facecolor','interp','Edgecolor','interp');
title('Diagramma Cromatico Cie xy');
xlabel('x Coordinate');
ylabel('y Coordinate');
%title('Piano Colori xy Cie1964 (Horseshoe)
(frontiera bianca) e visione sensore
(da 3 funzioni s1,s2,s3)(* blu=posizione bianco)')
title('Plane Colors xy Cie1964 (Horseshoe)
(white border) and sensor vision
(from 3 functions s1, s2, s3) (* = white position)');
text(0.05,0.86,'Green');
text(0.7,0.33,'Red');
text(0.07,0.04,'Blue');
text(0.45,0.58,'Yellow');
grid;
set(gca,'Layer','Top');
hold;
%plot(xbr,ybr,'k',xgb,ygb,'k',xgr,ygr,'k');
%plot(xw,yw,'b*');
%hold;
plot(ccx,ccy,'w.');
plot(ccsx,ccsy,'w-',ccsx,ccsy,'w.');
%text(ccsx,ccsy,num2str(jk));
```

```
% plot valori su grafico
lv=lambdain:passo:lambdafin;
for i=1:20:length(lv)
text(ccsx(i),ccsy(i),num2str(lv(i)));
end
%hh=line([ccsx(1) ccsx(length(ccsx))],
[ccsy(1) ccsy(length(ccsy))]);
hh=line([ccsx(4) ccsx(length(ccsx))],
[ccsy(4) ccsy(length(ccsy))]);
set(hh,'Color',[1 1 1],'Marker','.');
a=axis;
% prova tracciamento con riduzione spazio
% trial tracking with space reduction
plot(xwn,ywn,'m*');
%hold;
cx=[0.59054344 0.25823289 0.16420878 0.59054344];
cy=[0.3958799 0.69574172 0.0704781 0.3958799];
%plot(cx,cy,'w-',cx,cy,'ko')
%creazione grafico // creating figure
plot(irxc,igxc,'kp');

%title('Colour localization in the xy * magenta plane
= white point, 1 = Ill flat, 2 = Ill D50, 3 = Ill
D65, 4 = Ill D75, 5 = Ill F2, 6 = Ill F7, 7 = Ill F11')

%My micromorph + DSSC sensor
punti0=[0.677455570818292 0.322544429178399;
```

```
0.092131818314463  0.540108445101272;
0.207727258423574  1.477128268062870e-04;
0.677455570818292  0.322544429178399];

punti1=[0.683817757871573  0.316182241439364;
0.098072893423231  0.693065049883207;
0.167717094060689  0.020446255788578;
0.683817757871573  0.316182241439364];

[n,m]=size(punti0);
%pos=[1  3  4  2  5  1];
for  i=1:n-1



end
ordr=[1  2  3  1];
ordn=[1  2  3  1];
for  i=1:n-1
end
```

C. APPENDIX C

Appendix C

xyY to L*ab

```
prompt = 'What is the x1-value? ';
x1 = input(prompt);
prompt = 'What is the y1-value? ';
y1 = input(prompt);
prompt = 'What is the Y1-value? ';
Y1 = input(prompt);
fprintf(1, '\n');
prompt = 'What is the x2-value? ';
x2 = input(prompt);
prompt = 'What is the y2-value? ';
y2 = input(prompt);
prompt = 'What is the Y2-value? ';
Y2 = input(prompt);
X1 = x1 * ( Y1 / y1 );
Z1 = ( 1 - x1 - y1 ) * ( Y1 / y1 );
ReferenceX=95.047;
ReferenceY=100.000;
ReferenceZ=108.883;
```

```
varX1 = X1 / ReferenceX;
varY1 = Y1 / ReferenceY;
varZ1 = Z1/ ReferenceZ;
if ( varX1 > 0.008856 )
varX1 = varX1 ^ ( 1/3 );
else
varX1 = ( 7.787 * varX1 ) + ( 16 / 116 );
end
if ( varY1 > 0.008856 )
varY1 = varY1 ^ ( 1/3 );
else
varY1 = ( 7.787 * varY1 ) + ( 16 / 116 );
end
if ( varZ1 > 0.008856 )
varZ1 = varZ1 ^ ( 1/3 );
else
varZ1 = ( 7.787 * varZ1 ) + ( 16 / 116 );
end
CIEL1 = ( 116 * varY1 ) - 16;
CIEa1= 500 * ( varX1 - varY1 );
CIEb1= 200 * ( varY1 - varZ1 );
fprintf(1, '\n');
fprintf('CIE*a1 = %i\n', CIEa1);
fprintf('CIE*b1 = %i\n', CIEb1);
fprintf('CIE*Y1 = %i\n', CIEL1);
fprintf(1, '\n');
% fprintf('The colour transformations for x1= %a,
```

```
y1= %b, and Y1= %c are:\n',x1,y1,Y1);
% fprintf(1, '\n');
% fprintf('x becomes CIE*a1= %d\n',CIEa1);
% fprintf('y becomes CIE*b1= %d\n',CIEb1);
% fprintf('Y becomes CIE*L1= %d\n',CIEL1);
X2 = x2 * ( Y2 / y2 );
Z2 = ( 1 - x2 - y2 ) * ( Y2 / y2 );
ReferenceX=95.047;
ReferenceY=100.000;
ReferenceZ=108.883;
varX2 = X2 / ReferenceX;
varY2 = Y2 / ReferenceY;
varZ2 = Z2 / ReferenceZ;
if ( varX2 > 0.008856 )
varX2 = varX2 ^ ( 1/3 );
else
varX2 = ( 7.787 * varX2 ) + ( 16 / 116 );
end
if ( varY2 > 0.008856 )
varY2 = varY2 ^ ( 1/3 );
else
varY2 = ( 7.787 * varY2 ) + ( 16 / 116 );
end
if ( varZ2 > 0.008856 )
varZ2 = varZ2 ^ ( 1/3 );
else
varZ2 = ( 7.787 * varZ2 ) + ( 16 / 116 );
```

```
end
CIEL2 = ( 116 * varY2 ) - 16;
CIEa2 = 500 * ( varX2 - varY2 );
CIEb2 = 200 * ( varY2 - varZ2 );
fprintf(1, '\n');
fprintf('CIE*a2 = %i\n', CIEa2);
fprintf('CIE*b2 = %i\n', CIEb2);
fprintf('CIE*Y2 = %i\n', CIEL2);
fprintf(1, '\n');
DeltaE= sqrt( ( ( CIEL1 - CIEL2 ) ^ 2 ) +
( ( CIEa1 - CIEa2 ) ^2 ) + ( ( CIEb1 - CIEb2 ) ^ 2 ) );
fprintf('DeltaE = %i\n', DeltaE);
```